Mitochondrial fragmentation promotes inflammation resolution responses in macrophages via histone lactylation

By: Leah Isabelle Susser

A thesis submitted in partial fulfillment of the requirements for the
Doctorate in Philosophy degree in Biochemistry

Department of Biochemistry, Microbiology, & Immunology
Faculty of Medicine
University of Ottawa

uOttawa

Abstract

During the inflammatory response, macrophage phenotypes can be broadly classified as pro-inflammatory/classically activated 'M1', or pro-resolving/alternatively 'M2' macrophages. Although the classification of macrophages is general and assumes there are distinct phenotypes, in reality macrophages exist across a spectrum and must transform from a pro-inflammatory state to a pro-resolving state following an inflammatory insult. To adapt to changing metabolic needs of the cell, mitochondria undergo fusion and fission, which have important implications for cell fate and function. We ***hypothesized*** that mitochondrial fission and fusion directly contribute to macrophage function during the pro-inflammatory and pro-resolving phases. We find that mitochondrial length directly contributes to macrophage phenotype, primarily during the transition from a pro-inflammatory to a pro-resolving state. Phenocopying the elongated mitochondrial network (by disabling the fission machinery using siRNA) leads to a baseline reduction in the inflammatory marker IL-1β, but a normal inflammatory response to LPS, similar to control macrophages. In contrast, in macrophages with a phenocopied fragmented phenotype (by disabling the fusion machinery using siRNA) there is a heightened inflammatory response to LPS and increased signaling through the ATF4/c-Jun transcriptional axis compared to control macrophages. Importantly, macrophages with a fragmented mitochondrial phenotype show increased expression of pro-resolving mediator Arginase 1 and increased phagocytic capacity. Promoting mitochondrial fragmentation caused an increase in cellular lactate, and an increase in histone lactylation which caused an increase in Arginase 1 expression. Furthermore phenocopied mitochondrial fragmentation via MYLS22 (Opa1 inhibitor) also led to an improved zymosan induced peritonitis resolution timeline in-vivo.These studies demonstrate that a fragmented mitochondrial phenotype is critical for the pro-resolving response in macrophages and specifically drive epigenetic changes via lactylation of histones following an inflammatory insult.

Graphical Abstract

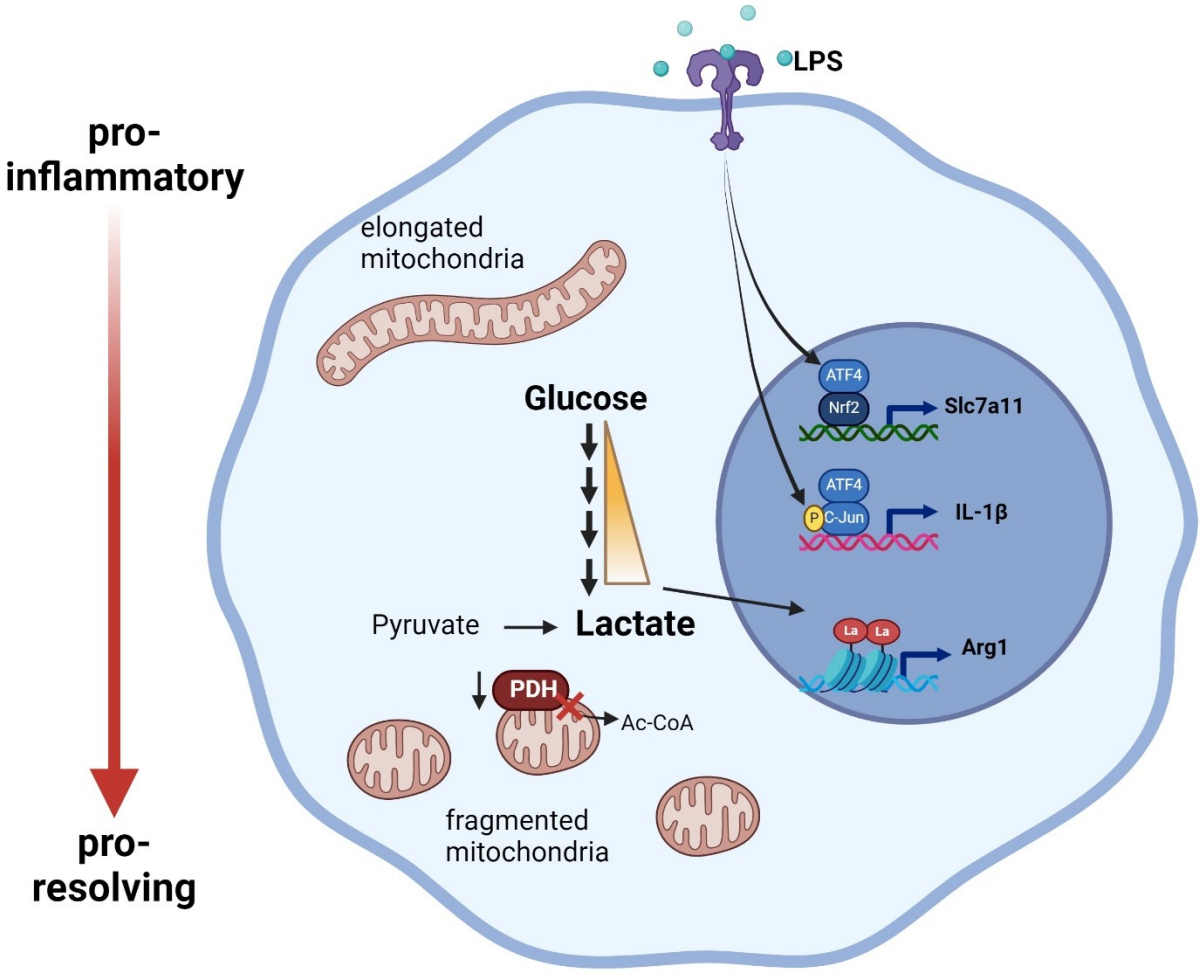

Acknowledgements

First and foremost, I would like to thank my supervisor, Dr. Katey Rayner, for giving me the opportunity to join the lab as a summer student and encouraging me to pursue my graduate studies. Over the years, she has provided me with the support and guidance to achieve more than I thought possible. Thank you for the time and mentorship you have given me over the last 7 years.

This project would not be possible without the guidance and encouragement of my co-supervisor Dr. Mireille Khacho. No matter the dead end, your fresh perspective helped me navigate forward.

I would like to express my gratitude to Dr. Mireille Ouimet, Dr. Erin Mulvihill, and Dr. Julie St-Pierre, all members of my thesis advisory committee. Their expertise, insight, and guidance have been invaluable in building my confidence in my research over the years. Thank you for being such strong examples of women in STEM.

To all the present and past lab members, thank you for making the lab such a fun and exciting place to work. I especially want to thank Michele Geoffrion (the knower of all things) for teaching me so much and being that foundation, I could go back to no matter the difficulty. I want to give special thanks to Dr. My-Anh Nguyen (my guru buddy ol pal) for training me in almost every technique I know and answering my ceaseless questions.

I cannot forget all the amazing friends I made at the Heart Institute over the years, who were always there to offer understanding, good talks, and laughter. I know you will be positive forces in my life no matter where in the world it takes us.

Thank you to my best friend for being my cheerleader who always believes in me and never fails to pick up the phone.

Lastly, thank you to my parents for their love and support not only through my Ph.D. but my entire life. You were there for every high and even lower low, and your love and patience got me through it. I hope to one day give back a fraction of what you have given me.

Preface

The following sections of this thesis have been previously published in *Molecular and Cellular Biology* in Oct 2023 (1) with some modifications having been completed thereafter: Chapter 2: Materials & Methods, Figures 3.1, 3.2, 4.1, 4,4, 4.5, 4.6, 4.7, 4.8 (as well as respective captions), and segments of Chapter 6: Discussion.

Table of Contents

List of Abbreviations

AcLDL	acetylated low-density lipoprotein
AgLDL	aggregated low-density lipoprotein
AIDS	acquired immunodeficient syndrome
APC	antigen-presenting cells
ARG1	arginase 1
ATF3	activating transcription factor 3
ATF4	activating transcription factor 4
ATP	adenosine triphosphate
BCAP	b-cell adaptor protein
BMDM	bone marrow-derived macrophages
CHIP	chromatin immunoprecipitation
DAMP	damage-associated molecular patterns
DNM2	dynamin 2
DRP1	dynamin-related protein 1
EMPF1	defective mitochondrial and peroxisomal fission-1
ER	endoplasmic reticulum
ETC	electron transport chain
FIS1	fission 1
GAPDH	glyceraldehyde 3-phosphate dehydrogenase
GLO2	glyoxalase2
GTP	guanisine triphosphate
HIF1α	hypoxia-inducible factor-1α
HIV	human immunodeficiency virus
HPLC	high-performance liquid chromatography
IFNγ	interferon gamma
IL-1β	interleukin 1 beta
IMM	inner mitochondrial membrane
INF2	inverted formin-2
IRG1	immune-responsive gene 1
KEAP1	kelch-like ECH-associated protein 1
KLA	lysine lactylation
KLF4	kruppel-like factor 4
LDH	lactate dehydrogenase
LGSH	lactylglutathione
LPS	lipopolysaccharides
MFF	mitochondrial fission factor
MFN	mitofusin
MHC	major histocompatibility complex
MS/MS	mass spectrometry

NADH	nicotinamide adenine dinucleotides
NaLa	sodium lactate
NFκB	nuclear factor kappa B
NK	natural killer cells
NRF2	nuclear factor erythroid 2–related factor 2
OMM	outer mitochondrial membrane
OPA1	optic atrophy 1
OxLDL	oxidized low-density lipoprotein
PAMP	pathogen-associated molecular patterns
PCAF	p300/CBP-associated factor
PDGF	platelet-derived growth factor
PDH	pyruvate dehydrogenase
PDHK	pyruvate dehydrogenase kinase
PGDH	prostaglandin dehydrogenase
PMAC	peritoneal macrophages
PPARγ	peroxisome proliferator-activated receptor gamma
RET	reverse electron transport
RNA	ribonucleic acid
ROS	reactive oxygen species
SDH	succinate dehydrogenase
SENP1	sentrin-specific protease 1
TCA	tricarboxylic acid cycle
TEM	transmission electron microscopy
TGFβ	transforming growth factor-beta
TNFα	tumour necrosis factor alpha
VEGF	vascular endothelial growth factors
ZIP	zymosan-induced peritonitis

List of Figures

Chapter 1: Introduction

1.1 Immune System

The immune system maintains tissue homeostasis and protects the body from invading foreign substances such as bacteria, fungi, yeast and viruses (2). Beyond the physical barriers which protect us from infection, the immune system can be viewed as having two "lines of defence": innate and adaptive immunity. Innate immunity is the first line of defence against invading pathogens (3). The innate immune response is antigen-independent and, therefore, cannot recognize or remember a pathogen for future exposure. However, through the use of pattern recognition receptors (PPRs), innate immune cells can distinguish between self and foreign body and respond rapidly to invading foreign substances. On the other hand, adaptive immunity is specific and acquired throughout life upon presentation of an antigen on the major histocompatibility complex (MHC) of antigen-presenting cells to T-cells, initiating the cell-mediated immune response followed by a humoral immune response. Thus, it involves a delay between exposure to the antigen and maximal immune response. The hallmark of adaptive immunity is the memory capacity, which enables the host to rapidly mount an effective immune response upon subsequent exposure to the antigen. Innate and adaptive immunity are complementary mechanisms, and defects in either system result in host vulnerability or inappropriate responses such as autoimmune disorders or allergies (3–5).

The cells and processes critical for effective innate immunity to pathogens have been widely studied. Innate immunity to pathogens relies on PRRs, which allow immune cells to rapidly detect and respond to a wide range of pathogens that share common structures, known

as pathogen-associated molecular patterns (PAMPs) or damage-associated molecular patterns (DAMPs). Examples include lipopolysaccharides (LPS), oxidized low-density lipoprotein (OxLDL) and double-stranded ribonucleic acid (RNA) (4). A vital function of the innate immune system is rapidly recruiting immune cells to sites of infection and inflammation. Recruitment is primarily induced through the production of cytokines and chemokines (small proteins involved in cell-cell communication). In addition to the cytokine response, another critical function of the innate immune system is phagocytosis, the process of engulfing microbes, cell debris, and infected cells. The phagocytic action of the innate immune response promotes the clearance of dead cells or antibody complexes and removes foreign substances.

Numerous cell types are involved in the innate immune response, such as macrophages, neutrophils, dendritic cells, mast cells, basophils, eosinophils, and natural killer (NK) cells (Figure 1.1). Both macrophages and neutrophils are considered phagocytes with a similar function: to engulf (phagocytose) foreign bodies and kill them through multiple cell death pathways. Neutrophils are short-lived phagocytes with the additional property of containing granules and enzyme pathways that assist in the elimination of pathogens. Macrophages are long-lived phagocytic cells with additional antigen-presenting properties. Macrophages, alongside B-cells and dendritic cells, use major histocompatibility complexes to present fragments of antigens to T-cells to mount an adaptive immune response (6).

The adaptive immune system's primary role is to amplify the immune response upon discovery through antibody production and to remember that antigen for a more rapid and

amplified response in the future. Two subclasses of lymphocytes, T-cell and B-cell, mediate the adaptive response (Figure 1.1). Upon recognition of antigen presentation, B-cells secrete antigen-specific antibodies, which in circulation protect in two significant ways: marking pathogens for easier discovery and preventing further binding by blocking their binding receptors. A subset of B-cells become memory cells to more rapidly produce antibodies upon future exposure. Upon antigen presentation, T cells perform two significant tasks: kill infected host cells to prevent further infection and produce cytokines that influence the innate immune response to either amplify or resolve the inflammation (e.g., IFNγ, IL-4, etc.). A subset of T-cells also become memory cells to destroy infected host cells more rapidly upon secondary exposure.

The innate and adaptive immune systems work together to maintain homeostasis and protect against infection. Although there is some built-in redundancy between cell type tasks, alteration in the function of any of these cell types results in disease. Autoimmune diseases are the result of overactive immune system attacking oneself causing bodily damage. Type 1 diabetes is caused by one's immune system attacking insulin-producing pancreatic Islets (7). Multiple sclerosis is caused by immune-mediated nerve damage (8). Crohn's disease and ulcerative colitis are characterized by immune damage to the intestinal lining (9). On the other hand, immunodeficiency results in illness and complications from normally benign pathogens. *Human immunodeficiency virus (HIV)* when left untreated result in acquired immunodeficient syndrome (AIDS) through depletion and damage of T-cells resulting in vulnerability to commonly transmitted pathogen such as pneumonia (10). A similar effect can be seen in the

case of Leukemia, whereby deficient cancerous immune cells result in frequent and severe infections. The above outlines only a few of the diseases and disorders associated with altered immune function (11). An effective innate and adaptive immune system is required for the maintenance of human health.

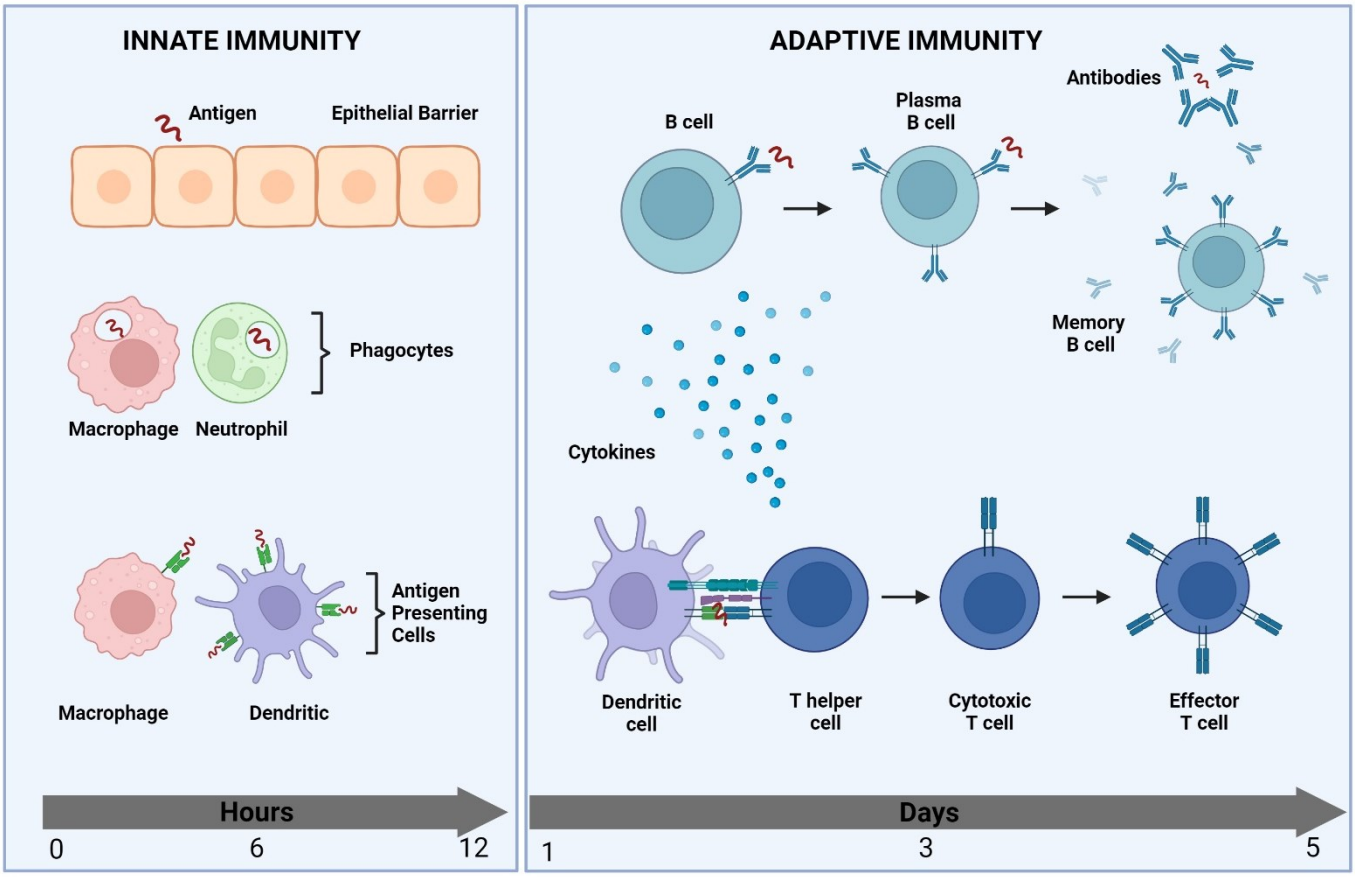

Figure 1.1: Innate and adaptive immunity timeline.
If a pathogen is able to get past the first layer of defense the skin barrier the innate immune response is rapidly initiated. Upon phagocytosis a fragment of the pathogen is presented on major histocompatibility complexes of antigen presenting cells (APCs) such. APCs present the antigen to T cells to initiate the slower adaptive immune response. Whereby T cells help attack and remove the pathogen. The released cytokines activate B cells which create antibodies against the pathogen for rapid action upon future exposures. B cells Adaptive immune responses develop later and require the activation of lymphocytes. The kinetics of the innate and adaptive immune responses are approximations and may vary in different infections.

1.2 Macrophages

Macrophages can be found in almost all organs in the body, including the liver, brain, bones, and lungs; they have specific functions in each organ. For instance, alveolar macrophages are necessary for processing surfactants, and macrophages in the gastrointestinal tract and adipose tissue play an integral role in maintaining homeostasis. Thus, each organ and the surrounding environment influence their properties during differentiation. Historically, it was believed that macrophages were solely derived from hematopoietic stem cells and locally differentiated into tissue-specific macrophages. Van Furth et al. proposed that tissue-resident macrophages are continuously repopulated by circulating monocytes in the blood, which arise from progenitors in adult bone marrow (12). However, Takahashi et al. demonstrated that macrophages were maintained in peripheral tissues by self-renewal from embryogenesis, in addition to the macrophages derived from hematopoietic stem cells (13, 14).

With the advancement of modern techniques and technology, such as novel mouse models, spatial single-cell omics and analysis pipelines it was discovered that within each organ niche, there is a combination of resident and recruited macrophages from different origins. For example, microglia in the central nervous system are primarily derived from the embryonic yolk sac which are maintained throughout life. Meanwhile, the intestinal tract is primarily embryonically derived, but the macrophages are replaced with bone marrow-derived macrophages immediately after birth. However, fetal liver-derived macrophages are dominant in most other organ tissues (15). In the case of disease or injury, monocyte-derived macrophages can, in part, replace long-lived resident macrophages within a niche. However,

they cannot fully recapitulate the original molecular signature imprinted on the fetal-derived macrophage from developing together within an organ. Thus, macrophage plasticity is specified by the maturation state of macrophage precursors and their ability to adapt to their specific niches (16–18).

Macrophages themselves have high plasticity and can exist on a spectrum of polarization based on their environmental cues. Macrophages exposed to pro-inflammatory stimuli, such as the invasion of a pathogen, are categorized as pro-inflammatory M1-like macrophages (19, 20). Generally, PAMPs, DAMPs, and inflammatory cytokines such as TNFα and IFNγ induce the M1 phenotype. M1 inflammatory macrophages were discovered as a response to bactericidal infection resulting in the release of inflammatory cytokines (ex: IL-1β, TNF-α, IL-12, IL-6, IL-2, NF-κB & iNOS), increased associated reactive oxygen species (ROS), and increased use of glycolysis as a primary form of metabolism (21, 22). To mimic this form of classical activation in vivo, LPS a component of the bacterial cell wall and activated T cell-produced cytokine interferon-gamma (IFNγ) are used. LPS stimulation induces the production of not only inflammatory cytokine but also ROS. LPS promotes ROS production by inhibiting complex II and III of the electron transport chain (ETC) and creating breaks in the TCA cycle at the citrate and succinate locations (23–25). Resulting in an interruption of the flow of metabolites and electrons marked by the accumulation of citrate and succinate, which have defined immunometabolism role. Those breaks effectively inhibit oxidative phosphorylation as the primary form of ATP production. Instead, electron resources are redirected to the formation of

ROS by reverse electron transport (RET) through complex I of the ETC (26, 27). ROS are then used to help kill foreign bacteria or infected cells they come across (28).

In contrast, macrophages exposed to pro-resolving stimuli, such as those involved in inflammation resolution, are classified as pro-resolving M2-like macrophages (29, 30). M2 macrophages, are considered pro-resolving due to their primary function being efferocytosis of apoptotic and toxic bodies—the efferocytosis process results in the release of anti-inflammatory cytokines IL-10 and TGFβ (31). IL-10 simultaneously promotes M2 macrophage polarization and inhibits M1 production of inflammatory cytokines. TGFβ encourages collagen production, thereby promoting angiogenesis, tissue repair and immunoregulation. M2 alternate activation is primarily induced by T helper 2 cell cytokine IL-4 (and IL-13) (21, 32). IL-4 also supports immunoregulation by suppressing M1 production of inflammatory cytokines through PPARγ.

Once an inflammatory reaction occurs within any given niche, bone marrow-derived monocytes infiltrate the inflammatory tissue and differentiate into macrophages. Generally, it is considered that embryonic-derived macrophages play a vital role in maintaining tissue homeostasis. In contrast, macrophages derived from bone marrow monocytes are strongly correlated to host defence reactions and inflammatory diseases. The phenotype of the macrophages, both recruited and resident to a tissue, can dictate the progression or regression of a disease. However, which phenotype of maximal benefit is context-dependent: M1-like

macrophages are most beneficial in the context of active infection and cancer, whereas M2-like macrophages are imperative for tissue repair and return to homeostasis (Figure 1.2).

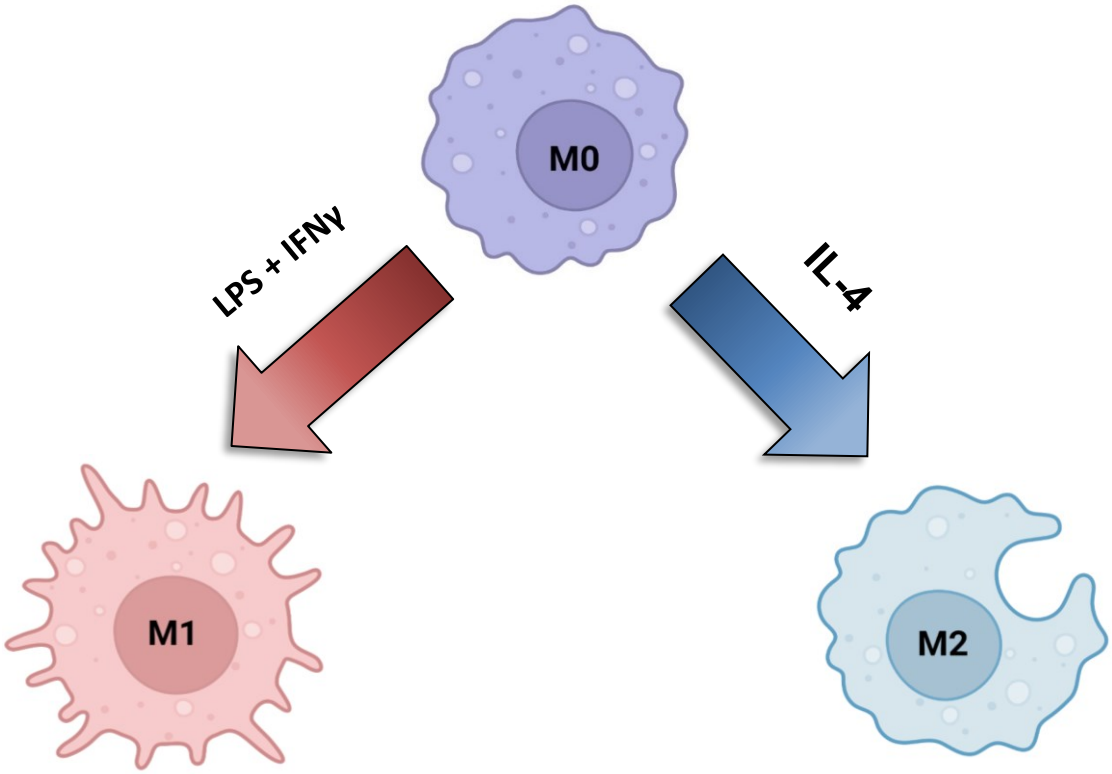

Pro-inflammatory:

- Secretes: TNF-α & IL-1β
- Markers: iNOS
- Functions:
  - Infection protection
  - Anti-cancer immunity
  - Atherosclerosis progression
  - Autoimmune diseases
- Glycolytic Metabolism

Anti-inflammatory:

- Secretes: IL-10, & TGF-β
- Markers: Arg1 & Fizz1
- Functions:
  - Tissue repair
  - Cancer progression
  - Atherosclerosis regression
  - Immunoregulation
- Oxidative metabolism

Figure 1.2: Flow chart of macrophage polarization phenotypes.
Macrophages exist on a spectrum of activation, with the two extremes being M1 or M2. Macrophages derived from monocytes become polarized into two phenotypes based on the cytokine they are exposed to. Pro-inflammatory cytokines LPS and IFNγ polarize macrophages to M1, and anti-inflammatory cytokines IL-4 (& IL-13) polarize macrophages to M2. M1 and M2 cells have very different metabolic preferences; M1s primarily use glycolytic metabolism, while M2s prefer oxidative metabolism. M1s are considered pro-inflammatory because they secrete TNF-α and IL-1β, promoting further inflammation, while M2s secrete IL-10 and TGF-β, which promotes angiogenesis and tissue repair. The ratio of M1-like vs M2-like macrophages can have a major impact on a disease's progression or regression. M1s, while great for infection protection and preventing cancer, can, in abundance, promote atherosclerosis progression and autoimmune diseases. M2s are integral to tissue repair and immunoregulation. They can even promote atherosclerosis regression, but in the case of cancer, an abundance of M2-like tumour-associated macrophages protects the tumour from self-detection, thereby promoting cancer progression. Disease by nature is the inability to return to homeostasis, and a significant part of that is shifts in macrophage phenotype therefore, determining novel factors that can influence the macrophage phenotype is of great interest in numerous disease contexts such as infection, cancer and atherosclerosis.

1.3 Atherosclerosis and macrophage innate immunity

Atherosclerosis is an inflammatory disease driven by the accumulation of cholesterol within the arterial walls (33). Cholesterol, when accumulated, can be modified either by acetylation, aggregation or oxidation, increasing their toxicity further. The body responds to this toxicity by recruiting macrophages to the arterial wall to efflux the excess cholesterol to restore homeostasis. However, disease occurs when the recruited macrophages become overwhelmed by toxic cholesterol, becoming foam cells with inhibited cholesterol efflux and metabolism capacity, requiring the recruitment of even more macrophages (34). This accumulation of inhibited foam cells, toxic cholesterol, and dead and dying macrophages forms a necrotic core (35). Necrotic cores have long been known as a hallmark of a progressing and vulnerable to rupture plaque.

One thing that drives the formation or stabilization of a lesion or enables plaque regression is the phenotype of the recruited macrophages. Macrophage phenotype depends on the stimulation they encounter and can be pro-inflammatory (M1-like) or pro-resolving (M2-like) (19). Within a complex lesion, this polarization phenotype is considered a continuum, but both phenotypes are known to present in human and mouse aortic lesions (36). M1-like macrophage and foam cells are dominant during atherosclerosis progression however upon regression the M2 macrophages are more abundant (Figure 1.3).

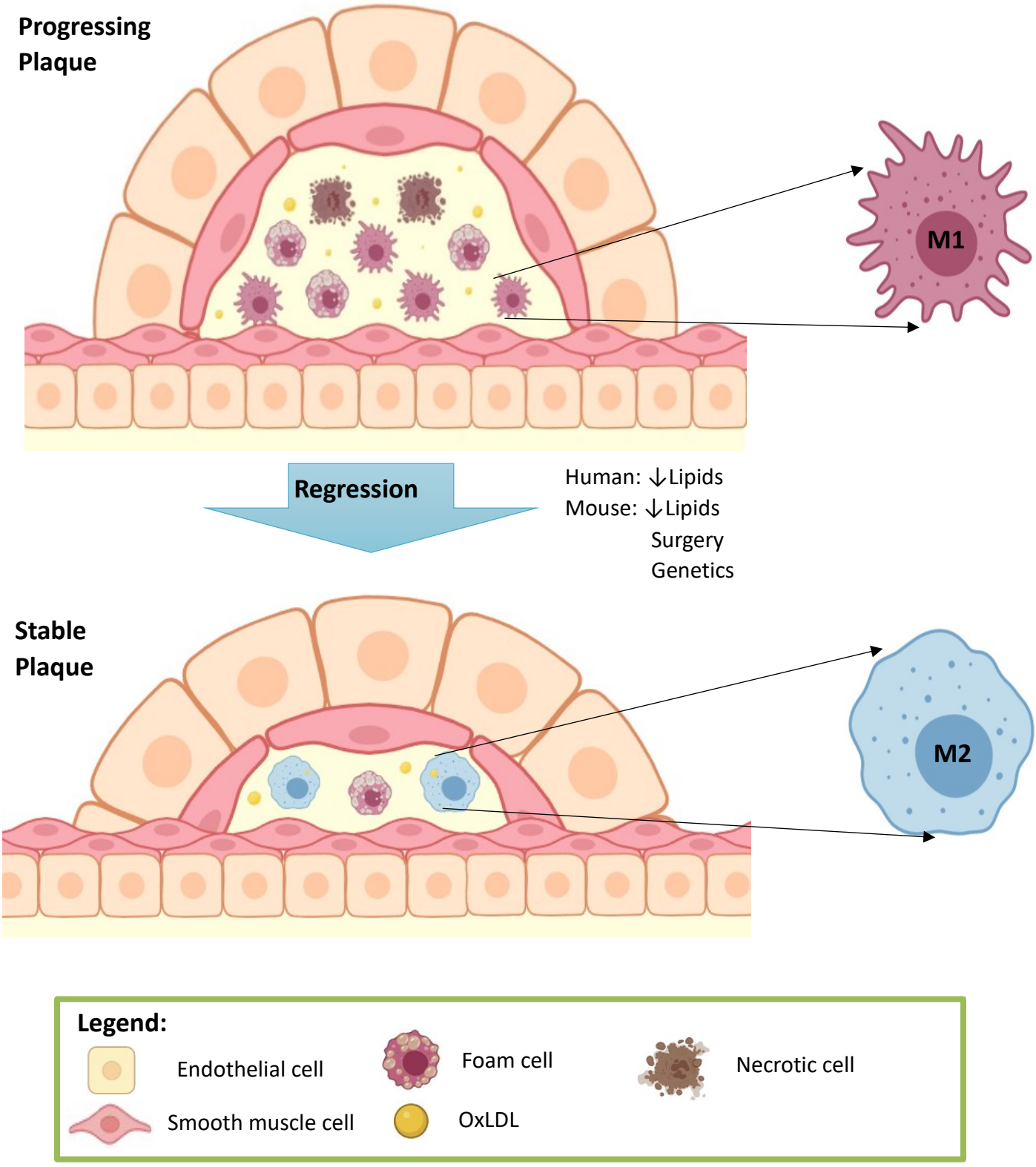
Progressing Plaque
M1
Regression
Human: ↓Lipids
Mouse: ↓Lipids
Surgery
Genetics
Stable Plaque
M2
Legend:
Endothelial cell
Foam cell
Necrotic cell
Smooth muscle cell
OxLDL

Figure 1.3: Illustration of the contents of progressing and regressing atherosclerosis plaques. Atherosclerosis is the formation of an inflammatory plaque due to the accumulation of excess cholesterol within the arterial wall. Macrophages are recruited to the arterial wall to efflux the excess cholesterol. Depending on the microenvironment of a plaque, such as the presence or absence of toxic oxidized LDL (oxLDL), those recruited macrophages undergo subsequent polarization into either a pro-inflammatory M1-like state or a pro-resolving M2-like state. A hallmark of progressing atherosclerosis lesions is a primarily M1-like macrophage population within the plaque, which sustains the inflammatory environment. In contrast, during lesion regression, the macrophage population is mostly M2-like and promotes lesion regression. To date, regression therapies have focused on statins (lipid-lowering therapies). Promoting macrophage commitment to M2 could be an untapped therapeutic target to stimulate plaque regression.

1.4 Mitochondrial dynamics and metabolic signaling

More than simply the site of metabolism and ATP production, mitochondria are double membrane-bound organelles found in almost every cell in the human body and eukaryotes as a whole. It is believed that mitochondria were originally prokaryotic cells capable of using oxygen to produce ATP, endocytosed into a symbiotic relationship into a eukaryotic cell. Mitochondria have a circular genome (~16 569 bp) and independent replication machinery. This genome is especially vulnerable to damage due to its proximity to ROS created by the ETC and lack of protective methylation (37–41). One way in which mitochondria protect themselves from DNA damage is by undergoing constant morphological changes via two equal but opposite processes of fission (fragmentation) and fusion (elongation) (42). Fission is the process by which mitochondria fragment, and it is carried out primarily by the cytosolic protein dynamin-related protein 1 (DRP1). Mitochondrial DNA (mtDNA) replication marks the site for the recruitment of the endoplasmic reticulum (ER) to contact the mitochondria at a site for impending midzone fission (43). In parallel, DRP1 oligomers are in constant balance between the cytosol and mitochondria, moving to the outer mitochondrial membrane (OMM) when post-translationally

activated by phosphorylation. At these sites, the ER-bound inverted formin-2 (INF2) and mitochondrial-bound Spire1C establish actin cables between the two organelles, with myosin II allowing actin contraction to provide the mechanical force to induce mitochondrial pre-constriction. ER-Ca^{2+} release into mitochondria, via mitochondrial calcium uniporter, leads to inner mitochondrial membrane (IMM) constriction upstream of DRP1 recruitment (44). At mitochondrial pre-constriction sites, adaptors of DRP1, MiD49/51 and mitochondrial fission factor (MFF) accumulate, and recruit activated DRP1 (phosphorylated), which oligomerizes in a ring-like structure around the mitochondrial tubule. Upon GTP hydrolysis, DRP1 changes conformation and increases mitochondrial constriction. DNM2 is recruited to DRP1-mediated constriction sites where it assembles and finishes membrane scission, leading to two daughter mitochondria. It is uncertain whether DNM2 is required to complete fission (45, 46). Peripheral fission is also mediated by DRP1; however, this process appears to rely on Fission 1 (FIS1) and lysosomal contact to mediate DRP1 assembly. Division at the periphery enables damaged material to be shed into smaller mitochondria destined for mitophagy, an important mechanism for mitochondrial quality control (43, 47–50). Fusion is the process by which mitochondria elongate, and it is carried out stepwise by first fusing the OMM and then the inner mitochondrial membrane (IMM). The outer membranes of two adjacent mitochondria are tethered by the interaction in trans of the HR2 domains of Mitofusin (MFN) 1 & 2. GTP binding and hydrolysis cause MFNs conformational change leading to OMM fusion. Following OMM fusion, optic atrophy 1 (OPA1) drives IMM fusion (51). Fusion causes the intermixing of the contents of the mitochondrial matrix of two discrete mitochondria. This process of complementation results in a healthier, elongated, single mitochondrion (52, 53). Both these

processes combined allow the mitochondria to act as part of a network to quickly adapt to any changing metabolic need or stress the cell meets (Figure 1.5).

The processes of fusion and fission are critical to cell function and adaptation, so much so that impairment in many of these proteins is associated with several devastating diseases. OPA1 impairment is associated with Optic Atrophy 1 disease, in which vision can be lost entirely from childhood (54). MFN2 mutations are associated with Charcot-Marie Tooth Disease type 2A, a congenital neuromuscular disorder that can result in lost motor functions over time (55–58). DRP1 mutations can result in encephalopathy from defective mitochondrial and peroxisomal fission 1 (EMPF1), which causes death in infancy due to a lack of neuronal development (59). Mff impairment is associated with EMPF2, which causes delayed psychomotor development and can cause seizures, optic atrophy and peripheral neuropathy. FIS1 impairment is related to Spinocerebellar ataxia 12, which can cause tremors and progressive cerebellar degeneration (59). All six essential fission and fusion proteins are also distantly associated with Alzheimer's disease due to altered levels within the frontal cortex, as well as in Parkinson's disease (59, 60). Along with these developmental diseases, the importance of our key fission and fusion proteins has been studied in the context of obesity, diabetes, cancer and cardiomyopathy. Complete knockout of MFN2 has been shown to cause cardiomyopathy, and overexpression creates ROS sensitivity in cardiomyocytes (57, 61–63). More recently, DRP1 has been studied in macrophages for its effects on efferocytosis in atherosclerosis. DRP1-mediated fission proves to be critical for the phagocytosis of secondary apoptotic bodies via ER Ca2+ signalling (64).

Mitochondrial dynamics plays a fundamental role in cell health and function, but in addition to that, fission and fusion have also been shown to play a directional role in cell differentiation. Neuronal stem cell self-renewal or differentiation commitment has been demonstrated to be directed by mitochondrial morphology (65–67). Under low ROS stimulation, neuronal stem cells maintain elongated mitochondria, leading to stem cell renewal through notch signalling. Under moderate ROS stimulation, neuronal stem cells have fragmented mitochondria, leading to NRF2 signalling and progenitor cell commitment (68, 69). Additionally, the adult skeletal muscle stem cells' state of quiescence has been shown to be directed by mitochondrial morphology. Adult skeletal muscle stem cell mitochondria rapidly fragment upon an activation stimulus via systemic HGF/mTOR to drive the exit from deep quiescence. Deletion of the mitochondrial fusion protein OPA1 transitions adult skeletal muscle stem cells into G-alert quiescence, causing premature activation and depletion upon a stimulus (70–73). The process of stem cell differentiation is similar to the maturation of immune cells from their precursors, and indeed, T cell commitment to an effector or memory cell phenotype is also directed through mitochondrial dynamics. OPA1 enables T cell commitment to the memory cell phenotype by controlling cristae morphology, thereby impacting metabolic potential (74). Effector T cells are characterized as having a fission-associated expansion of cristae, leading to inefficient oxidative phosphorylation and a compensatory use of glycolysis as a primary form of metabolism (75). Mitochondrial dynamics has been proven to play a directional role in neuronal and T-cell commitment (71, 74). The role mitochondrial fission and fusion may play in macrophage polarization requires further discovery.

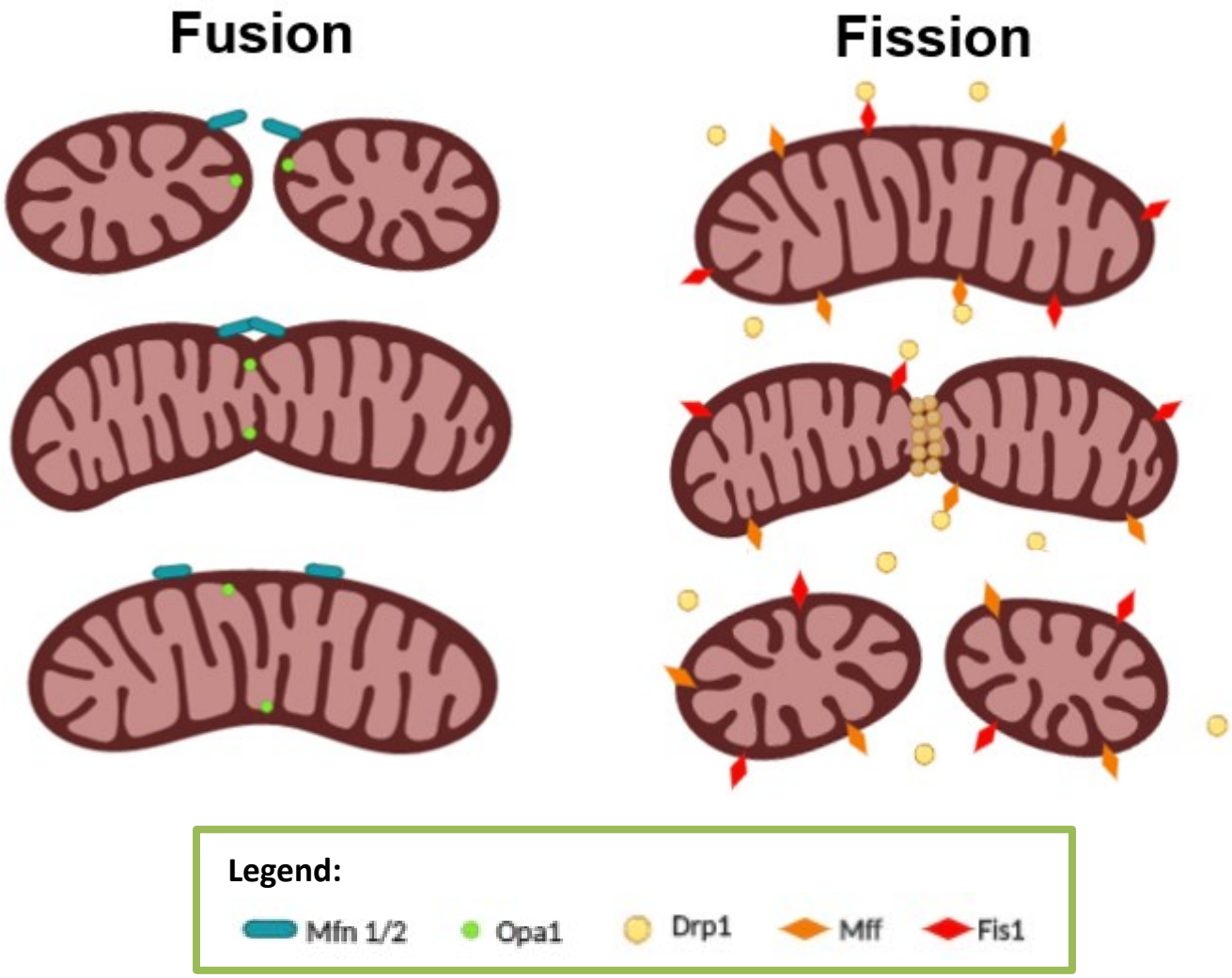

Figure 1.4: Illustration of the mitochondrial fission and fusion process and the proteins involved.
Mitochondrial dynamics is the process by which mitochondria adapt to the needs of the cell and repair mitochondrial damage, encompassing two well-defined processes of fusion (elongation) and fission (fragmentation). Fusion is carried out by mitofusin 1 & 2 (MFN1 & MFN2) on the outer mitochondrial membrane and optic atrophy 1 (OPA1) on the inner mitochondrial membrane which sequentially fuse to combine two small mitochondria into one longer mitochondrion. Elongated mitochondria are thought to be more metabolically efficient due to tighter cristae junctions allowing for electron transport chair super complex formation. Fission is primarily carried out by cytosolic dynamin-related protein 1 (DRP1), which is recruited to the outer mitochondrial membrane by two independent proteins, mitochondrial fission factor (MFF) and fission 1 (FIS1). DRP1 encircles the outer mitochondrial membrane, pinching them together until two smaller mitochondria can be formed from 1 longer mitochondrion. The mitochondrial network within a cell is continuously undergoing the dynamic process of fission and fusion to meet the needs of the cell.

1.5 Macrophage metabolism

Pro-inflammatory M1 macrophages primarily use glycolytic metabolism, and this means that upon LPS stimulation, the majority of ATP is produced directly from the glycolysis pathway and substrate level phosphorylation. To restore the NAD+/NADH ratio, pyruvate is converted into lactate instead of feeding into the Tricarboxylic acid cycle (TCA). LPS stimulation also results in two major breaks in the TCA cycle at isocitrate and succinate dehydrogenase, resulting in the cumulation of citrate and succinate, respectively (23, 25, 76). Both citrate and succinate have been shown to have additional roles in cell signalling. Succinate stabilizes the transcription factor hypoxia-inducible factor-1α (HIF-1α) in activated macrophages, resulting in the release of IL-1β (24, 77–79). Citrate is involved in fatty acid synthesis for membrane biogenesis and generates itaconic acid via the enzyme immune-responsive gene 1 (IRG1). Itaconate modifies KEAP1, leading to Nrf2 activation and promoting the expression of anti-inflammatory and antioxidant genes (69, 80, 81). It follows that macrophage metabolic preferences and the metabolites they accumulate are more than the consequence of metabolism but part of the signalling pathway associated with their polarization (Figure 1.5).

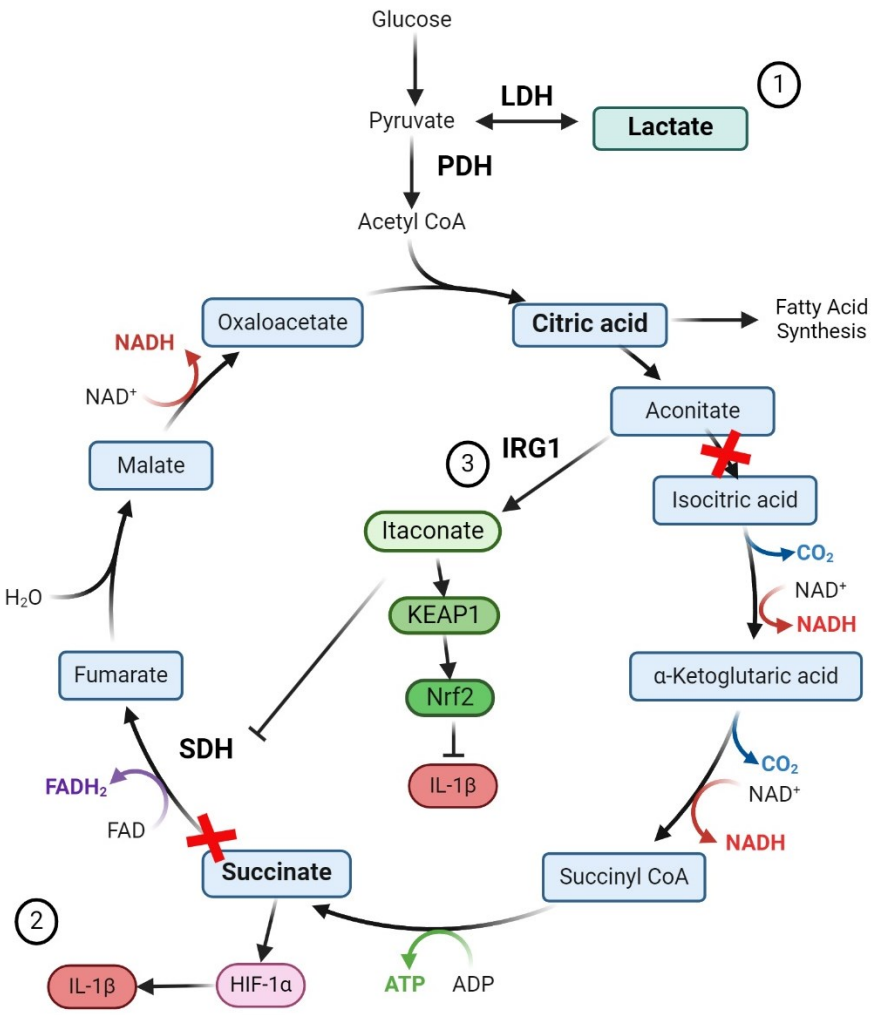

Figure 1.5: Metabolite shift induced by proinflammatory stimulation in macrophages.
Pro-inflammatory stimulation promotes a shift in metabolic preference towards glycolysis. This results in two major breaks within the TCA cycle, creating reservoirs of three major metabolites: Citrate, Succinate and Lactate. Those metabolites in addition to their role in the TCA cycle also play roles in cell signaling, specifically in macrophage inflammatory responses. Succinate the first metabolite to accumulate, stabilize HIF-1α promoting IL-1β responses. Citrate plays a critical role in fatty acid synthesis, however Aconitate its derivative created Itaconate via IRG1. Itaconate Inhibits succinate dehydrogenase (SDH) further accumulating succinate and via the KEAP1-Nrf2 pathway, initiates protective antioxidant responses. Lastly lactate has been linked to a new post translational histone modification lactylation which turns on pro-resolving machinery such as arginase 1. The accumulation of these metabolites plays a role in initiating and resolving inflammatory responses in macrophages.

1.6 Lactate

Lactate has historically been thought of as a waste product of glycolysis. However, modern research has shown that lactate is a principal messenger in the complex feedback loop system composed of glucose metabolism, redox homeostasis, and histone post-translational modification termed the lactate clock (82, 83). Lactate production is promoted when the glycolysis pathway is activated to compensate for an ATP deficency from an inhibited tricarboxylic acid (TCA) cycle. Specifically, cytoplasmic glucose is converted to pyruvate through a series of classic catalytic reactions. Pyruvate is reduced to lactate via lactate dehydrogenase (LDH) (84, 85), and can be reversed by that same enzyme. Pyruvate dehydrogenase (PDH), then catalyzes pyruvate to acetyl-CoA, which can then enter the TCA cycle (86). Hence, the balance between glycolysis and PDH is a crucial determinant of lactate levels (Figure 1.4).

As an essential metabolic substrate, lactate is an intercellular and inter-tissue redox signalling molecule. Lactate can affect the cellular production of reactive oxygen species (ROS) through enzymatically and non-enzymatically catalyzed reactions. Perhaps best known is the chemistry by which ROS are generated as the result of mitochondrial respiration (82, 87); less studied are lactate-iron interactions capable of generating ROS. Redox homeostasis is maintained by the transport of electrons via nicotinamide adenine dinucleotides (NAD+ or NADP+), which are then reduced to NADH or NADPH (88). The reoxidation of NADH or NADPH then releases electrons through mitochondrial respiration or lactate fermentation. Cytoplasmic LDH and mitochondrial ETC complex I drive the oxidation of NADH to NAD+ in several ways. First, the production and removal of the metabolic intermediate lactate through the oxidation

of NADH to NAD+ and H+, thus maintaining electron flux. NADH oxidation is accompanied by LDH-mediated catalysis of lactate to pyruvate (89, 90). High lactate concentrations have been shown to increase the NADH/NAD+ ratio, inhibiting GAPDH and PGDH activity and, subsequently, glycolysis and mitochondrial respiration (91). In summary, lactate levels reflect the cytosolic redox state of the NADH/NAD+ couple.

While the metabolic impact of lactate has been a point of study for many years, the discovery of lactate-modified histones only became apparent with the advancement of high-performance liquid chromatography (HPLC)–tandem mass spectrometry (MS/MS) technology where they identified a lactly group on the lysine ε-amino group of histones (92). This study demonstrated the presence of histone lysine lactylation (KLA) for the first time. It indicated that KLA is a new form of epigenetic post-translational modification. Recently, many studies have shown the accumulation of histone KLA on gene promoters in cells stimulated by hypoxia, interferon (IFN)-γ, LPS, or bacterial attack to produce lactate (92, 93), thereby directly regulating gene expression (92).

To date, research on Kla has focused primarily on histone modification. Histone KLA differs from histone acetylation primarily due to its unique time dynamics. Histone KLA is significantly increased on the promoters of M2-like genes in the late stages of M1 macrophage polarization, suggesting that histone KLA acts as a lactate clock promoting the macrophage transition from a pro-inflammatory to a pro-resolving (94, 95). This switch occurs in the later stages of inflammation and is closely aligned with wound healing. Ricardo et al. revealed that mice with

macrophage-specific B cell adaptor protein (BCAP) deletion had decreased ARG1 and KLF4 expression, failed to recover from dextran sodium sulphate-induced colitis, and died (93). Other studies found that BCAP deficiency impaired aerobic glycolysis and reduced lactate production, decreasing histone KLA (93). Adding exogenous sodium lactate (NaLa) to BCAP-deficient bone marrow-derived macrophages (BMDMs) rescued the phenotype, promoting histone KLA and recovering the decreases in ARG1 and KLF4 expression (93). Another recent study found that lactate human alveolar macrophages led to an increase in histone KLA (96). Results from CHIP assays using lactate-treated BMDMs confirmed increased histone KLA in the promoter regions of the ARG1, PDGF, and VEGF genes, resulting in their significant upregulation (97–101). In summary, these examples demonstrate that lactate activates gene expression by inducing histone lactylation of the promoters associated with pro-resolving mediators (Figure 1.4). KLA has also been found to occur on nonhistone proteins; however, this is less studied and requires further research.

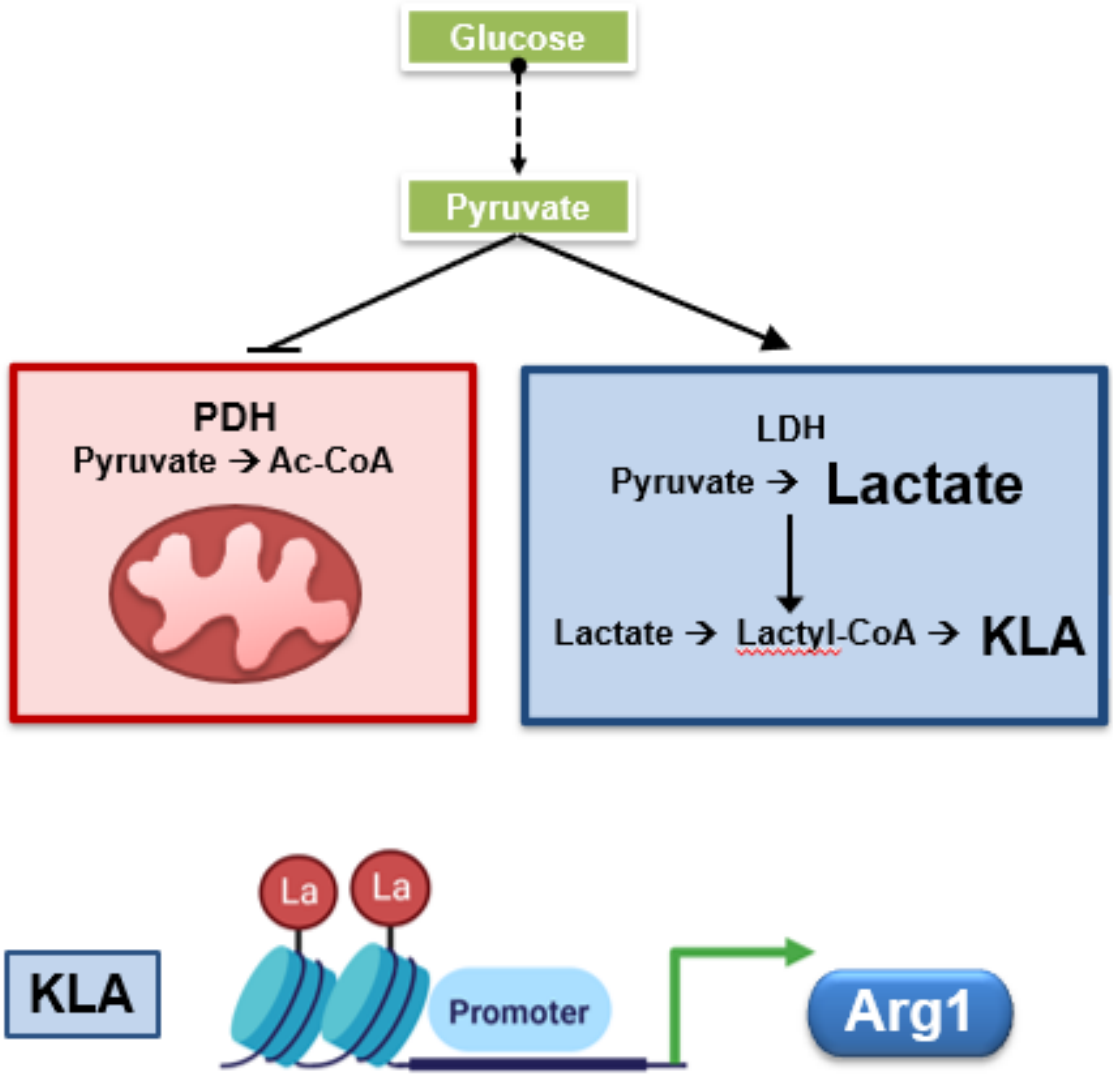

Figure 1.6: LPS mediated initiation of lactate clock post-inflammatory response in macrophages.
Pro-inflammatory stimulation such as LPS actively impairs the TCA cycle, shifting metabolism to primarily glycolysis. During glycolysis, pyruvate can be shifted from going into the TCA cycle to producing lactate. Lactate, when abundant, can lactylate (add a Lactly group) proteins similarly to acetylation. Like acetylation, one well-studied post-translational modification is histone lactylation. Histone lactylation turns on the promoter regions of pro-resolving genes such as ARG1. Lactylation thereby acts as a lactate clock mechanism where post-inflammatory response, the resulting accumulation of lactate due to an impaired TCA cycle, turns on the resolution programming to return to homeostasis. There are likely proteins in addition to histones being lactylated that aid in the post-inflammatory resolution response, but this is less defined and requires further research.

1.7 Hypothesis

We **hypothesize** that mitochondrial fission and fusion directly contribute to macrophage function during the pro-inflammatory and pro-resolving phases.

1.8 Aims

1.8.1 *Determine if fission and/or fusion direct macrophage polarization*.

a) Characterize mitochondrial dynamics across macrophage phenotypes.

b) Characterize the effect of impaired fission or fusion on macrophage phenotype.

1.8.2 Characterize the role of mitochondrial dynamics on the endogenous LPS response.

a) Characterized the effect of impaired fission and fusion upon inflammatory stimulation.

b) Determine the mechanism behind changes in IL-1β.

c) Determine the mechanism behind changes in ARG1.

1.8.3 Determine the role of mitochondrial-mediated lactylation on inflammation resolution in vivo.

a) Characterize and define the model of zymosan-induced peritonitis.

b) Test effect of LDH inhibitor sodium oxamate on zymosan-induced peritonitis resolution.

c) Test effect of OPA1 inhibitor MYLS22 on zymosan-induced peritonitis resolution.

Chapter 2: Materials and Methods

2.1 Animal Procedures

C57BL/6 (wild type, Charles River Laboratories) mice were maintained and housed in the University of Ottawa Heart Institute (UOHI) Animal Care and Veterinary facility. Mice ranged in age between 4-10 months with equal distribution of males and females.

2.2 Cell Culture

Murine bone marrow-derived macrophages (BMDM) were obtained by flushing the femur and tibia in DMEM high glucose media (Gibco, 11965092) supplemented with 20% L929 conditioned media (a source of MCSF produced in-house from L929 cell culture), 10% heat-inactivated FBS (Gibco, 12483020) and 1% Antibiotic Antimycotic Solution (Gibco, 15240062). Monocytes were left to differentiate for 6 days in an incubator at 37°C with 5% CO_2. On day 6 the differentiated macrophages were lifted using 50mM EDTA, counted and plated according to experimental conditions. All experimental procedures were started on day 7.

Human monocytic THP-1 cell line were maintained in culture in RPMI medium (Gibco, 21870076) supplemented with 10% of heat-inactivated FBS (Gibco, 12483020), 10mM Hepes (Gibco, 15630080), 10mM L-Glutamine (Gibco, 25030149), 1mM sodium pyruvate (Gibco, 11360070), 2.5 g/l D-glucose (Merck), 1% Penicillin-Streptomycin (Gibco, 15140122) and 50pM β-mercaptoethanol (Gibco; 31350–010). THP-1 monocytes were differentiated into macrophages through incubation with 100nM PMA (Sigma, P1585) in full media for 72h.

Peritoneal macrophages (PMACs) were obtained 96h post thioglycolate intraperitoneal injection by peritoneal lavage with ice cold phosphate buffer saline (PBS). PMACs were then

resuspended in DMEM high glucose media (Gibco, 11965092) supplemented with 10% heat-inactivated FBS (Gibco, 12483020). Cells were plated and allowed to adhere for 4-6h in advance of treatment or fixation.

2.3 Macrophage Treatments

BMDM macrophages were polarized to M1 or M2 through treatment with 100 ng/ml LPS (Sigma, L4391) and 100 ng/ml IFNγ (R&D, 485-MI-100) or 10ng/ml IL-4 (R&D, 404-ML-010) for 24h. THP-1 macrophages were polarized to M1 or M2 by incubation with 20 ng/ml IFNγ (PeproTech, 300-02) and 100 ng/ml LPS (Sigma, L4391) or 20 ng/ml IL-4 (PeproTech, #200-04) and 20 ng/ml IL-13 (PeproTech, 200-13) for 24h. LPS timecourses were performed in full media with 100ng/ml LPS (Sigma, L4391) with or without 10mM sodium oxamate (SelleckChem, S6871). IL-4 timecourses were performed in full media with 10ng/ml IL-4 (R&D, 404-ML-010).

2.4 SiRNA Knockdown

Fission knockdown macrophages were obtained by 72h siRNA co-transfection with 40nM *Drp1* siRNA (Qiagen, SI0098226), 10nM *Mff* siRNA (Qiagen, SI00855918) and 10nM *Fis1* siRNA (Qiagen, SI0145779) in OPTIMEM media (Gibco, 11058021) with Lipofectamine RNA iMAX transfection reagent (Life technologies, 13778150) used according to manufacturers instructions. Fusion knockdown cells were obtained using the same method with 20nM *Opa1* siRNA (Qiagen, SI01365707), 20nm *Mfn1* siRNA (Qiagen, SI01304387), 20nM *Mfn2* siRNA (Qiagen, SI04392010). Knockdown efficiency was determined in comparison to control cells transfected with 60nM negative control siRNA (Qiagen, 1027310).

2.5 RNA Isolation & RT-qPCR

Total RNA was isolated using Trizol (Invitrogen, 15596018) according to manufacturers instruction. The cDNA reactions were prepared from 750ng of total RNA using iScript reverse transcription supermix (Bio-Rad, 1708841) and a 1:5 dilution was used for qPCR. Real-time quantitative PCR reactions were carried out using primer sequences obtained from the Harvard Medical School PrimerBank database and SYBR Green dye (Bio-Rad, 1725275). Data were normalized to either SRP14, TFAM or HPRT gene expression using the comparative ΔΔCt method and calculated fold changes relative to the controls.

Gene		Forward Primer (5'->3')	Reverse Primer (5'->3')
Fusion:	Opa1	TGGAAAATGGTTCGAGAGTCAG	CATTCCGTCTCTAGGTTAAAGCG
	Mfn1	CCTACTGCTCCTTCTAACCCA	AGGGACGCCAATCCTGTGA
	Mfn2	TGACCTGAATTGTGACAAGCTG	AGACTGACTGCCGTATCTGGT
Fission:	Drp1	TTACGGTTCCCTAAACTTCACG	GTCACGGGCAACCTTTTACGA
	Mff	AGCTGCCGCCACTTCTAATC	TGCATCTACCACAGTCATGTCA
	Fis1	TGTCCAAGAGCACGCAATTTG	CCTCGCACATACTTTAGAGCCTT
M1:	Tnfa	CCCTCACACTCAGATCATCT	GCTACGACGTGGGCTACAG
	IL1B	GCAACTGTTCCTGAACTCAACT	ATCTTTTGGGGTCCGTCAACT
	iNOS	GTTCTCAGCCCAACAATACAAGA	GTGGACGGGTCGATGTCAC
M2:	Arg1	GGTCCACCCTGACCTATGTGT	ACGATGTCTTTGGCAGATATGC
	Fizz1	AAGCCTACACTGTGTTTCCTTTT	GCTTCCTTGATCCTTTGATCCAC
	IL-10	GCTCTTACTGACTGGCATGAG	CGCAGCTCTAGGAGCATGTG
Other:	Slc7a11	GTCTGCCTGTGGAGTACTGT	ATTACGAGCAGTTCCACCCA
House-keeping:	HPRT	TCAGTCAACGGGGGACATAAA	GGGGCTGTACTGCTTAACCAG
	TFAM	ATTCCGAAGTGTTTTTCCAGCA	TCTGAAAGTTTTGCATCTGGGT
	SRP14	CAGCGTGTTCATCACCCTCAA	GGCTCTCAACAGACACTTGTTTT

2.6 Western Blots

Total protein was extracted on ice in radioimmunoprecipitation assay buffer (RIPA) containing protease (Roche, 4693132001) and phosphatase (Roche, 4906837001) inhibitors. Proteins were

separated on acrylamide gels of varying percentages and transferred to 0.22µM polyvinylidene difluoride (PVDF) membranes. Membranes were blocked in 5% Skim milk or 5% Bovine serum albumin (BSA), depending on the antibody manufacturers' specifications. Primary antibodies were incubated on the membrane overnight at 4°C in 1% blocking. Membranes were incubated with LI-COR Secondaries (IRDye 800CW α-Rabbit & IRDye 680RD α-Mouse) at room temperature for an hour and imaged on the LI-COR Odyssey imaging system. Protein bands were quantified on Image J and normalized to housekeeping bands, either HSP90 or β-actin. Proteins ATF4, Phos C-Jun, KLA and ARG1 required the use of HRP secondaries and chemiluminescence to be detected. Full list of antibodies and their catalogue numbers can be found in Supplemental table 2.

2.7 Immunofluorescence Microscopy

For all immunofluorescence microscopy, the macrophages were plated on glass coverslips within a 24-well plate. At the end of treatment (either polarization or siRNA transfection), the macrophages were fixed with 4% paraformaldehyde for 15min at 37°C, followed by 10min of quenching by 10mM NH_4Cl. The cells were permeabilized with 0.1% Triton X-100 for 10min. 10% FBS was used as a blocking agent and incubated on the coverslips for 30min. Primary antibodies were then incubated for an hour in 5% FBS followed by secondary antibodies also in 5% FBS for an hour. Primary antibodies used are detailed in the associated figure legends. Secondaries used were Alexa Fluor 555 or 488 in the associated species. 1ug/ml Dapi (Becton Dickinson, 564907) was used as a nuclear dye and incubated on the coverslips for 5min. Coverslips were then washed and mounted using Dako Fluorescence mounting media

(Cedarlane, S3022380-2) on microscopy slides (Fisher Scientific, 12-552). Cells were imaged within 2 days at 63x on a Zeiss LSM 880 microscope. Mitochondrial length was measured manually using the ImageJ software and presented as mean length (μM) per cell. HIF-1α nuclear translocation was also measured on ImageJ, whereby we quantified the total mean fluorescence intensity (MFI) per cell and the MFI within the nucleus. Data is presented as a ratio of nuclear/cytoplasmic MFI per cell.

2.8 Transmission Electron Microscopy

Cells were fixed for 60min in 2% PFA and 2.5% Glutaraldehyde. The samples were processed and imaged at the University of Ottawa Heart Institute Cell Imaging and Histology Core Facility according to standard protocols. Those images were quantified for mitochondrial length and cristae width using the ImageJ software. All dynamic events (either fission or fusion) were quantified as a ratio between static vs dynamic mitochondria per cell.

2.9 Phagocytosis Assay

Cells plated on glass coverslips within a 24-well plate were incubated with equal concentrations of polystyrene fluoresbrite YG microspheres (Polysciences, 17154-10) for 2h at 37°C. The wells were washed with PBS to remove excess beads, then fixed and stained for Tom20 according to the above IF protocol. The cells were imaged within 2 days at 63x on a Zeiss LSM 880 microscope. Images were manually quantified for the number of internalized fluorescent beads per cell on Image J.

2.10 Il-1β ELISA

Fission and fusion knockdown cells were assessed for changes in IL-1β secretion upon LPS (100ng/ul) stimulation with and without 5mM ATP (Bio-Rad, 1725275). Cell media was collected at end of LPS treatment centrifuged at 1200G for 5min to discard any cell debris. Media was quantified for secreted IL-1β by Mouse IL-1 beta Quantikine ELISA Kit (R&D, MLB00C) according to the manufacturer's instruction.

2.11 Lactate levels

Cell lysate or exudate was collected and analysed for lactate levels using the L-Lactate Assay Kit (ab65331) or D-Lactate Assay Kit (ab83439) according to manufacturers' instructions.

2.12 Zymosan Induces Peritonitis Resolution Model

Zymosan A (Sigma Z-4250, Saccharomyces cerevisiae) powder was suspended in Saline (5mg/ml), sonicated and 200ul was injected intraperitoneally (IP). After the reported time, mice were euthanized by CO_2, and peritoneal lavage was collected ~10ml ice-cold PBS collected in 50ml falcon. Cells were centrifuged at 500xG for 5min at 4°C, remove supernatant and resuspended pellet in 100ul FACS buffer (PBS with 3% FBS and 0.5mM EDTA). Perform red blood cell lysis (BD Pharm lyse, 555899) for 5min at room temperature with agitation. Quench the reaction with FACs buffer and centrifuge at 500xG for 5min at 4°C, remove supernatant and resuspend pellet in 2ml FACS buffer. Count cells and aliquot for all forms of analysis. Primary analyses include flow cytometry, microscopy, lactate levels, and western blots. Drug intervention was performed by IP injection 24h after Zymosan. MYLS22 (Selleckchem, S9885)

was injected IP at 10mg/kg suspended in vehicle (10% DMSO, 40% PEG300, 5% Tween-80, 45% saline) at 2.82mM. Sodium oxamate (Selleckchem, S6871) was injected IP at 500mg/kg suspended in saline at 198.14mM. Injection volume was corrected for differences in weight with additional vehicle or saline and drug effects were determined in comparison to mice given an equal volume of vehicle or saline.

2.13 Flow Cytometry

Cell suspensions of 1 million cells per mouse were blocked with FC block (BD, 553142) for 5min then stained with anti-mouse antibodies LY6G-BV421, CD11b-alexafluor488, F4/80-PE-Cy7 and LY6C-APC for 20min. Followed by staining with fixable viability dye 510 (BD, 564406) for 30min. Cells were washed with FACs buffer and then fixed for 15min using Cytofix (BD, 554655). Cells were washed 2x with FACs buffer and then resuspended in 150ul final volume. Samples were protected from light and stored at 4°C. Data was acquired on MACSQuant Analyzer 10 Flow cytometer within 24h of staining and analyzed with FlowJo software.

2.14 Statistical analysis

All data involving statistics are presented as mean ± SEM. The same control was used for individual comparisons to Fission KD or Fusion KD. The statistical significance of the differences between groups was determined on Prism V9.5.0 software (GraphPad Software Inc) using unpaired student t-tests, multiple unpaired t-tests or one-way ANOVA. Normal distribution was determined by the Shapiro-Wilk test. The number of replicates and the statistical test used are described in the figure legends.

2.15 Figures

All pathway/mechanism illustrations presented were made using Biorender combining components of previously discovered pathways to best illustrate the key findings outlined within the thesis. The remainder of the figures were made from original data using a combination of GraphPad, Illustrator and Powerpoint.

Chapter 3: Characterization of macrophage mitochondrial dynamics

3.1 Introduction

Macrophages have been established to exist on a spectrum of activation based on the stimulus they have been exposed to. This can be simplified as pro-inflammatory M1-like and anti-inflammatory M2-like macrophages. M1-like macrophages secret pro-inflammatory cytokines such as TNFα and IL-1β and are very beneficial in the context of infection protection and anti-cancer immunity. M2-like macrophages are pro-resolving because they promote tissue repair, immunoregulation, and atherosclerosis regression through the secretion of TGFβ and IL-10 as well as intracellular arginase 1 (ARG1). The abundance of either phenotype and the transition between these states is of great importance for better understanding inflammation and its resolution (102–106).

This thesis aims to determine what role mitochondrial fission and fusion play in inflammation and its resolution, stemming from the distinct metabolic preference of each phenotype. M1s primarily use glycolytic metabolism, while M2s prefer oxidative metabolism. On a mitochondrial morphology level, this suggests that cells preferring oxidative metabolism require more efficient and, therefore, longer mitochondria. Mitochondrial morphology, although linked to metabolic needs, is a dynamic process constantly undergoing events of fission (fragmentation) and fusion (elongation). Mitochondrial dynamics have been shown to be integral to cell fate decisions in both stem and T-cells. To determine how mitochondrial dynamics impact macrophage fate decisions, we characterized mitochondrial network morphology in M1 vs M2 macrophages. If mitochondrial dynamics plays a role in macrophage

polarization, we hypothesize that macrophage phenotypes have distinct mitochondrial network morphologies.

3.2 Results

3.2.1 Macrophage polarization influences mitochondrial fission and fusion

To understand how macrophage polarization affects mitochondrial morphology, we first characterized the mitochondrial network of bone marrow-derived macrophages (BMDMs) polarized to traditional M1 or M2 phenotypes. We observed that macrophages stimulated with LPS and IFNγ for 24h (proinflammatory or M1) have a significantly longer mitochondrial network compared to both unpolarized macrophages (resting, M0) and IL-4 stimulated macrophages (pro-resolving or M2) (**Figure 3.1a, b, c**). The increase in mitochondrial length was observed as early as two hours after stimulation and before establishing an M1 identity (**Figure 3.1d, e**). Mitochondrial morphology and changes in mitochondrial length between M0, M1 and M2 macrophages were confirmed by transmission electron microscopy, showing longer mitochondria in M1 and a higher ratio of mitochondria undergoing dynamic events (either fission or fusion) (**Figure 3.1f-h**). Furthermore, we saw increased cristae width in M1 macrophages compared to M0 and M2 (**Figure 3.1i**). BMDM M1 macrophage mitochondrial network elongation was conserved in human THP-1 macrophages polarized to M1 with LPS + IFNγ in comparison to M0 & M2 (**Figure 3.2a-c**). These data demonstrate that proinflammatory and M1 macrophages adopt an elongated mitochondrial network, whereas resting and M2 macrophages adopt a shorter mitochondrial network corresponding to their polarized phenotype.

Figure 3.1

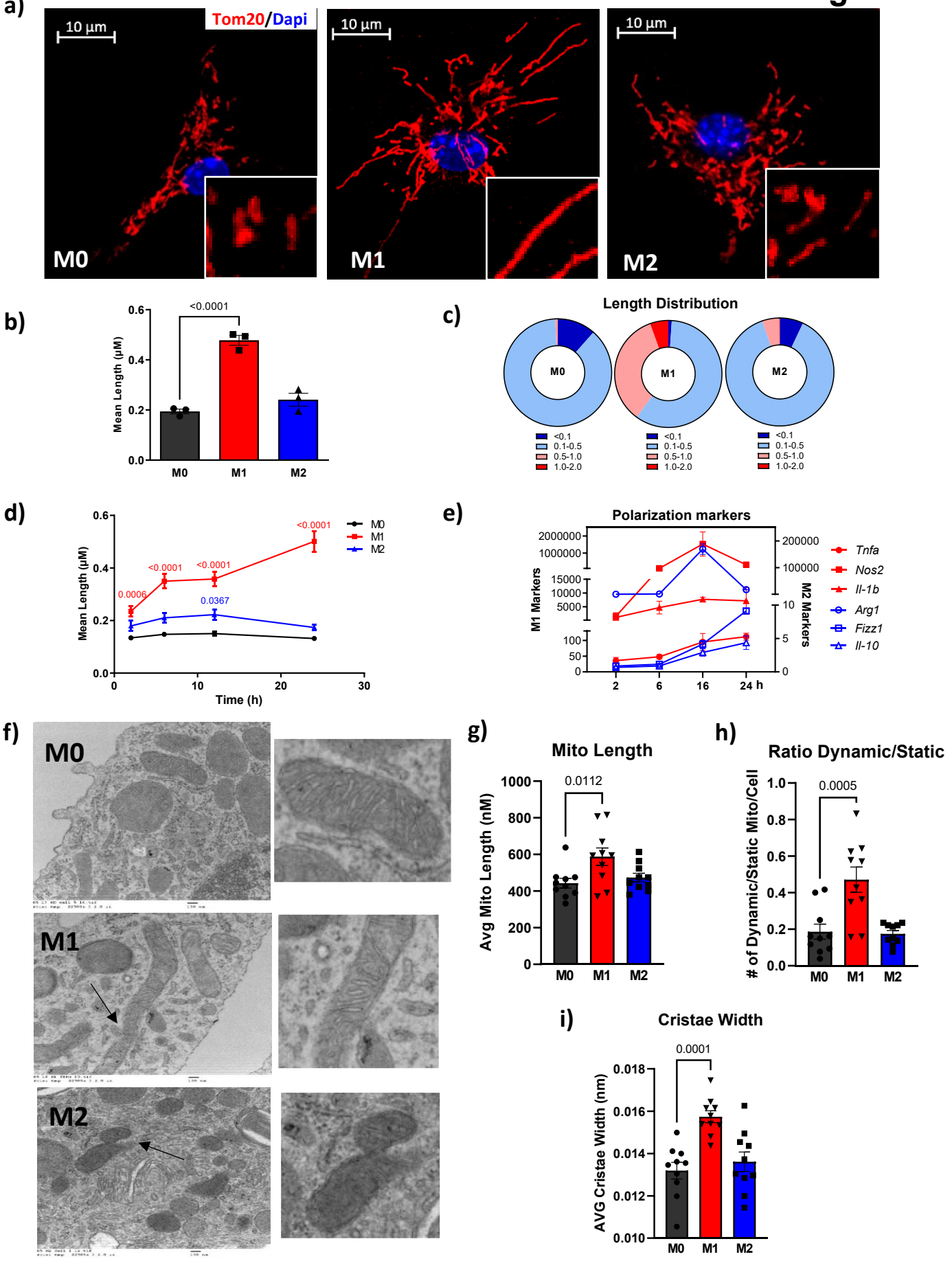
a)
Tom20/Dapi
10 µm
M0
M1
M2
b)
Mean Length (µM)
<0.0001
c)
Length Distribution
<0.1
0.1-0.5
0.5-1.0
1.0-2.0
d)
Mean Length (µM)
Time (h)
<0.0001
0.0006
0.0367
e)
Polarization markers
M1 Markers
M2 Markers
Tnfa
Nos2
Il-1b
Arg1
Fizz1
Il-10
f)
g)
Mito Length
Avg Mito Length (nM)
0.0112
h)
Ratio Dynamic/Static
# of Dynamic/Static Mito/Cell
0.0005
i)
Cristae Width
AVG Cristae Width (nm)
0.0001

Figure 3.1: Elongated mitochondria are associated with a pro-inflammatory macrophage phenotype. Bone marrow derived macrophages (BMDMs) were differentiated and then polarized for 24h before being fixed and analyzed by microscopy. a) Representative immunofluorescence (IF) microscopy of polarized macrophages mitochondrial network (Tom 20 in red & Dapi in blue). b) Quantification of BMDM mean mitochondrial length measured manually on Image J (n=3 mice with 30 cell minimum per group per n). c) Polarized macrophages mitochondrial length distribution (n=3 mice). d) Quantification of mitochondrial length over time (n=3 mice). f) Gene expression of M1 & M2 markers over time (n=10 mice). g) Representative transmission electron microscopy (TEM) images of M0, M1 and M2 BMDMs. h) Quantification of average mitochondrial length (n=10 cells). i) Ratio of dynamic over static mitochondria with dynamic events defined as membrane pinching examples indicated by arrows (n=10 cells). j) Quantification of average cristae width (n=10 cells). Data are presented as the mean of biological replicates +/- SEM. Statistical analysis by one-way ANOVA.

Figure 3.2

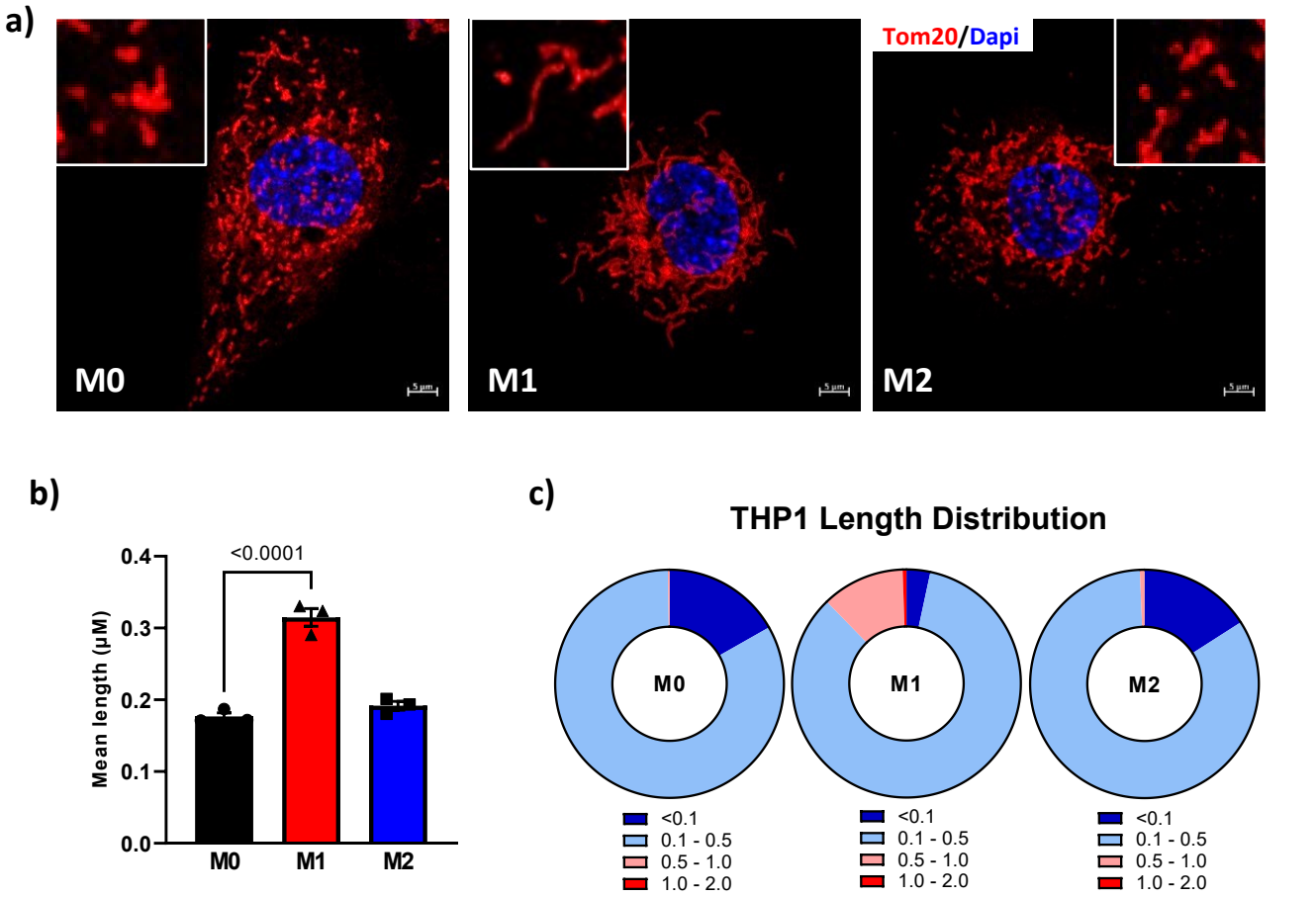

Figure 3.2: M1 elongated mitochondrial network is conserved in human THP1 macrophages.
THP-1 monocytes were differentiated into macrophages through incubation with 100nM PMA in full media for 72h. THP-1 macrophages were polarized to M1 or M2 by incubation with 20 ng/ml IFN-γ and 100 ng/ml LPS or 20 ng/ml IL-4 and 20 ng/ml IL-13 for 24h. a) Representative IF microscopy of polarized THP1 macrophages mitochondrial network (Tom 20 in red & Dapi in blue). b) Quantification of THP1 mean mitochondrial length measured manually on Image J. c) Polarized THP1 mitochondrial length distribution (n=3). Data are presented as the mean of biological replicates +/- SEM. Statistical analysis by one-way ANOVA. N refers to the number of mice. Mean mitochondrial length refers to the mean of a minimum of 30 cells per n per group.

3.2.2 Pro-atherogenic stimuli promote mitochondrial elongation.

In atherosclerosis, overabundant lipids trapped within the vascular wall become modified primarily through oxidation or acetylation. These atherogenic stimuli induce an M1-like phenotype on foamy macrophages. Therefore, we assessed if modified lipids Acetylated LDL (AcLDL, 37.5ug/ml), Aggregated LDL (AgLDL, 100 ug/ml) and Oxidized LDL (OxLDL, 50ug/ml) also induced an elongated mitochondrial phenotype in BMDMs. Differentiated BMDMs were lipid-loaded for 72h and assessed for lipid loading and mitochondrial morphology using live cell microscopy. All three forms of lipids formed lipid droplets and induced an elongated mitochondrial network (**Figure 3.3a**, **b**). The most significant elongation was seen in OxLDL-loaded macrophages. Additionally, we assessed mitochondrial morphology upon *in vivo* lipid loading from two weeks of a high-fat diet on mouse peritoneal macrophages (PMAC). PMACs are macrophages recruited into the peritoneal cavity upon induction of sterile inflammation via thioglycolate intraperitoneal injection. Two weeks of high-fat diet-induced significant PMAC mitochondrial network elongation compared to chow-fed aged, matched mice (**Figure 3.3c, d**). Together, this data indicates that mitochondrial network elongation is correlated with not only classical M1 stimuli but also pro-atherogenic stimuli.

Figure 3.3

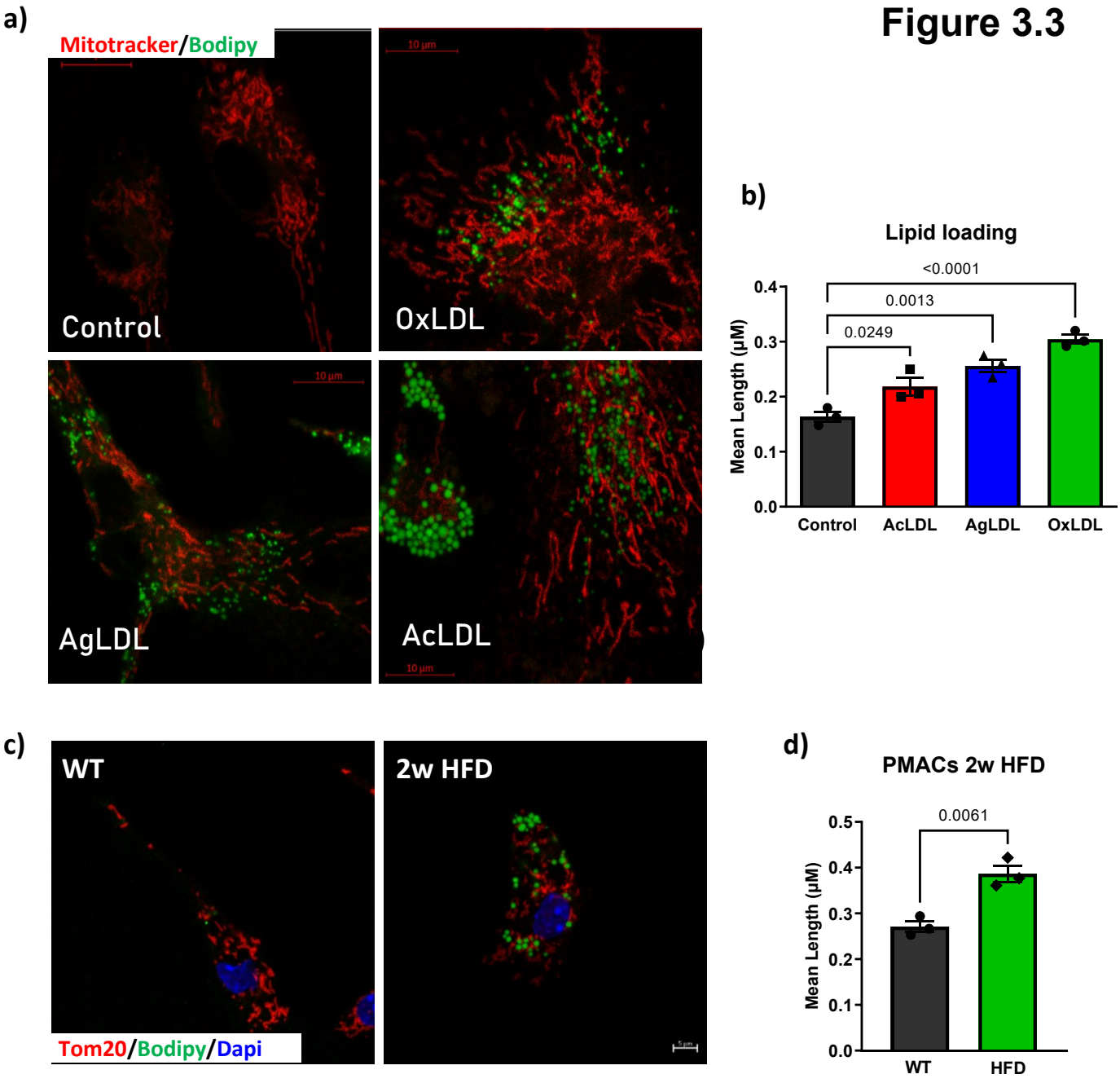
a)
Mitotracker/Bodipy
Control
OxLDL
AgLDL
AcLDL
10 µm
b)
Lipid loading
<0.0001
0.0013
0.0249
Mean Length (µM)
0.0
0.1
0.2
0.3
0.4
Control
AcLDL
AgLDL
OxLDL
c)
WT
2w HFD
Tom20/Bodipy/Dapi
d)
PMACs 2w HFD
0.0061
Mean Length (µM)
0.0
0.1
0.2
0.3
0.4
0.5
WT
HFD

Figure 3.3: Pro-atherogenic stimulation promotes an M1-like elongated mitochondrial network. BMDM macrophages were lipid-loaded with either oxidized, aggregated, or acetylated LDL for 72h. a) Representative IF microscopy of lipid-loaded BMDMs (Mitotracker in red & Bodipy in green). b) Quantification of mitochondrial length in lipid-loaded macrophages (n=3 mice). PMACs were isolated from mice fed either Chow or a high-fat diet for two weeks. c) Representative IF microscopy of in-vivo loaded PMACS (Tom 20 in red, Bodipy in green & Dapi in blue). d) Quantification of in-vivo loaded peritoneal macrophages mitochondrial length (n=3 mice). Data are presented as the mean of biological replicates +/- SEM. Statistical analysis by one-way ANOVA or unpaired student t-test. N refers to the number of mice. Mean mitochondrial length refers to the mean of a minimum of 30 cells per n per group.

3.2.3 Mitochondrial elongation is integral to macrophage phenotype transitioning

Although *in vitro*, we broadly characterize macrophages as M1 or M2, within the body, macrophages exist on a spectrum of polarization. Thus, it is also critical to characterize macrophage transitioning between phenotypes. To assess the role of mitochondrial elongation on the capacity of the macrophages to switch between macrophage phenotypes, the M1 stimuli (LPS + IFNγ) were replaced with the M2 stimuli (IL-4) or vice versa after 6h of polarization and left in new stimulus for an additional 18h (Total 24h). The time point of 6h was chosen because we had previously confirmed significant elongation after 6h (**Figure 3.1d**). Cells transitioning from M1 to M2 and M2 to M1 stimuli had significantly elongated mitochondrial networks similar to fully polarized M1 macrophages (**Figure 3.4a, b**). Despite the elongated mitochondria, both M1 to M2 and M2 to M1 expressed their terminal phenotype polarization markers *Nos2* for M1 and *Arg1* for M2 as determined by qPCR (**Figure 3.4c, d**). Together, this suggests that these cells were indeed transitioning but had not fully become the other phenotype. Giving some indication that elongation could play an initiation role in this process.

Figure 3.4

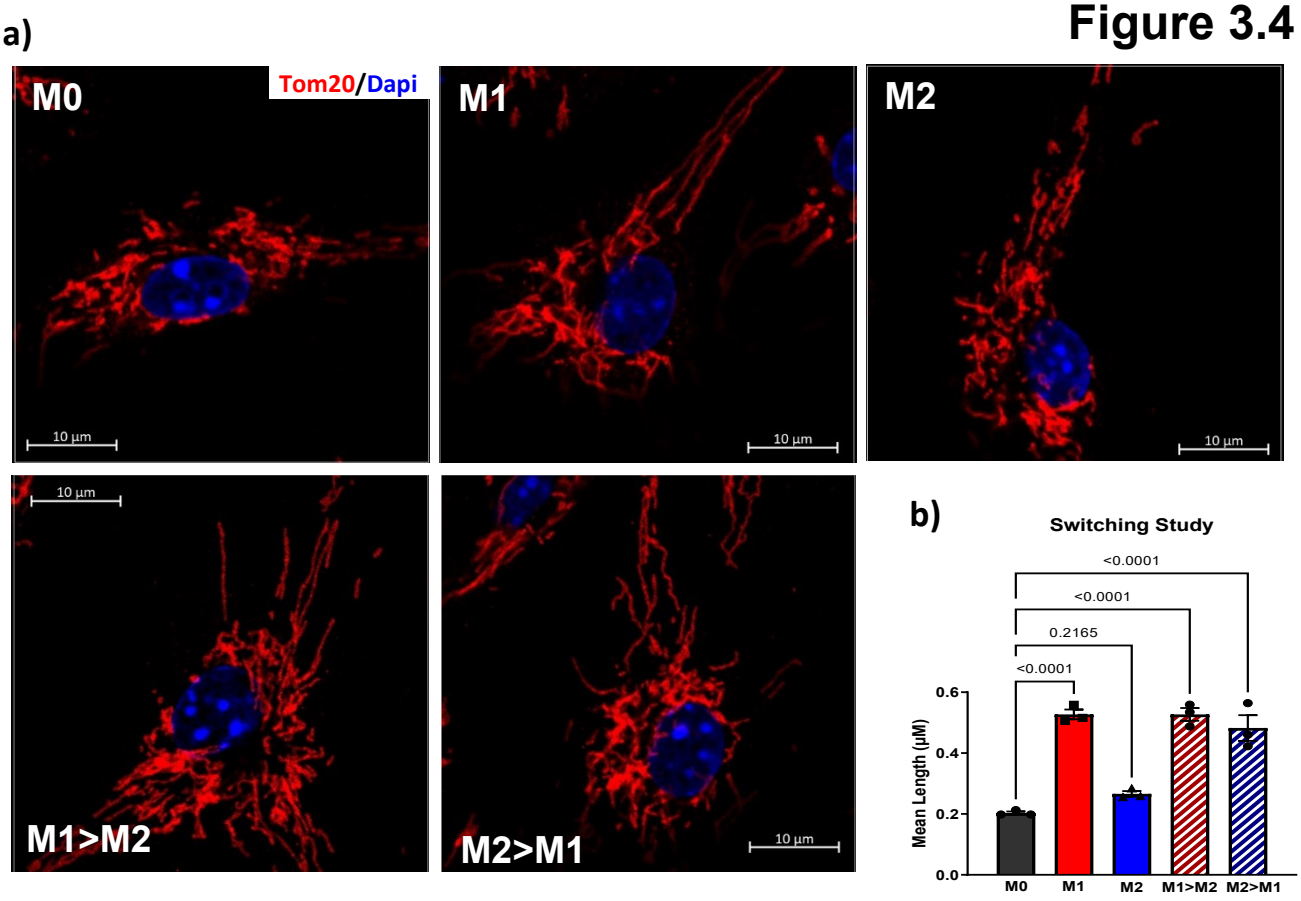
a)
M0
Tom20/Dapi
M1
M2
M1>M2
M2>M1
10 µm
b)
Switching Study
<0.0001
<0.0001
0.2165
<0.0001
Mean Length (µM)
0.0
0.2
0.4
0.6
M0
M1
M2
M1>M2
M2>M1
c)
M1 Marker: Nos2
0.2505
0.9910
>0.9999
0.7495
Fold Change
0
1000000
2000000
3000000
4000000
M0
M1
M2
M1>M2
M2>M1
d)
M2 Marker: Arg1
0.7556
<0.0001
0.1716
0.7259
Fold Change
0
10000
20000
30000
40000
M0
M1
M2
M1>M2
M2>M1

Figure 3.4: Mitochondrial network elongation is a key component of macrophage phenotype transitioning.
Differentiated BMDMs were stimulated for 24h with either M1 stimuli (LPS + IFNγ), M2 stimuli (IL-4) or the stimuli were swapped after 6h. a) Representative IF microscopy of stimulated BMDMs (Tom 20 in red & Dapi in blue). b) Quantification of mitochondrial length in transitioning macrophages (n=3). c) Gene expression of M1 marker *Nos2* (n=3). d) Gene expression of M2 marker *Arg1* (n=3). Data are presented as the mean of biological replicates +/- SEM. Statistical analysis by one-way ANOVA. N refers to the number of mice. Mean mitochondrial length refers to the mean of a minimum of 30 cells per n per group.

3.2.4 Sodium pyruvate supplementation alters the M1 elongation phenotype.

We observed that pro-inflammatory M1 macrophages have an elongated mitochondrial network when compared to pro-resolving M2 or basal M0s. However, historically it was believed that LPS stimulation induced a fragmented mitochondrial phenotype, which correlates with the increased glycolysis associated with M1 polarization (107, 108). Some of that discrepancy can be attributed to our characterization method. We evaluated mitochondrial length by staining for an outer membrane protein, Tom20, which is *(i)* not subject to changes in mitochondrial leakage (as is the case with Mitotracker), *(ii)* distinct from other measures of inner mitochondrial membrane proteins that may change with metabolic shifts (i.e. complex I) and *(iii)* more robustly reflects the mitochondrial membrane structure and length (68, 109, 110). Additionally, mitochondrial dyes used in live cell imaging can be toxic to cells and thus cause additional mitochondrial stress, which may be exacerbated upon co-stimulation with inflammatory factors like LPS.

An additional source of discrepancy is media sodium pyruvate supplementation. Sodium pyruvate directly feeds into the TCA cycle, alleviating some of the pressure LPS treatment

creates. We assessed the effect of sodium pyruvate supplementation on mitochondrial length during LPS treatment. Supplementation with sodium pyruvate diminished the elongation phenotype in our LPS-treated cells in accordance with increasing sodium pyruvate concentrations (**Figure 3.5a, b**). Therefore, if others supplemented their media with sodium pyruvate in addition to different quantification methods, it could have masked the M1 elongated mitochondrial phenotype we have characterized. We conclude that pro-inflammatory macrophages have a predominantly elongated mitochondrial network, whereas resting and M2 macrophages have a predominantly fragmented mitochondrial network.

Figure 3.5

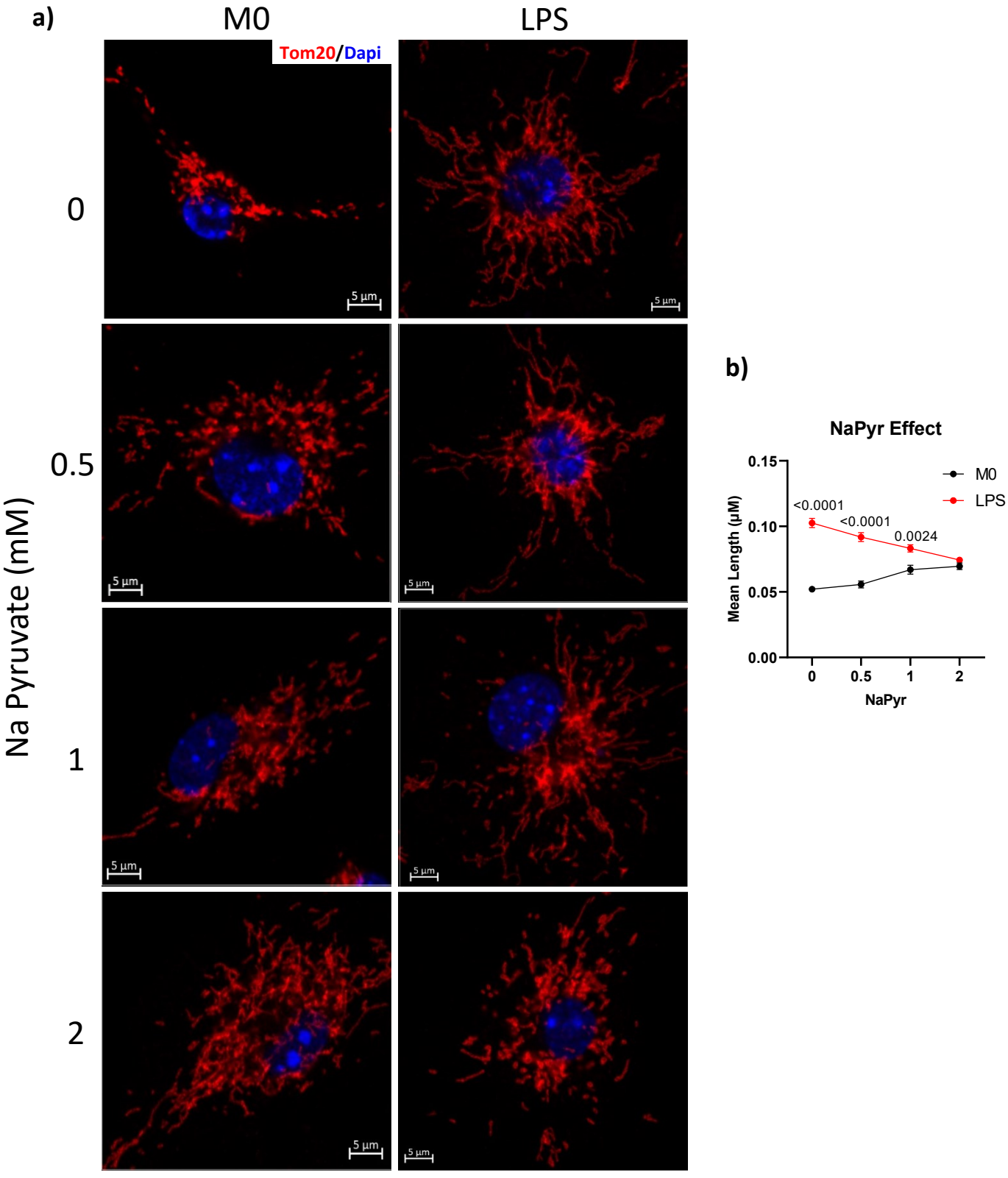
a)
M0
LPS
Tom20/Dapi
Na Pyruvate (mM)
0
0.5
1
2
5 µm
b)
NaPyr Effect
Mean Length (µM)
0.15
0.10
0.05
0.00
M0
LPS
<0.0001
<0.0001
0.0024
0
0.5
1
2
NaPyr

Figure 3.5: Sodium pyruvate supplementation alters mitochondrial network morphology.
Differentiated BMDMs were stimulated with LPS (100ng/ul) for 24h. Media was supplemented with indicated concentrations of sodium pyruvate. Differentiation media does not contain sodium pyruvate. a) Representative IF microscopy (Tom 20 in red & Dapi in blue). b) Quantification of mitochondrial length (n=3). Data are presented as the mean of biological replicates +/- SEM. Statistical analysis performed was multiple unpaired t-tests with Holm-Šídák correction. N refers to the number of mice. Mean mitochondrial length refers to the mean of a minimum of 30 cells per n per group.

3.2 Conclusions

It has been established that M1 macrophages prefer glycolytic metabolism and, thus, do not require hyper-efficient elongated mitochondria. The data shown above, however, indicates that M1 macrophages have an elongated phenotype. This phenotype occurs upon pro-inflammatory stimulation and happens quickly. Elongation can be seen as early as two hours into polarization before M1 polarization markers become elevated. In addition to elongation being seen even during stimulus-switching, this suggests that mitochondria elongation may play an initiating role in macrophage polarization.

The data above suggests that macrophage fate decisions, similar to T cell commitment to effector vs memory cell or neuronal and muscle stem cell commitment, could be directed by mitochondrial dynamics. M1 mitochondrial network elongation could play a critical role in macrophage inflammation and resolution responses. To test if mitochondrial dynamics play a directional role in macrophage fate decisions and determine a potential mechanism for this effect, we performed mitochondrial dynamics impairment of function studies.

Chapter 4: Impaired mitochondrial dynamics impact on inflammation resolution

4.1 Introduction

Previous studies have demonstrated a role for key mitochondrial fission and fusion proteins, namely DRP1, MFN2 and OPA1, in various aspects of macrophage inflammatory responses, sometimes with disparate results. Genetic deletion of *Drp1*- a critical mediator of mitochondrial fission- leads to reduced inflammatory responses measured by cytokine expression (107). Similarly, genetic deletion of either *Mfn2* or *Opa1* each of whom promote mitochondrial fusion- also results in reduced inflammatory gene activation. Collectively, these data suggest that macrophages require a functional and dynamic mitochondrial network to maintain inflammatory responses. It is possible that deletion of a single member of the fission or fusion machinery may have non-mitochondrial effects (e.g. the non-mitochondrial functions of DRP1 are also lost) and/or complete loss of these key proteins may result in adaptations that alter cell function. As such, we used an alternative approach, where siRNA knockdown of all 3 major fission or fusion machinery acutely induces the loss of functional mitochondrial fission or fusion. Based on the previously published work, we hypothesize that impairing mitochondrial dynamics will alter macrophage phenotype and inflammatory responses.

4.2 Results

4.2.1 Characterization of siRNA-mediated triple fission and fusion knockdown.

To determine whether mitochondrial fission and/or fusion directs macrophage M1 or M2 polarization, we developed a model wherein the mitochondrial dynamics machinery was silenced using a combination of siRNAs. SiRNAs targeting *Drp1*, *Mff* and *Fis1* were used to

prevent mitochondrial fission (Fission KD) phenocopying the hyperfused M1 mitochondrial network (**Figure 4.1a**) and siRNA targeting *Opa1*, *Mfn1*, and *Mfn2* were used to prevent mitochondrial fusion (Fusion KD) phenocopying the fragmented M2 mitochondrial network (**Figure 4.1b**). Fission knockdown resulted in a significantly elongated mitochondrial network compared to control siRNA-treated macrophages (**Figure 4.1c, e**). Fusion knockdown resulted in a significantly fragmented mitochondrial network compared to control siRNA-treated macrophages (**Figure 4.1d, f**). We confirmed knockdown for each siRNA combination at both the mRNA and protein levels (**Figure 4.1g-j**). We assessed pro- and anti-inflammatory gene expression in macrophages from Fission & Fusion KD cells at baseline. Unstimulated fusion KD macrophages had decreased expression of the M1 markers *Il1b & Tnfα*, whereas *Nos2* expression was increased, which corresponds with decreased M2 marker *Arg1* (**Figure 4.1k, l**). Impaired mitochondrial fusion in unstimulated macrophages similarly resulted in decreased M1 marker *Il1b, & Tnfα* gene expression; however, *Nos2* gene expression was also decreased, corresponding with increased M2 markers *Arg1* & *Fizz1* (**Figure 4.1m, n**). Together, this data indicated that mitochondrial network morphology impacts basal macrophage inflammatory marker gene expression.

Figure 4.1

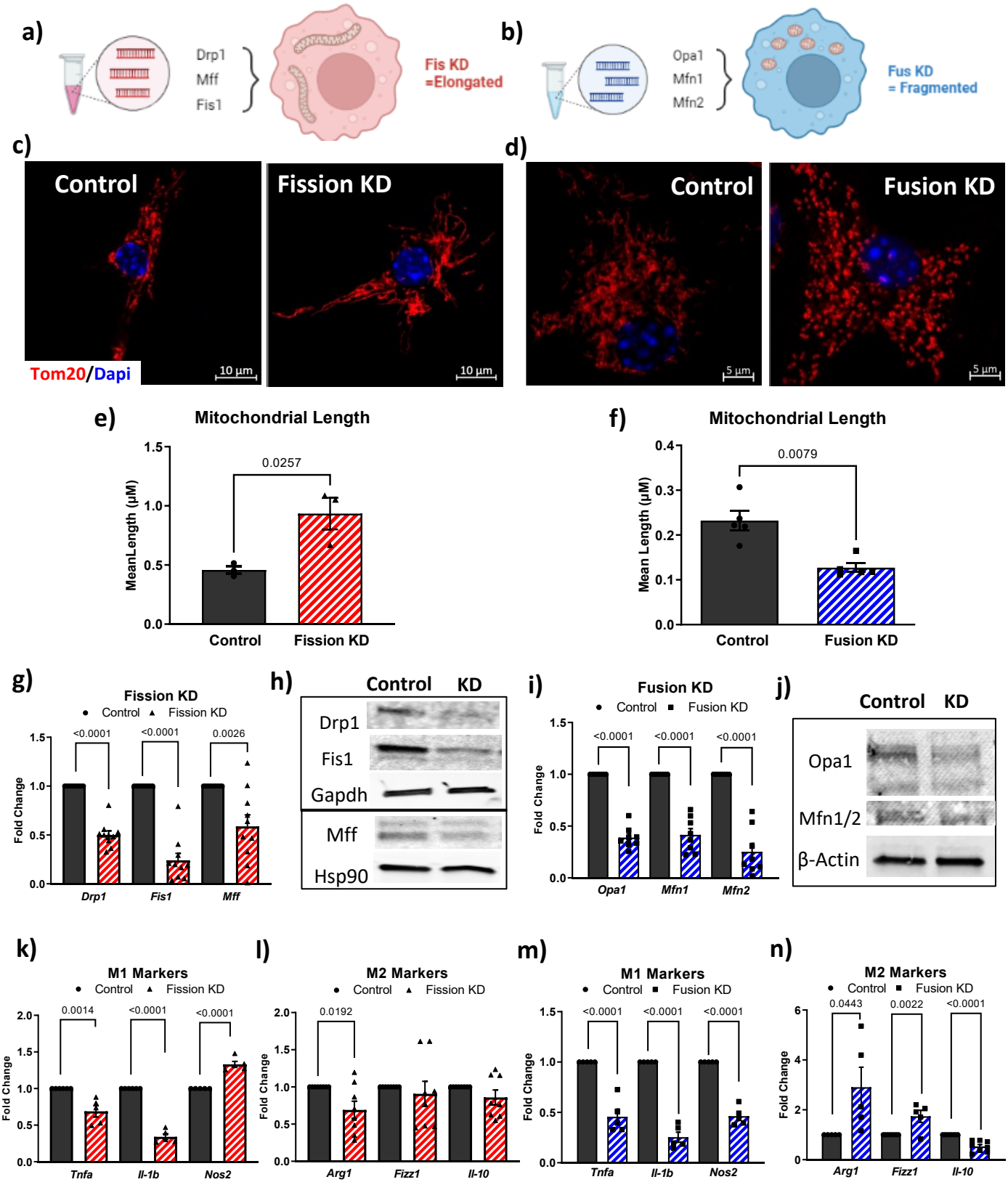
a)
Drp1
Mff
Fis1
Fis KD
=Elongated
b)
Opa1
Mfn1
Mfn2
Fus KD
= Fragmented
c)
Control
Fission KD
Tom20/Dapi
10 µm
d)
Control
Fusion KD
5 µm
e)
Mitochondrial Length
MeanLength (µM)
0.0257
Control
Fission KD
f)
Mitochondrial Length
Mean Length (µM)
0.0079
Control
Fusion KD
g)
Fission KD
Control
Fission KD
<0.0001
<0.0001
0.0026
Fold Change
Drp1
Fis1
Mff
h)
Control
KD
Drp1
Fis1
Gapdh
Mff
Hsp90
i)
Fusion KD
Control
Fusion KD
<0.0001
<0.0001
<0.0001
Fold Change
Opa1
Mfn1
Mfn2
j)
Control
KD
Opa1
Mfn1/2
β-Actin
k)
M1 Markers
Control
Fission KD
0.0014
<0.0001
<0.0001
Fold Change
Tnfa
Il-1b
Nos2
l)
M2 Markers
Control
Fission KD
0.0192
Fold Change
Arg1
Fizz1
Il-10
m)
M1 Markers
Control
Fusion KD
<0.0001
<0.0001
<0.0001
Fold Change
Tnfa
Il-1b
Nos2
n)
M2 Markers
Control
Fusion KD
0.0443
0.0022
<0.0001
Fold Change
Arg1
Fizz1
Il-10

Figure 4.1: Impairing mitochondrial fission or fusion in resting macrophages alters inflammatory gene expression.

BMDMs were transfected with siRNA against all three fission or fusion proteins for 72h. a) Infographic of triple siRNA fission knockdown (Fis KD). b) Infographic of triple siRNA fusion knockdown (Fus KD). c) Representative IF microscopy Fis KD. d) Representative IF microscopy Fus KD. e) Quantification of mean Fis KD mitochondrial length (n=3). f) Quantification of mean Fus KD mitochondrial length (n=5). g) Quantification of Fis KD efficiency by qPCR (n=10). h) Verification of Fis KD by Western blot. i) Quantification of Fus KD efficiency by qPCR (n=8). j) Effect of Fis KD on M1 marker gene expression (n=6). k) Effect of Fis KD on M2 marker gene expression (n=8). l) Effect of Fus KD on M1 marker gene expression (n=5). m) Effect of Fus KD on M2 marker gene expression (n=5). Data are presented as the mean of biological replicates +/- SEM. Statistical analysis by unpaired student t-test. N refers to the number of mice.

4.2.2 Single gene siRNA mediated knockdown implications.

To elucidate how our findings fit into the common literature, we performed single siRNA knockdowns for each fission and fusion protein. In summary, individual siRNA knockdowns of *Drp1, Fis1, Mff, Opa1*, and *Mfn1* had significantly decreased *Il1b* gene expression, the same as we observed with the triple Fusion KD (**Figures 4.2 & 4.3**). Mfn2, which is known to have numerous non-mitochondrial roles, had a significant increase in *Arg1* but no significant change in *Il1b* upon knockdown (**Figure 4.2h, i**). Generally, our triple knockdown model recapitulates the effects on IL1b and Arg1 of the individual protein knockdown model but is amplified due to the complete functional impairment. Specific single protein knockout with known additional roles (ie: Mfn2 and ER tethering) vary more in their effects on polarization markers.

Figure 4.2

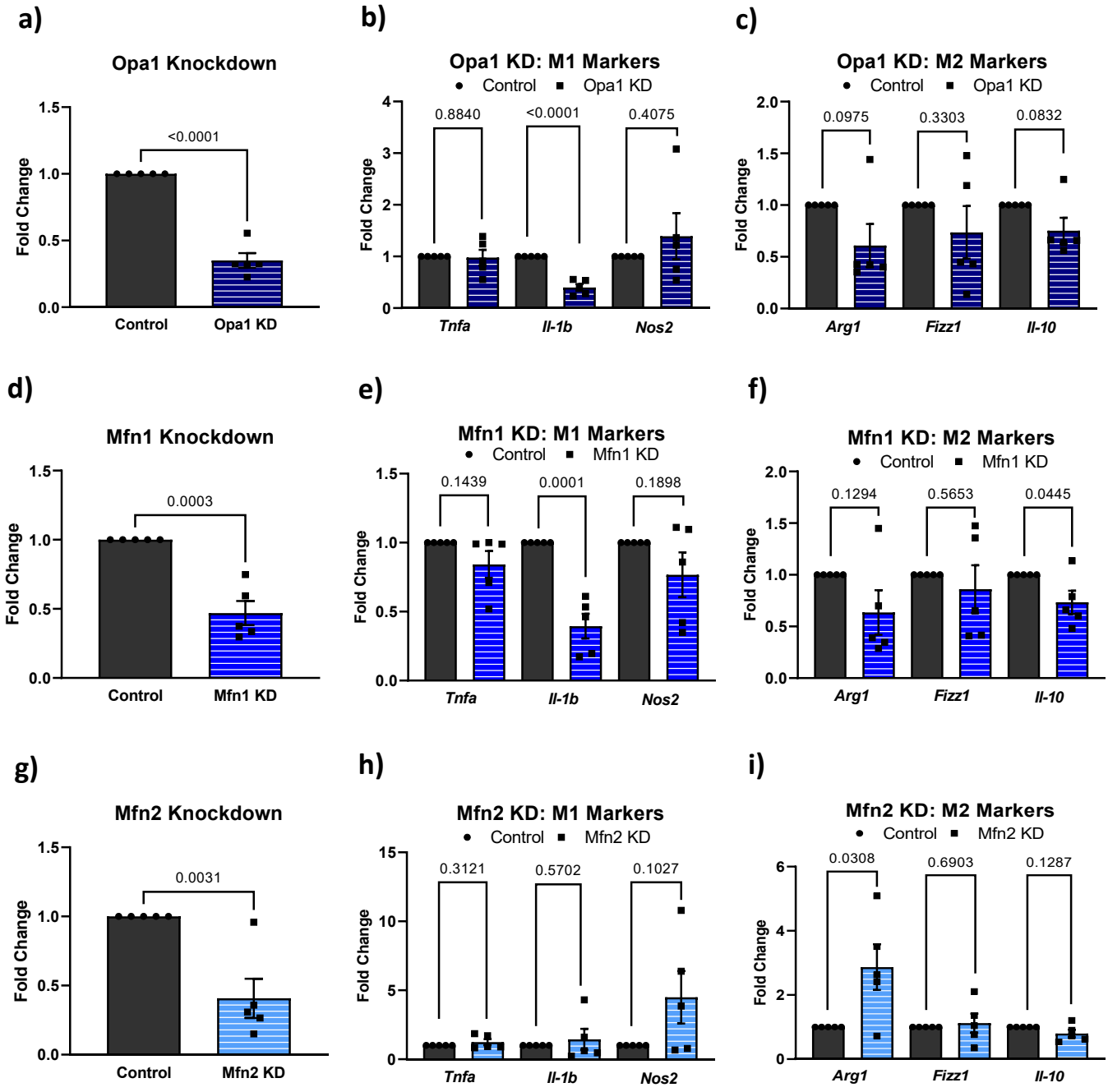

Figure 4.2: Determine the effect of single fusion protein knockdown on polarization.
BMDMs were transfected with either Opa1 (20nM), Mfn1 (20nM) or Mfn2 (20nm) siRNA for 72h than assessed for knockdown (KD) and polarization markers gene expression by qPCR. a) Opa1 KD efficiency (n=5). b) Opa1 KD impact on M1 markers (n=5). c) Opa1 KD impact on M2 markers (n=5). d) Mfn1 KD efficiency (n=5). e) Mfn1 KD impact on M1 markers (n=5). f) Mfn1 KD impact on M2 markers (n=5). g) Mfn2 KD efficiency (n=5). h) Mfn2 KD impact on M1 markers (n=5). i) Mfn2 KD impact on M2 markers (n=5). Data are presented as the mean of biological replicates +/- SEM. Statistical analysis of a, d, g by unpaired student t-test and the rest by multiple unpaired t-tests with Holm-Šídák correction. N refers to the number of mice.

Figure 4.3

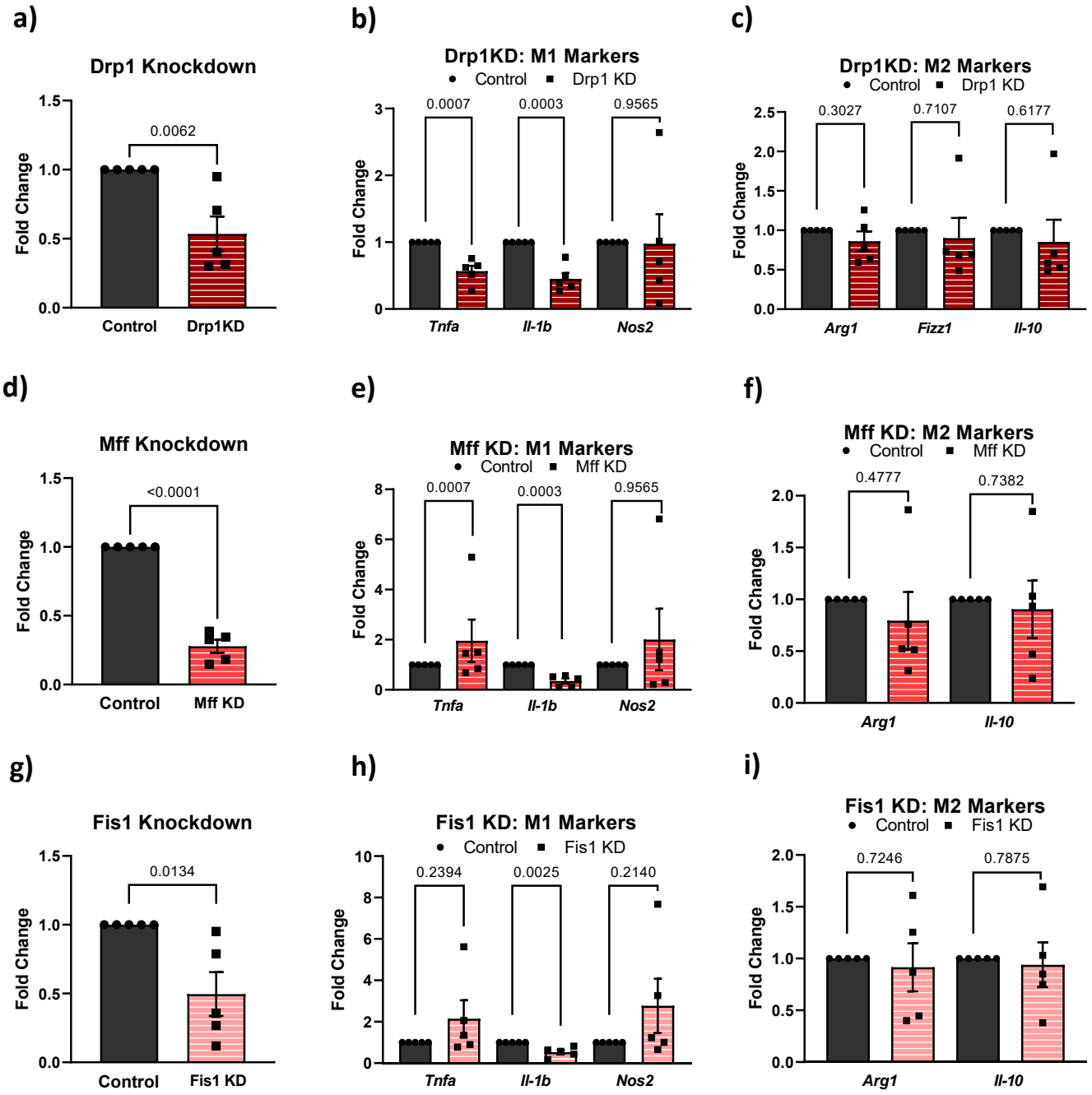

Figure 4.3: Determine the effect of single fission protein knockdown on polarization.
BMDMs were transfected with either Drp1 (40nM), Mff (10nM) or Fis1 (10nm) siRNA for 72h than assessed for knockdown and polarization markers gene expression by qPCR. a) Drp1 KD efficiency (n=5). b) Drp1 KD impact on M1 markers (n=5). c) Drp1 KD impact on M2 markers (n=5). d) Mff KD efficiency (n=5). e) Mff KD impact on M1 markers (n=5). f) Mff KD impact on M2 markers (n=5). g) Fis1 KD efficiency (n=5). h) Fis1 KD impact on M1 markers (n=5). i) Fis1 KD impact on M2 markers (n=5). Data are presented as the mean of biological replicates +/- SEM. Statistical analysis of a, d, g by unpaired student t-test and the rest by multiple unpaired t-tests with Holm-Šídák correction. N refers to the number of mice.

4.2.3 Implication of fission and fusion knockdown on inflammatory progression.

To determine whether macrophages with impaired mitochondrial dynamic respond normally to an inflammatory stimulus, we assessed *Il1b* gene expression after LPS stimulation. Macrophages with hyperfused mitochondria had decreased *Il1b* gene expression after 24h of LPS stimulation compared to controls (**Figure 4.4a, b**). To assess how changes in gene expression may impact protein function, we examined the expression of the precursor, mature and secreted forms of IL-1β protein in response to LPS stimulation over time. The loss of mitochondrial fission had no effect on either pro-IL-1β or IL-1β secretion (**Figure 4.4c, d, f**). To determine whether elongated mitochondria influenced the full activation of IL-1β protein secretion, which requires the engagement of the NLPR3 inflammasome via a priming and an activation signal, we tested an *in-vitro* model of inflammasome activation with LPS priming followed by ATP activation (111–114). Priming with LPS and subsequent activation by ATP in macrophages with hyperfused mitochondria resulted in equivalent IL-1β release compared to controls, indicating a normal inflammasome priming and activation process (**Figure 4.4g**). Together, these data indicate that while mitochondrial fusion appears to control the basal expression of macrophage *Il1b* gene expression, it has little influence on IL-1β protein secretion upon inflammatory stimulation. Therefore, although M1 macrophages adopt a lengthened mitochondrial network in parallel with their pro-inflammatory gene expression state, forcing an elongated mitochondrial network does not directly cause a heightened inflammatory response to LPS.

To determine whether preventing mitochondrial fusion would result in an impaired inflammatory response, we stimulated control and fusion KD macrophages with LPS. Impaired mitochondrial fusion results in increased *Il1b* gene expression after 6 and 24h (**Figure 4.4b)**. Activation of IL-1β protein was assessed after LPS stimulation where loss of mitochondrial fusion results in an increase in pro-IL-1β at 6h and 24h (**Figure 4.4c, e**) and a corresponding small but not statistically significant increase in IL-1β secretion at 24h (**Figure 4.4h**). Upon inflammasome activation with LPS and ATP (as described above), loss of mitochondrial fusion led to a significant increase in IL-1β secretion (**Figure 4.4i**). These data are similar to what is observed in a parallel model of impaired mitochondrial fusion where genetic loss of OPA1 led to an increase in IL-1β secretion upon inflammasome activation (115), and support that this is likely due to functional losses in mitochondrial fusion.

Figure 4.4

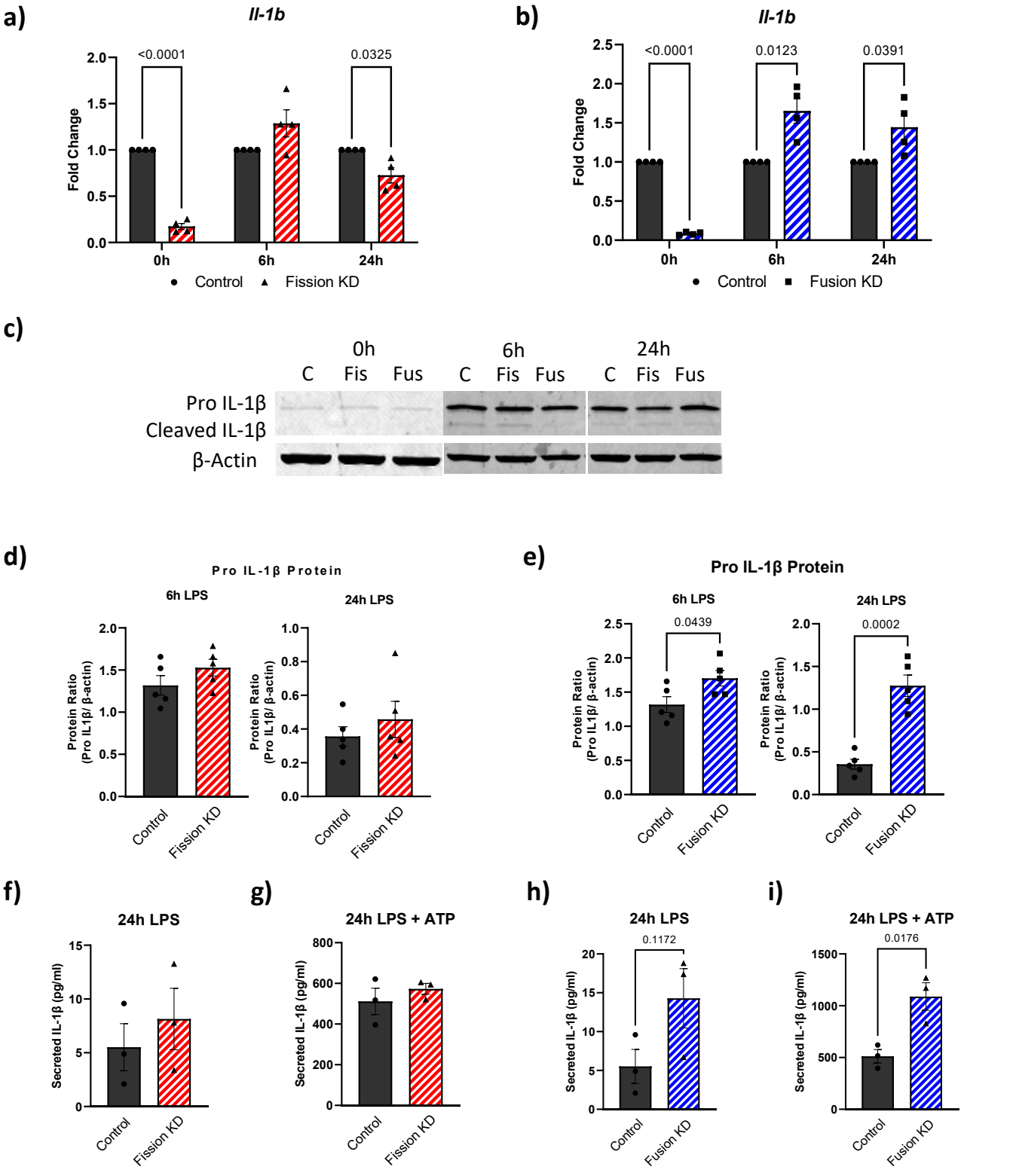
a)
Il-1b
<0.0001
0.0325
Fold Change
0h
6h
24h
Control
Fission KD
b)
Il-1b
<0.0001
0.0123
0.0391
Fold Change
Control
Fusion KD
c)
0h
6h
24h
C
Fis
Fus
Pro IL-1β
Cleaved IL-1β
β-Actin
d)
Pro IL-1β Protein
6h LPS
24h LPS
Protein Ratio (Pro IL1β/ β-actin)
Control
Fission KD
e)
Pro IL-1β Protein
6h LPS
0.0439
24h LPS
0.0002
Protein Ratio (Pro IL1β/ β-actin)
Control
Fusion KD
f)
24h LPS
Secreted IL-1β (pg/ml)
Control
Fission KD
g)
24h LPS + ATP
Secreted IL-1β (pg/ml)
Control
Fission KD
h)
24h LPS
0.1172
Secreted IL-1β (pg/ml)
Control
Fusion KD
i)
24h LPS + ATP
0.0176
Secreted IL-1β (pg/ml)
Control
Fusion KD

Figure 4.4: Impairing mitochondrial fission & fusion alters inflammatory progression in LPS-stimulated macrophages.

Fission and Fusion KD BMDMs were stimulated with LPS (100ng/ml) for the indicated time. a) *IL-1b* gene expression upon LPS stimulation in fission KD cells (n=4). b) *IL-1b* gene expression upon LPS stimulation in fusion KD cells (n=4). c) Representative western blot of IL-1β protein over time once stimulated with LPS d) Quantification of fission KD pro-IL1β protein levels normalized to β-Actin (n=5). e) Quantification of fusion KD pro-IL-1β protein levels normalized to β-Actin (n=5). f) Secreted IL-1β levels in fission KD cells upon 24h LPS stimulation measured by ELISA (n=3). g) Secreted IL-1β levels in fission KD cells upon 24h LPS + 30min ATP stimulation measured by ELISA (n=3). h) Secreted IL-1β levels in fusion KD cells upon 24h LPS stimulation measured by ELISA (n=3). i) Secreted IL-1β levels in fusion KD cells upon 24h LPS + 30min ATP stimulation measured by ELISA (n=3). Statistical analysis performed was multiple unpaired t-tests with Holm-Šídák correction (a-b) and unpaired student t-test (d-j). N refers to the number of mice.

4.2.4 Fusion KD cells initiate alternate Il-1b transcription ATF4/c-Jun pathway upon LPS stimulation

To investigate how mitochondrial fusion alters the expression of IL-1β upon LPS stimulation, we investigated transcriptional pathways known to promote cytokine production. We first assessed NFκB activity, which is a potent inducer of *Il1b* expression and is quickly activated upon LPS stimulation, where the p65 subunit becomes phosphorylated and translocates to the nucleus to activate inflammatory gene expression (116–118). We assessed NFkB activity via measuring the phosphorylation of the p65 subunit by Western blot. Surprisingly, despite increases in *Il1b* gene expression upon loss of mitochondrial fusion, we find that p65 phosphorylation is significantly decreased after 24h of LPS stimulation (**Figure 4.5a, b**). These data indicate that the observed increase in IL-1β expression and secretion upon loss of mitochondrial fusion may be caused by an alternative NFκB-independent mechanism. HIF1α nuclear translocation- which is stimulated in response to LPS and drives inflammatory cytokine production downstream of NFκB was next assessed by microscopy (119). Upon LPS

stimulation, the loss of mitochondrial fusion caused a decrease in HIF1α nuclear translocation (**Figure 4.5c**). This observed decrease in HIF-1α translocation would not be expected to result in increased IL-1β secretion upon LPS stimulation; therefore we looked into alternative pathways that are known to be upstream of inflammatory stimulation and may activate cytokine expression. We assessed the activity of the ATF4/c-jun transcriptional pathway, which can promote *Il1b* expression in response to LPS (120). When mitochondrial fusion is impaired, both ATF4 and phosphorylated c-Jun are significantly increased after 6h of LPS stimulation (**Figure 4.5d-g**). To confirm the increase in ATF4 activity upon knockdown of mitochondrial fusion, another ATF4-responsive gene, *Slc7a11* was measured after both 6h and 24h of LPS stimulation (121), and indeed was increased in macrophages with fusion KD (**Figure 4.5h**). *Slc7a11* can also be induced through ROS-mediated NRF2 nuclear translocation; however, we found no significant changes in mitochondrial ROS levels or NRF2 nuclear translocation, indicating that the increase in *Slc7a11* can likely be associated with ATF4 activity (**Figure 4.5i, j**). Together, these data indicate that, in response to inflammatory stimulation, mitochondrial fusion contributes to the macrophage inflammatory IL-1β response, possibly via activation of the ATF4/c-jun axis.

Figure 4.5

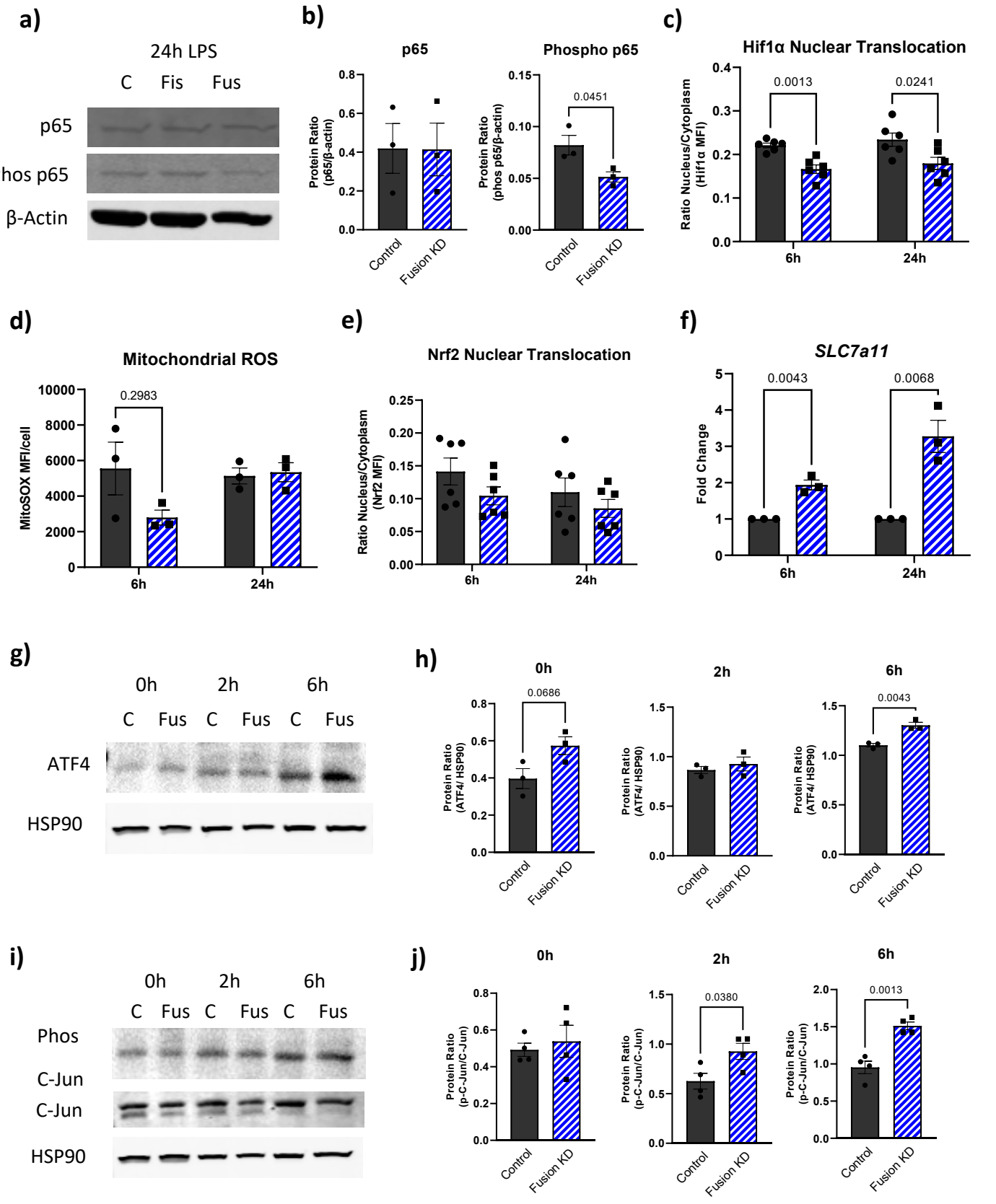
a)
24h LPS
C
Fis
Fus
p65
Phos p65
β-Actin
b)
p65
Protein Ratio (p65/β-actin)
Control
Fusion KD
Phospho p65
Protein Ratio (phos p65/β-actin)
0.0451
c)
Hif1α Nuclear Translocation
Ratio Nucleus/Cytoplasm (Hif1α MFI)
0.0013
0.0241
6h
24h
d)
Mitochondrial ROS
MitoSOX MFI/cell
0.2983
e)
Nrf2 Nuclear Translocation
Ratio Nucleus/Cytoplasm (Nrf2 MFI)
f)
SLC7a11
Fold Change
0.0043
0.0068
g)
0h
2h
6h
C
Fus
ATF4
HSP90
h)
Protein Ratio (ATF4/ HSP90)
0.0686
0.0043
i)
Phos
C-Jun
j)
Protein Ratio (p-C-Jun/C-Jun)
0.0380
0.0013

Figure 4.5: Fusion knockdown shift in IL-1β after LPS stimulation associated with ATF4 and phosphorylated C-Jun transcription factors.

a) Representative western blot of p65 and phosphorylated p65 upon 24h LPS stimulation. b) Quantification of p65 and phosphorylated p65 normalized to β-actin (n=3). c) Quantification of Hif1α nuclear translocation from IF microscopy (n=6). d) Reactive oxygen species (ROS) as measured by MitoSOX mean fluorescence intensity per cell (n=3) e) Quantification of Nrf2 nuclear translocation from IF microscopy (n=6). f) SLC7a11 gene expression as indication of Nrf2 activity (n=3). g) Representative western blot of ATF4 upon LPS stimulation. h) Quantification of ATF4 normalized to HSP90 (n=3). i) Representative western blot of C-Jun and phosphorylated C-Jun upon LPS stimulation. j) Quantification of phosphorylated C-Jun normalized to HSP90 (n=3). Statistical analysis by unpaired student t-test except for c-f, where multiple unpaired t-tests with Holm-Šídák correction were applied. N refers to the number of mice.

4.2.5 Fusion KD promotes post-inflammatory resolution responses.

Given that M2 macrophages had a more fragmented mitochondrial network compared to M1 macrophages (**Figure 3.1a, b**) and that loss of mitochondrial fusion led to an increase in baseline expression of *Arg1* (**Figure 4.1n**), we sought to determine whether mitochondrial fusion alters the anti-inflammatory macrophage phenotype during the resolution phase of inflammation. Arginase 1 is a critical enzyme in macrophages that promotes the resolution of inflammation by reducing nitric oxide signaling, promoting L-arginine metabolism to assist in tissue repair (122). In normal macrophages, *Arg1* expression is temporally activated by LPS, with expression appearing late following LPS stimulation, following the peak of the pro-inflammatory response (123). We, therefore, assessed whether a fragmented mitochondrial network influenced the late activation of *Arg1*. Upon LPS stimulation, *Arg1* gene expression was maximally increased in mitochondrial fusion-impaired cells after 24h, translating to an increased protein level at 48h (**Figure 4.6a-c**). IL-4 is a potent inducer of M2 macrophage responses and is produced by Th2 cells to trigger the anti-inflammatory program in macrophages (124, 125). We, therefore, assessed the impact of impaired mitochondrial fusion

upon direct anti-inflammatory stimulation using IL-4. *Arg1* gene and protein expression were both increased upon fusion KD after 24h of IL-4 treatment (**Figure 4.6d-f)**. To test how mitochondrial fusion impacts macrophage plasticity, we first stimulated cells with LPS for 6h, after which we stimulated them with IL-4, to accelerate the pro-resolving phase. Loss of mitochondrial fusion increased *Arg1* gene expression and protein compared to control cells, indicating a heightened pro-resolving response (**Figure 4.6g-i**). A key function of M2 pro-resolving macrophages is phagocytic capacity; therefore, we measured phagocytosis of latex beads. Loss of mitochondrial fusion resulted in an increase in phagocytosis compared to controls basally and under LPS, IL-4 or combined stimulation. (**Figure 4.6j-m**). Together, these data indicate that inducing a fragmented mitochondrial phenotype promotes inflammation resolution following inflammatory or anti-inflammatory activation.

Figure 4.6

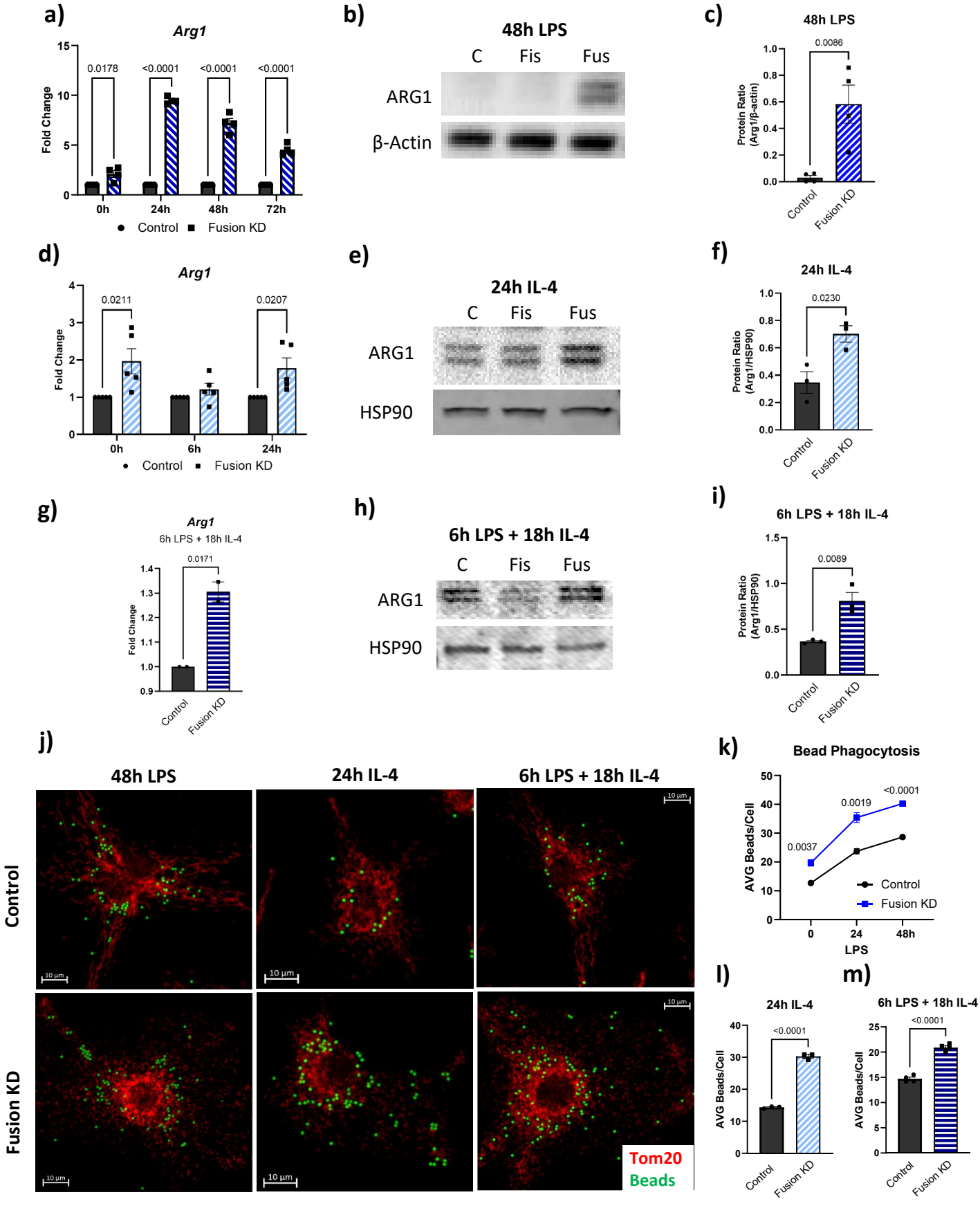
a)
Arg1
Fold Change
0.0178
<0.0001
<0.0001
<0.0001
0h
24h
48h
72h
Control
Fusion KD
b)
48h LPS
C
Fis
Fus
ARG1
β-Actin
c)
48h LPS
0.0086
Protein Ratio (Arg1/β-actin)
Control
Fusion KD
d)
Arg1
Fold Change
0.0211
0.0207
0h
6h
24h
Control
Fusion KD
e)
24h IL-4
C
Fis
Fus
ARG1
HSP90
f)
24h IL-4
0.0230
Protein Ratio (Arg1/HSP90)
Control
Fusion KD
g)
Arg1
6h LPS + 18h IL-4
0.0171
Fold Change
Control
Fusion KD
h)
6h LPS + 18h IL-4
C
Fis
Fus
ARG1
HSP90
i)
6h LPS + 18h IL-4
0.0089
Protein Ratio (Arg1/HSP90)
Control
Fusion KD
j)
48h LPS
24h IL-4
6h LPS + 18h IL-4
Control
Fusion KD
10 µm
Tom20
Beads
k)
Bead Phagocytosis
AVG Beads/Cell
0.0037
0.0019
<0.0001
Control
Fusion KD
0
24
48h
LPS
l)
24h IL-4
<0.0001
AVG Beads/Cell
Control
Fusion KD
m)
6h LPS + 18h IL-4
<0.0001
AVG Beads/Cell
Control
Fusion KD

Figure 4.6: Silencing mitochondrial fusion machinery promotes a pro-resolving macrophage phenotype.

a) *Arg1* gene expression over time upon LPS stimulation (n=4). b) Representative ARG1 western blot after 48h of LPS stimulation. c) Quantification of ARG1 protein levels normalized to β-actin after 48h LPS stimulation (n=4). d) *Arg1* gene expression over time upon IL-4 stimulation (n=5). e) Representative ARG1 western blot after 24h of IL-4 stimulation. f) Quantification of ARG1 protein levels normalized to HSP90 after 24h IL-4 stimulation (n=3). g) *Arg1* gene expression upon 6h LPS + 18h IL-4 stimulation (n=2). h) Representative ARG1 western blot after 6h LPS + 18h IL-4 stimulation. i) Quantification of ARG1 protein levels normalized to HSP90 after 6h LPS + 18h IL-4 stimulation (n=3). j) Representative immunofluorescence microscopy of bead phagocytosis (Mitotracker in red and Beads in green). k) Quantification of bead phagocytosis in fusion KD cells under LPS stimulation (n=4). l) Quantification of bead phagocytosis in fusion KD cells under IL-4 stimulation (n=3). m) Quantification of bead phagocytosis in fusion KD cells under 6h LPS + 18h IL-4 stimulation (n=4). Western blot molecular weights ARG1 40kDa, β-actin 45kDa, HSP90 90kDa. Data are presented as the mean of biological replicates +/- SEM. Statistical analysis c, f, g, i, l, m by unpaired student t-test and a, d, k by multiple unpaired t-tests with Holm-Šídák correction. N refers to the number of mice.

4.2.6 Mitochondrial fragmentation promotes post-inflammatory resolution via histone lactylation.

Pro-inflammatory macrophages are highly glycolytic, and as a result, produce high levels of lactate upon inflammatory stimulation (83, 126). Lactate is a powerful signaling molecule and is known to promote M2-like responses in tumour macrophages (127). It was recently shown that once sufficiently elevated, lactate causes a change in gene expression via lactylation of lysine residue on histones, turning on pro-resolving machinery such as ARG1 (82, 92, 128, 129). We observed an increase in *Arg1* expression in macrophages with fragmented mitochondria and therefore hypothesized that lactate may play a role. To understand whether mitochondrial fragmentation promotes changes in lactate metabolism, we assessed lactate levels in control and Fusion KD cells upon LPS stimulation. After 24h of LPS treatment, lactate levels were increased in Fusion KD compared to controls (**Figure 4.7a**). In agreement with the increase in lactate levels, histone lactylation (marked by the pan-histone lactylation antibody, KLA) was

increased with knockdown of mitochondrial fusion after 24h of LPS stimulation **(Figure 4.7b-c).** Both lactate and histone lactylation were equivalent to that of control macrophages after 48h of LPS stimulation suggesting fusion KD shifts the homeostatic lactylation mechanism earlier (**Figure 4.7a-c**). To better understand the increase in lactate and KLA upon loss of mitochondrial fusion, we first measured the expression of pyruvate dehydrogenase (PDH), which converts pyruvate to acetyl-CoA to enter the TCA cycle (83). Upon loss of mitochondrial fusion, we observe a decrease in PDH expression after 24h of LPS stimulation (**Figure 4.7d-e**). It would be expected that lower PDH expression in cells with fragmented mitochondria would result in reduced conversion of pyruvate to acetyl-coA, and an increase in conversion of pyruvate to lactate (130). To test this hypothesis, we inhibited lactate accumulation by inhibiting the activity of lactate dehydrogenase (LDH) using oxamate (127, 131–133). Co-treatment of macrophages with LPS and oxamate for 48h prevented the induction of ARG1 protein in Fusion KD macrophages (**Figure 4.7f, g**) and induction of KLA in control cells **(Figure 4.7h, i).** In summary, the above data indicate that increased lactate accumulation in cells with fragmented mitochondria is driving the increase in *Arg1* expression in macrophages following inflammatory activation.

Figure 4.7

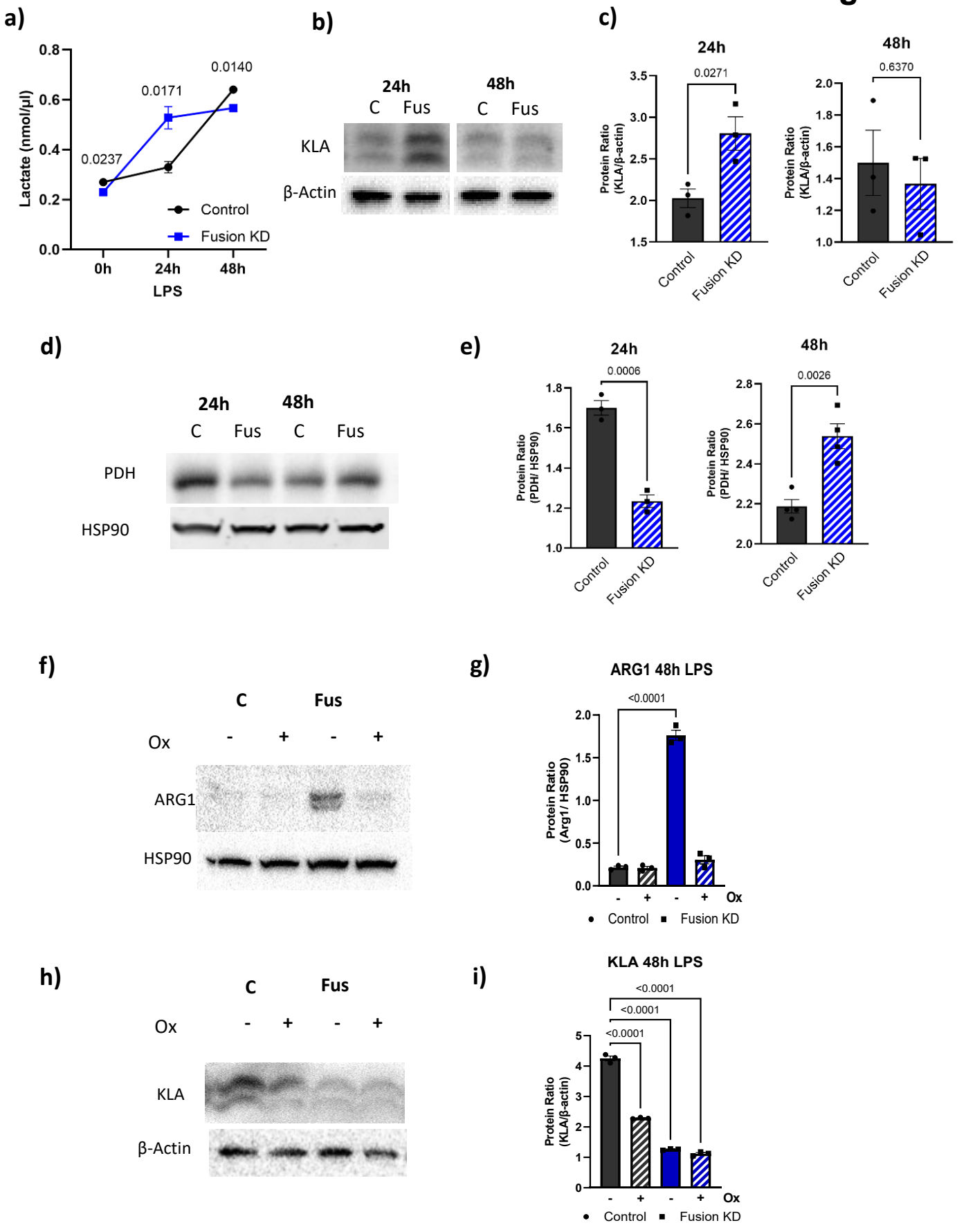
a)
Lactate (nmol/µl)
0.8
0.6
0.4
0.2
0.0
0.0237
0.0171
0.0140
Control
Fusion KD
0h
24h
48h
LPS
b)
24h
48h
C
Fus
C
Fus
KLA
β-Actin
c)
24h
0.0271
Protein Ratio (KLA/β-actin)
3.5
3.0
2.5
2.0
1.5
Control
Fusion KD
48h
0.6370
Protein Ratio (KLA/β-actin)
2.0
1.8
1.6
1.4
1.2
1.0
Control
Fusion KD
d)
24h
48h
C
Fus
C
Fus
PDH
HSP90
e)
24h
0.0006
Protein Ratio (PDH/ HSP90)
1.8
1.6
1.4
1.2
1.0
Control
Fusion KD
48h
0.0026
Protein Ratio (PDH/ HSP90)
2.8
2.6
2.4
2.2
2.0
Control
Fusion KD
f)
C
Fus
Ox
-
+
-
+
ARG1
HSP90
g)
ARG1 48h LPS
<0.0001
Protein Ratio (Arg1/ HSP90)
2.0
1.5
1.0
0.5
0.0
-
+
-
+
Ox
Control
Fusion KD
h)
C
Fus
Ox
-
+
-
+
KLA
β-Actin
i)
KLA 48h LPS
<0.0001
<0.0001
<0.0001
Protein Ratio (KLA/β-actin)
5
4
3
2
1
0
-
+
-
+
Ox
Control
Fusion KD

Figure 4.7: Silencing mitochondrial fusion machinery alters cellular lactate levels, increases histone lactylation and reduces PDH.

a) Lactate levels over time in fusion KD cells compared to control cells (n=3). b) Representative western blot of histone lactylation (KLA) over time. c) Quantification KLA in fusion KD cells after 24 & 48h LPS stimulation (n=3). d) Representative western blot of pyruvate dehydrogenase levels over time. e) Quantification PDH in fusion KD cells after 24 & 48h LPS stimulation (n=3). f) Representative western blot of ARG1 in control vs fusion KD cells upon 48h LPS stimulation with LDH inhibitor sodium oxamate. g) Quantification ARG1 in fusion KD cells after 48h LPS stimulation with sodium oxamate (n=3). h) Representative western blot of KLA in control vs fusion KD cells upon 48h LPS stimulation with sodium oxamate. i) Quantification KLA in fusion KD cells after 48h LPS stimulation with sodium oxamate (n=3). Western blot molecular weights KLA 15kDa, PDH 43 kDa, ARG1 40kDa, β-actin 45kDa & HSP90 90kDa.Data are presented as the mean of biological replicates +/- SEM. Statistical analysis a, c, e by unpaired student t-test and g, i, by one-way ANOVA. N refers to the number of mice.

4.2.7 The lactate clock is associated with endogenous mitochondrial fragmentation.

The observation that siRNA-induced mitochondrial fragmentation resulted in an increase in histone lactylation and *Arg1* expression prompted us to examine whether this also occurs during the physiological macrophage resolution response. Having observed a fragmented mitochondrial network in IL-4 treated M2 polarized macrophages, so we next sought to characterize the mitochondrial phenotype of macrophages as they enter the pro-resolving phase after LPS exposure- during which the switch to histone lactylation occurs and *Arg1* expression is induced. Analysis of mitochondrial morphology after 24, 48 and 72h following LPS stimulation revealed maximal mitochondrial elongation at 24h and a return to near baseline length after 48 and 72h (**Figure 4.8a-c**). There was a corresponding increase in lactate (**Figure 4.8d**) and histone lactylation, as measured by KLA, between 24-72h (**Figure 4.8e**). Furthermore, co-treatment with LDH inhibitor sodium oxamate and LPS for 72h prevented the induction of both ARG1 and KLA (**Figure 4.8g-j**). Together, these data indicate that a fragmented mitochondrial network is associated with an increase in histone lactylation during the resolution phase of inflammation.

Figure 4.8

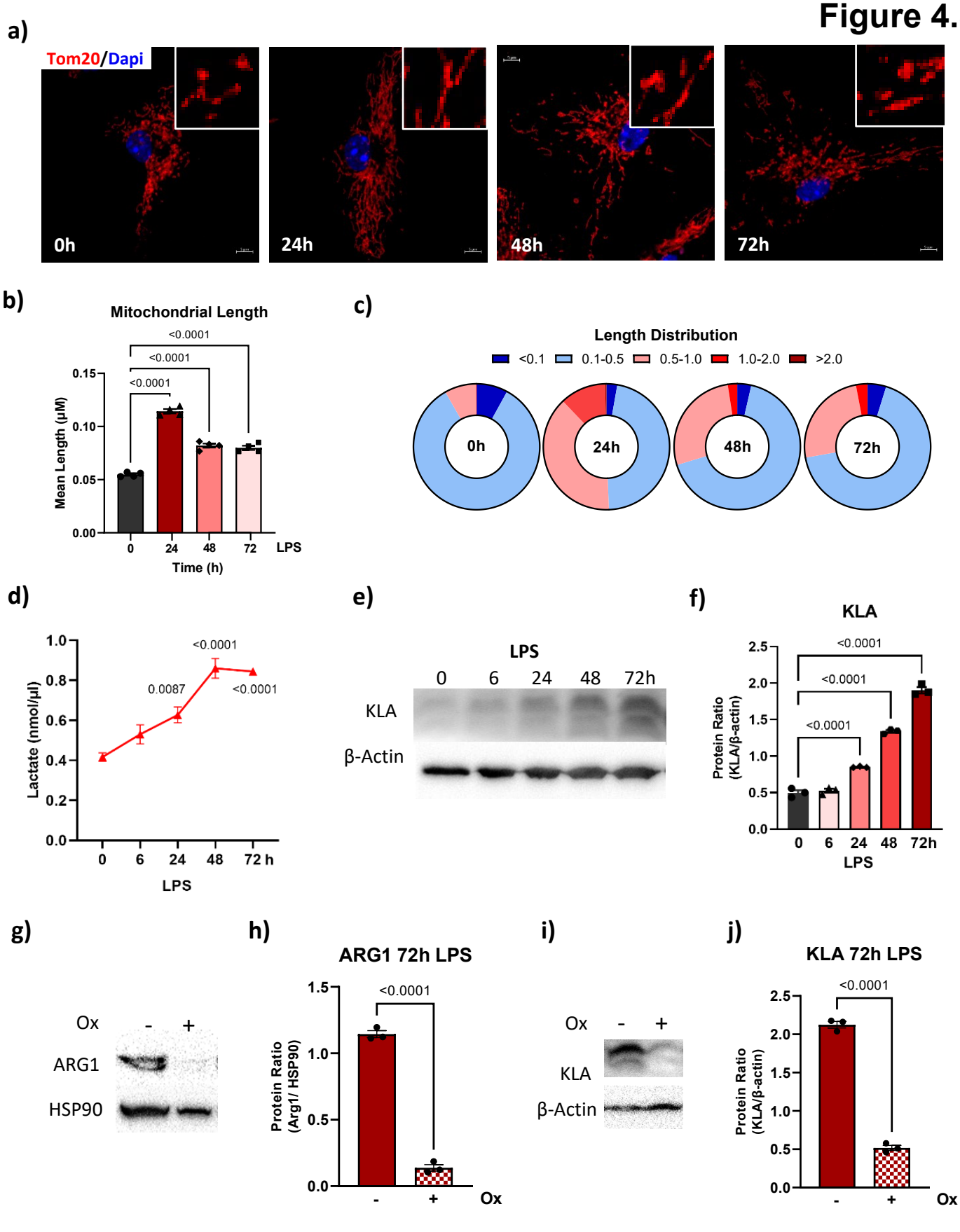
a)
Tom20/Dapi
0h
24h
48h
72h
b)
Mitochondrial Length
<0.0001
<0.0001
<0.0001
Mean Length (µM)
0.15
0.10
0.05
0.00
0
24
48
72
LPS
Time (h)
c)
Length Distribution
<0.1
0.1-0.5
0.5-1.0
1.0-2.0
>2.0
0h
24h
48h
72h
d)
Lactate (nmol/µl)
1.0
0.8
0.6
0.4
0.2
0.0
<0.0001
0.0087
<0.0001
0
6
24
48
72 h
LPS
e)
LPS
0
6
24
48
72h
KLA
β-Actin
f)
KLA
<0.0001
<0.0001
<0.0001
Protein Ratio (KLA/β-actin)
2.5
2.0
1.5
1.0
0.5
0.0
0
6
24
48
72h
LPS
g)
Ox
-
+
ARG1
HSP90
h)
ARG1 72h LPS
<0.0001
Protein Ratio (Arg1/ HSP90)
1.5
1.0
0.5
0.0
-
+
Ox
i)
Ox
-
+
KLA
β-Actin
j)
KLA 72h LPS
<0.0001
Protein Ratio (KLA/β-actin)
2.5
2.0
1.5
1.0
0.5
0.0
-
+
Ox

Figure 4.8: Endogenous fragmentation is correlated with lactate clock initiation.
a) Representative images of mitochondrial network morphology upon late-stage LPS stimulation (Tom 20 in red & Dapi in blue). b) Quantification of average mitochondrial length per cell (n=4) c) Average mitochondrial length distribution per time point (n=4). d) Lactate levels upon LPS stimulation in control cells with statistics vs 0h (n=3). e) Representative time-course western blot of histone lactylation (KLA) in untransfected BMDMs upon LPS stimulation. f) Quantification of KLA upon LPS stimulation in untransfected BMDMs (n=3). g) Representative western blot of ARG1 in control cells upon 72h LPS stimulation with sodium oxamate. h) Quantification of ARG1 in control cells 72h LPS stimulation with or without sodium oxamate (n=3). i) Representative western blot of KLA upon 72h LPS stimulation with sodium oxamate. j) Quantification of KLA upon 72h LPS stimulation with or without sodium oxamate (n=3). Western blot molecular weights KLA 15kDa, ARG1 40kDa, β-actin 45kDa & HSP90 90kDa. Data are presented as the mean of biological replicates +/- SEM. Statistical analysis d, h, j by unpaired student t-test and b, f by one-way ANOVA. N refers to the number of mice.

4.2 Conclusions

The data above indicates that mitochondrial fusion plays a role in macrophage resolution response. In response to inflammatory stimulation, macrophages with impaired mitochondrial fusion have an early inflammatory IL-1β response, possibly via activation of the ATF4/c-jun axis. However, most strikingly, a fragmented mitochondrial phenotype promotes inflammation resolution following inflammatory or anti-inflammatory activation. Impaired mitochondrial fusion results in faster lactate accumulation upon LPS stimulation. The resulting lactate accumulation drives the macrophage post-inflammatory resolution response (increase in *Arg1* expression) via histone lactylation. Furthermore, mitochondrial fragmentation is associated with the initiation of the lactate clock, restoring homeostasis post-inflammation.

Chapter 5: Mitochondrial fragmentation promotes inflammation resolution *in vivo*

5.1 Introduction

The previous chapters showed the mechanism by which mitochondrial fragmentation promotes inflammation resolution, specifically in macrophages. Based on those findings, we hypothesize that promoting mitochondrial fragmentation would promote inflammation resolution *in vivo*. The model we chose to test this hypothesis is zymosan-induced peritonitis (ZIP) (134–138). Zymosan produces a form of sterile inflammation which, when injected into the peritoneum, induces the recruitment of neutrophils followed by monocytes and then macrophages. This model was chosen because the recruitment and resolution timeline has been well established, allowing us to see if intervention by either inhibiting histone lactylation or promoting mitochondrial fragmentation can alter that timeline.

5.2 Results

5.2.1 Characterize zymosan-induced peritonitis in-vivo resolution model.

To establish and validate the zymosan-induced peritonitis *in vivo* recruitment and resolution model, we performed a time course study. Mice were injected with 1mg per mouse of zymosan and euthanized for peritoneal lavage at specified time points (**Figure 5.1a**). Flow cytometry was used to characterize the infiltration and resolution of neutrophils (CD11b+, Ly6C+ and Ly6G+) monocytes (CD11b+, LY6C+, and Ly6G-) and macrophages (CD11b+ and F4/80+) upon zymosan-induced peritonitis(136, 137, 139, 140). We found peak neutrophil infiltration at 6h, monocyte at 24h and macrophage recruitment at 72h (**Figure 5.1b-e**). As our *in vitro* work focused on the impact of mitochondrial fragmentation and lactylation on

macrophages, we identified 24h post-Zymosan as the optimal point of drug intervention when macrophage recruitment begins. To further correlate our *in vivo* model to our *in vitro* data, we quantified mitochondrial length across the recruitment and resolution timeline. We observed increasing mitochondrial length up to 72h following zymosan injection, at which point endogenous fragmentation could be seen during the resolution phase(**Figure 5.1f, g**).

Figure 5.1

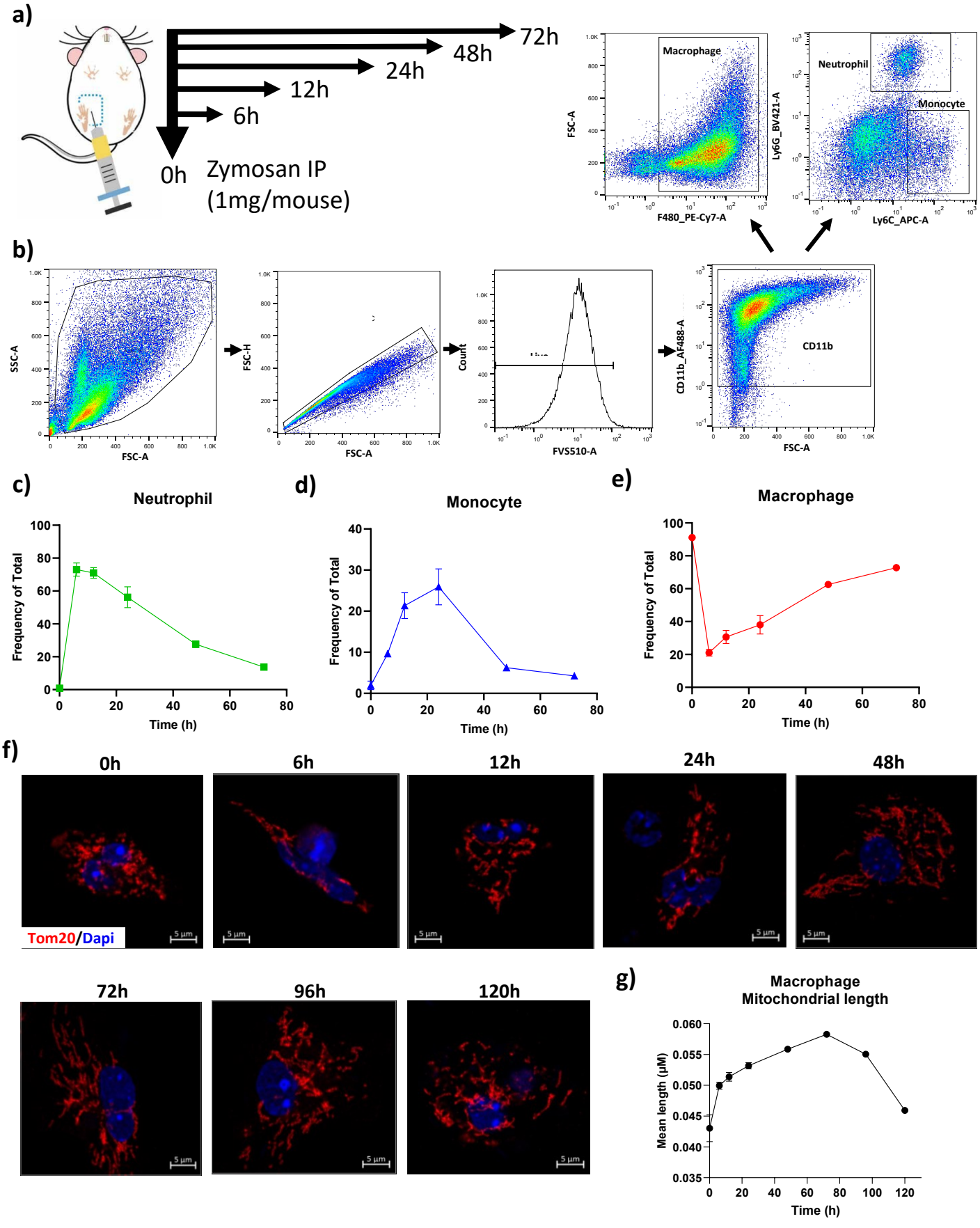
a)
72h
48h
24h
12h
6h
0h
Zymosan IP
(1mg/mouse)
Macrophage
Neutrophil
Monocyte
FSC-A
F480_PE-Cy7-A
Ly6G_BV421-A
Ly6C_APC-A
b)
SSC-A
FSC-A
FSC-H
Count
FVS510-A
CD11b_AF488-A
CD11b
c)
Neutrophil
Frequency of Total
Time (h)
d)
Monocyte
e)
Macrophage
f)
0h
6h
12h
24h
48h
Tom20/Dapi
5 µm
72h
96h
120h
g)
Macrophage
Mitochondrial length
Mean length (µM)

Figure 5.1: Zymosan-induced peritonitis characterization.
C57BL/6 wild-type mice were injected with 1mg per mouse Zymosan A in saline by intraperitoneal injection. Mice were euthanized at specified times by CO2, and then peritoneal lavage was collected for further analysis. a) Zymosan-induced peritonitis (ZIP) resolution model timeline. b) Representative flow cytometry gating strategy to identify the neutrophil, monocyte and macrophage populations within the peritoneal lavage. c) Neutrophil frequency over time (n=2). d) Monocyte frequency over time (n=2). e) Macrophage frequency over time (n=2). f) Representative immunofluorescent microscopy of peritoneal macrophage (PMAC) mitochondrial morphology over time (Tom 20 in red & Dapi in blue). g) Quantification of PMAC mitochondrial length over time (n=2). Data are presented as the mean of biological replicates +/- SEM. N refers to the number of mice.

5.2.2 Mitochondrial fragmentation shifts the lactate clock in vivo.

To assess the impact of mitochondrial fragmentation on inflammation resolution *in vivo*, we performed a zymosan-induced peritonitis resolution study with impaired mitochondrial fusion. We chose to promote mitochondrial fragmentation with an acute OPA1 chemical inhibitor called MYLS22 (115, 141–145). MYLS22 was confirmed to initiate mitochondrial fragmentation in BMDMS after 24h of treatment at a similar level to that of our Fusion KD cells (**Figure 5.2a, b**). This allows for a comparable extent of mitochondrial fragmentation to our fusion KD cells without the time constraints associated with siRNA-mediated knockdown.

Figure 5.2

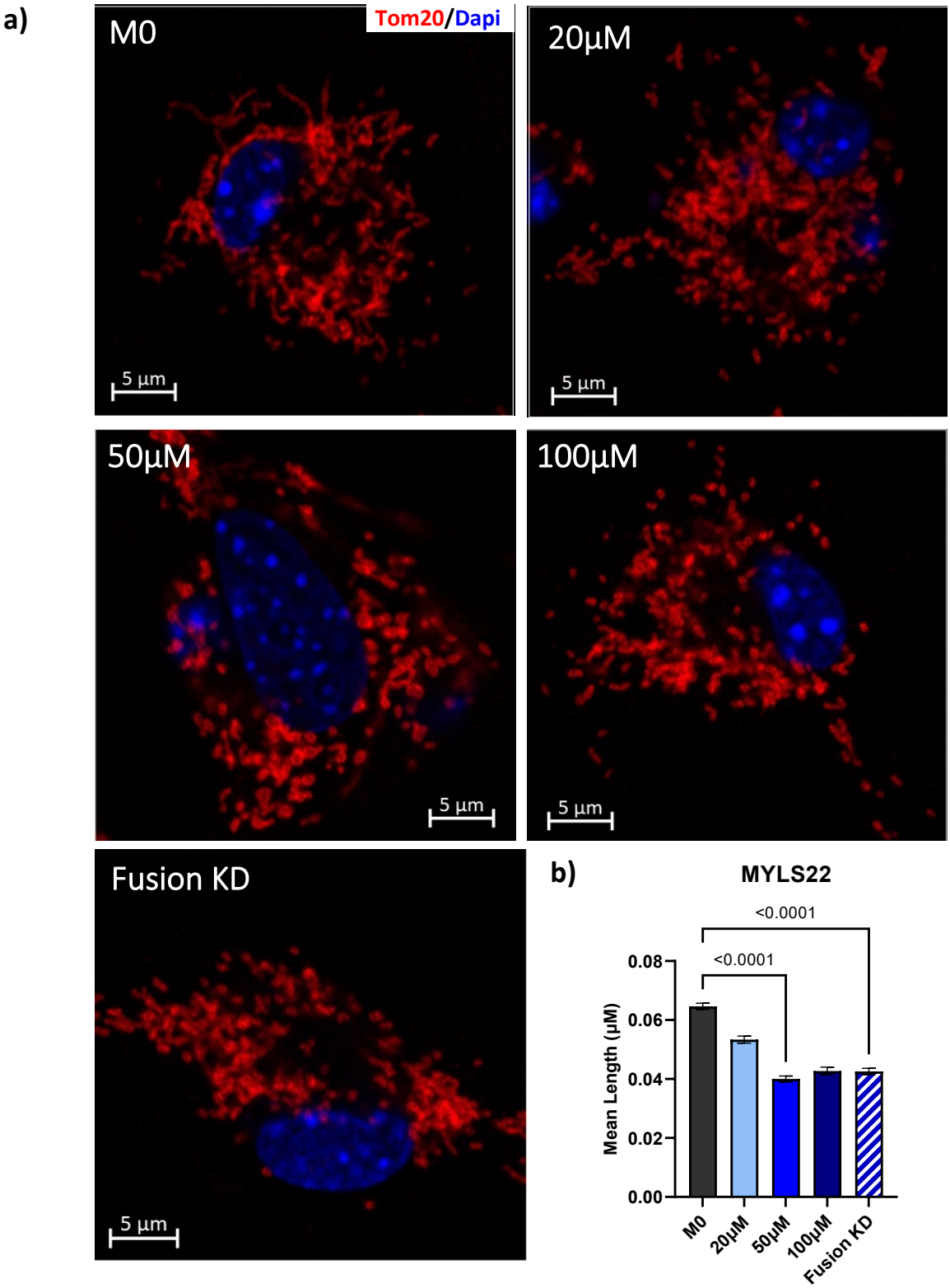
a)
M0
Tom20/Dapi
5 µm
20µM
5 µm
50µM
5 µm
100µM
5 µm
Fusion KD
5 µm
b)
MYLS22
<0.0001
<0.0001
Mean Length (µM)
0.08
0.06
0.04
0.02
0.00
M0
20µM
50µM
100µM
Fusion KD

Figure 5.2: OPA1 inhibitor MYLS22 validation.
BMDMs were treated with MYLS22 for 24h and validated against optimized 72h siRNA Fusion KD protocol. a) Representative immunofluorescent microscopy of MYLS22 treated BMDMs (Tom 20 in red & Dapi in blue). b) Quantification of mitochondrial length (n=2 mice). Data are presented as the mean of biological replicates +/- SEM. Statistical analysis by one-way ANOVA.

To determine if mitochondrial fragmentation can promote inflammation resolution *in vivo*, we administered 10mg/kg MYLS22 by intraperitoneal injection 24h post-zymosan (144, 146–148). Mice were sacrificed at 24-hour intervals for peritoneal lavage (**Figure 5.3a**). The lavage was assessed for cellular contents by flow cytometry, and mitochondrial morphology was observed by microscopy. MYLS22 treatment decreased the frequency of neutrophils and monocytes over time compared to vehicle-treated mice (**Figure 5.3b, c**). Additionally, MYLS22 significantly decreased macrophage recruitment throughout zymosan resolution (Figure 3d). The decrease in macrophage recruitment correlates with MYLS22-mediated mitochondrial fragmentation (**Figure 5.3e, f**). To assess whether mitochondrial fragmentation promotes inflammation resolution via histone lactylation, we measured KLA and ARG1 protein levels. MYLS22 shifted maximal KLA & ARG1 protein expression earlier to 96h post-zymosan, whereas vehicle-treated cells KLA and ARG1 levels were most elevated after 120h post-zymosan (**Figure 5.3g-j**). In summary, MYLS22-mediated mitochondrial fragmentation promotes inflammation resolution *in vivo,* potentially via a shift in the lactate clock.

Figure 5.3

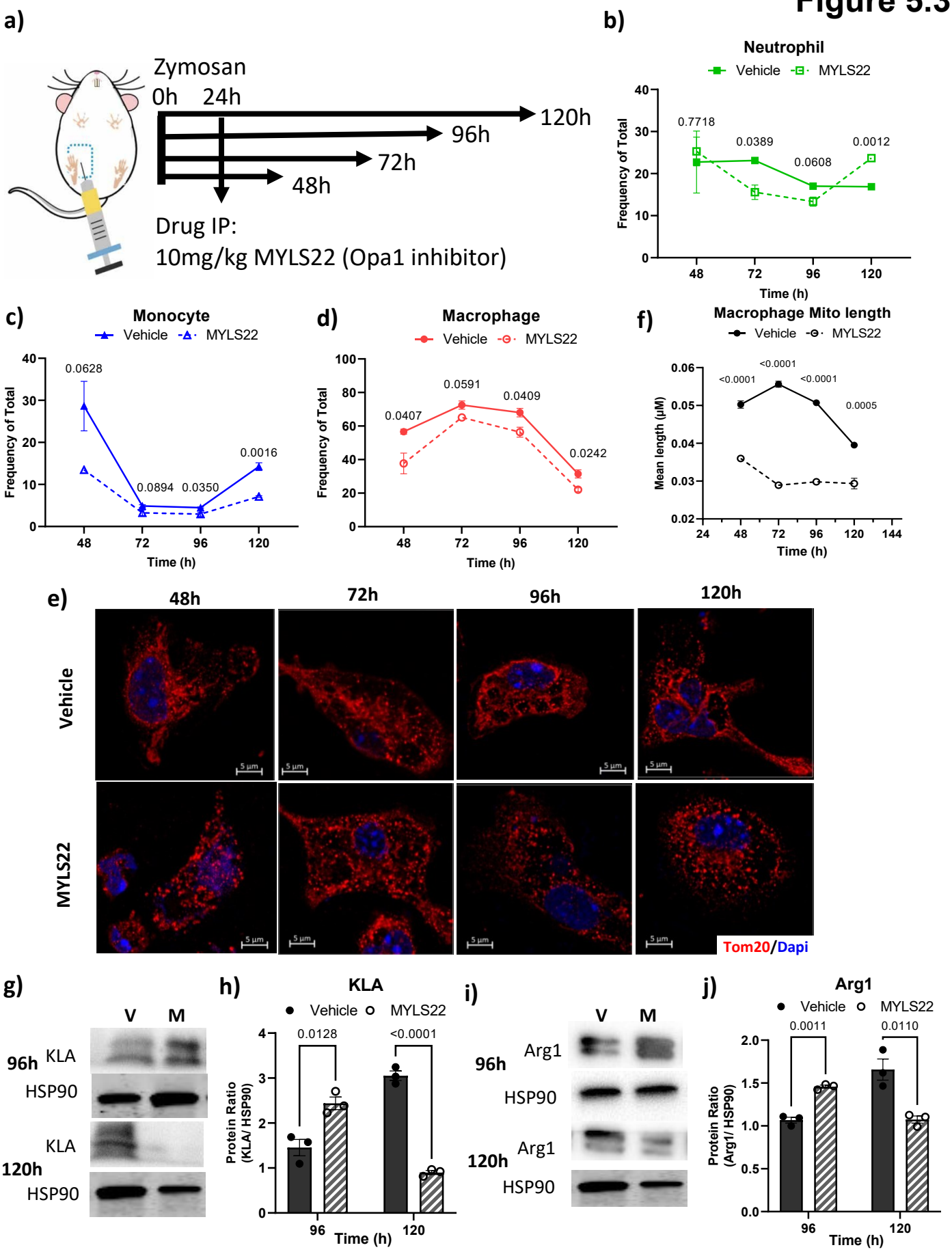
a)
Zymosan
0h 24h
120h
96h
72h
48h
Drug IP:
10mg/kg MYLS22 (Opa1 inhibitor)
b)
Neutrophil
Vehicle MYLS22
Frequency of Total
0.7718
0.0389
0.0608
0.0012
Time (h)
c)
Monocyte
Vehicle MYLS22
Frequency of Total
0.0628
0.0894
0.0350
0.0016
Time (h)
d)
Macrophage
Vehicle MYLS22
Frequency of Total
0.0407
0.0591
0.0409
0.0242
Time (h)
f)
Macrophage Mito length
Vehicle MYLS22
Mean length (µM)
<0.0001
<0.0001
<0.0001
0.0005
Time (h)
e)
48h
72h
96h
120h
Vehicle
MYLS22
Tom20/Dapi
g)
V M
96h KLA
HSP90
KLA
120h
HSP90
h)
KLA
Vehicle MYLS22
Protein Ratio (KLA/ HSP90)
0.0128
<0.0001
Time (h)
i)
V M
96h Arg1
HSP90
Arg1
120h
HSP90
j)
Arg1
Vehicle MYLS22
Protein Ratio (Arg1/ HSP90)
0.0011
0.0110
Time (h)

Figure 5.3: MYLS22 shifts ZIP resolution timeline.
C57BL/6 wild-type mice were injected intraperitoneally with 1 mg per mouse Zymosan A, followed by 10 mg per kg MYLS22 or vehicle 24 hours later. Mice were euthanized at specified times from Zymosan injection by CO2, and then peritoneal lavage was collected for further analysis. a) MYLS22 intervention ZIP resolution timeline. b) Neutrophil frequency over time (n=3). c) Monocyte frequency over time (n=3). d) Macrophage frequency over time (n=3). e) Representative immunofluorescent microscopy of peritoneal macrophage (PMAC) mitochondrial morphology. f) Quantification of PMAC mitochondrial length over time (n=3). g) Representative western blot of histone lactylation (KLA). h) Quantification KLA at 96h and 120h of the ZIP resolution timeline (n=3). i) Representative western blot of Arginase 1 (Arg1) over time. j) Quantification Arg1 at 96h and 120h of the ZIP resolution timeline (n=3). Data are presented as the mean of biological replicates +/- SEM. Statistical analysis by multiple unpaired t-tests with Holm-Šídák correction. N refers to the number of mice.

5.2.3 Inhibiting lactate accumulation impacts in-vivo inflammatory response.

Next, we assessed whether impairing histone lactylation would impede zymosan-induced peritonitis resolution to determine if the lactylation pathway we identified *in vitro* plays a prominent role in inflammation resolution *in vivo*. To prevent histone lactylation, we used sodium oxamate, a lactate dehydrogenase inhibitor, thereby preventing lactate accumulation. We administered 500mg/kg sodium oxamate by intraperitoneal injection 24h post-zymosan(131–133, 149–151). Mice were sacrificed at 24-hour intervals for peritoneal lavage (**Figure 5.4a**). The lavage was assessed for cellular contents by flow cytometry, and cellular/extracellular lactate levels were assessed by colorimetric assay. Sodium oxamate treatment increased the frequency of neutrophils and monocytes over time compared to saline-treated mice (**Figure 5.4b, c**). Additionally, sodium oxamate significantly increased macrophage recruitment throughout the zymosan resolution timeline (**Figure 5.4d**). The increase in macrophage recruitment correlates with the sodium oxamate-mediated decrease in cellular and extracellular L-lactate (**Figure 5.4e, f**). This correlation was confirmed by sodium

oxamate decreasing KLA and ARG1 protein levels up to 120h post-zymosan. In conclusion, impairing lactate accumulation via sodium oxamate promotes inflammation; thus, histone lactylation is a key component of inflammation resolution *in vivo*.

Figure 5.4

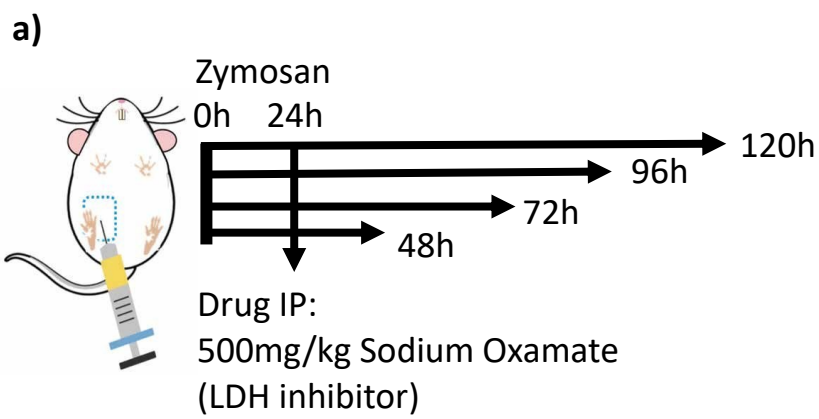
a)
Zymosan
0h 24h
120h
96h
72h
48h
Drug IP:
500mg/kg Sodium Oxamate
(LDH inhibitor)

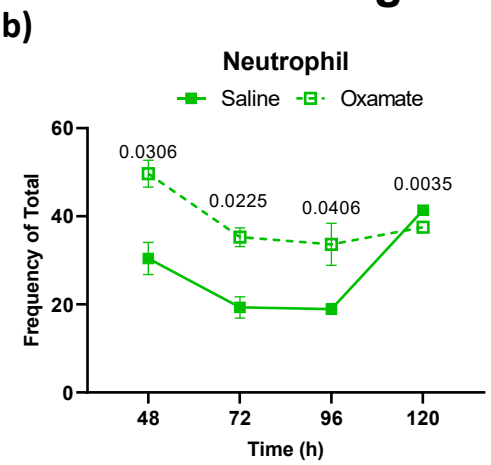
b)
Neutrophil
Saline
Oxamate
Frequency of Total
0.0306
0.0225
0.0406
0.0035
Time (h)

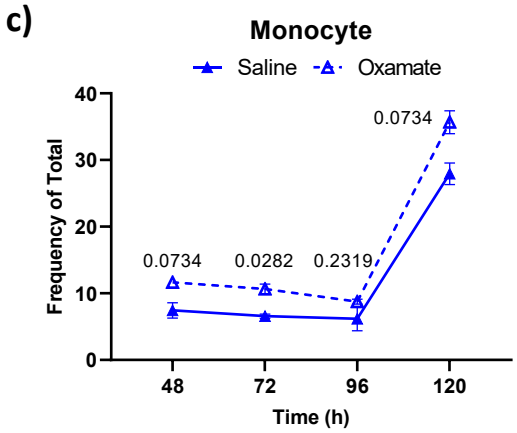
c)
Monocyte
Saline
Oxamate
Frequency of Total
0.0734
0.0734
0.0282
0.2319
Time (h)

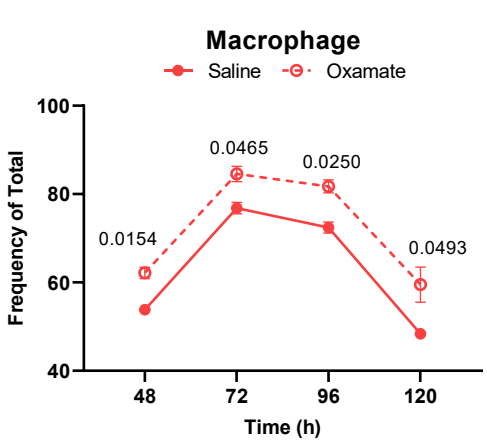
d)
Macrophage
Saline
Oxamate
Frequency of Total
0.0154
0.0465
0.0250
0.0493
Time (h)

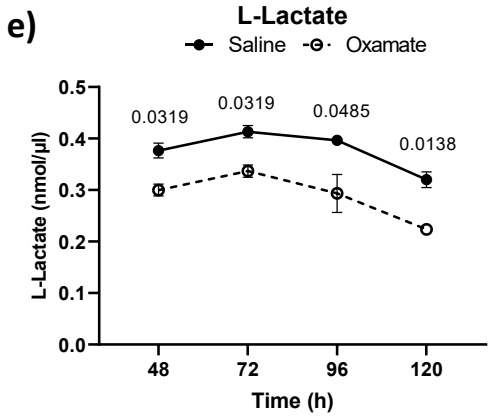
e)
L-Lactate
Saline
Oxamate
L-Lactate (nmol/µl)
0.0319
0.0319
0.0485
0.0138
Time (h)

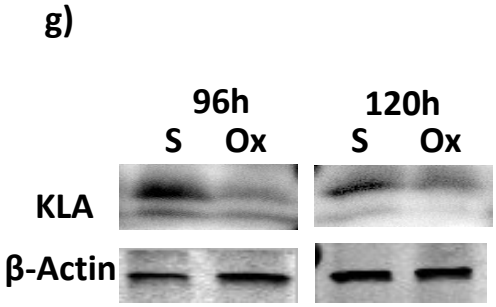
g)
96h
120h
S
Ox
S
Ox
KLA
β-Actin

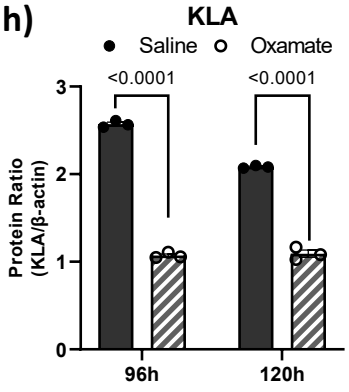
h)
KLA
Saline
Oxamate
<0.0001
<0.0001
Protein Ratio
(KLA/β-actin)
96h
120h

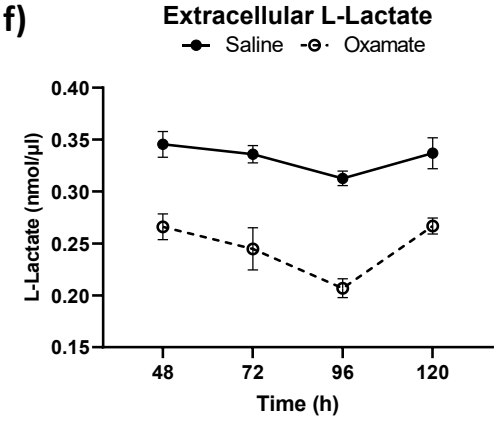
f)
Extracellular L-Lactate
Saline
Oxamate
L-Lactate (nmol/µl)
Time (h)

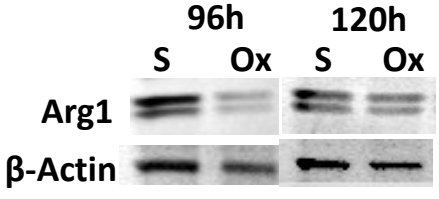
i)
96h
120h
S
Ox
S
Ox
Arg1
β-Actin

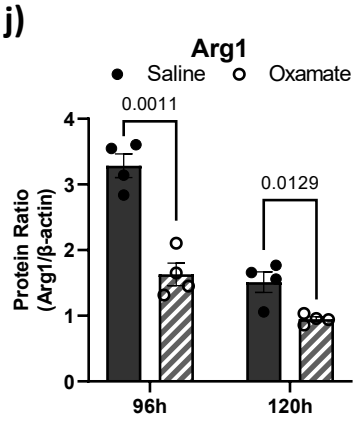
j)
Arg1
Saline
Oxamate
0.0011
0.0129
Protein Ratio
(Arg1/β-actin)
96h
120h

Figure 5.4: Sodium Oxamate (Ox) prolongs ZIP resolution timeline.
C57BL/6 wild-type mice were injected intraperitoneally with 1 mg per mouse Zymosan A, followed by 500 mg per kg Oxamate or saline 24 hours later. Mice were euthanized at specified times from Zymosan injection by CO_2, and then peritoneal lavage was collected for further analysis. a) Oxamate intervention ZIP resolution timeline. b) Neutrophil frequency over time (n=3). c) Monocyte frequency over time (n=3). d) Macrophage frequency over time (n=3). e) Cellular L-lactate levels over time (n=3). f) Extracellular L-lactate levels over time (n=3). g) Representative western blot of histone lactylation (KLA) over time. h) Quantification KLA at 96h and 120h of the ZIP resolution timeline (n=3). i) Representative western blot of Arginase 1 (Arg1) over time. j) Quantification Arg1 at 96h and 120h of the ZIP resolution timeline (n=3). Data are presented as the mean of biological replicates +/- SEM. Statistical analysis by multiple unpaired t-tests with Holm-Šídák correction. N refers to the number of mice.

5.2.4 Alternative implications of lactate accumulation.

Lactate is commonly produced as three isomers: L-lactate, D-lactate, and racemic DL-lactate. L-lactate is the main form in the human body and can be metabolized from pyruvate to lactate by L-lactate dehydrogenase (L-LDH). On the other hand, D-lactate is a primary metabolite in gut bacteria (152). However, recent studies have discovered that D-LDH is expressed in human and mammalian mitochondria (153). Mitochondrial D-LDH converts D-lactate to pyruvate as part of methylglyoxal detoxification using Cytochrome C as an electron acceptor (154, 155). Lysine D-lactylation is said to occur but by a non-enzymatic acyl transfer (156). The extent to which histone D-lactylation participates in the lactate clock to initiate post-inflammatory resolution remains to be studied (83, 127, 157, 158). We measured cellular D-Lactate by colorimetric assay and identified relatively high D-Lactate during zymosan-induced peritonitis accumulating in a very similar pattern to L-Lactate. Treatment with sodium oxamate also significantly decreased cellular D-lactate (**Figure 5.5a**). However, extra-cellular D-lactate was very low, and thus, the zymosan-induced peritonitis D-lactate accumulation cannot be

dismissed as gut bacteria leakage from mistaken colon perforation (**Figure 5.5b**). It, therefore, follows that D-lactate and L-lactate may be participating in the lactate clock response.

Figure 5.5

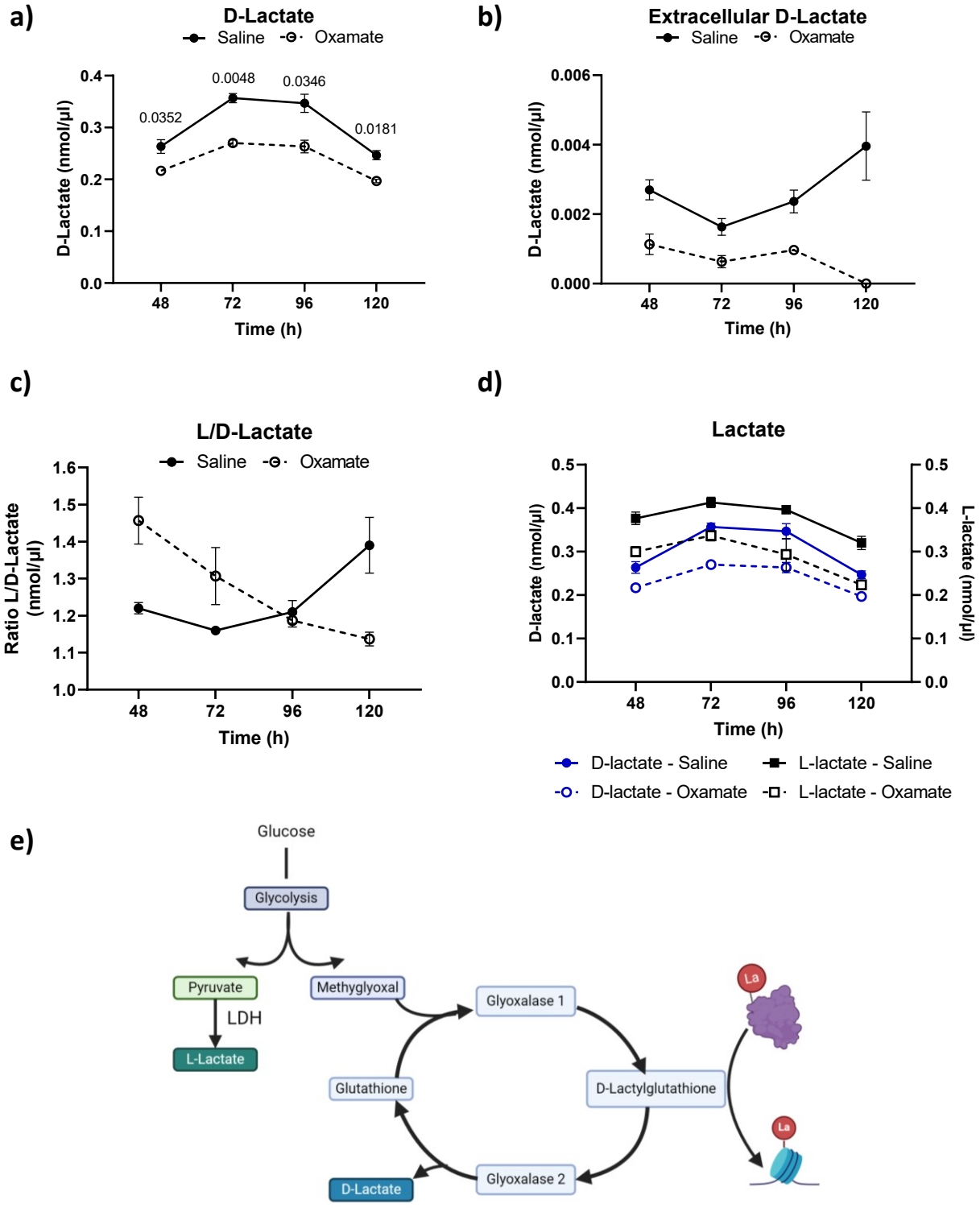

Figure 5.5: D-lactate present during ZIP resolution.
C57BL/6 wild-type mice were injected intraperitoneally with 1 mg per mouse Zymosan A, followed by 500 mg per kg Oxamate or saline 24 hours later. Mice were euthanized at specified times from Zymosan injection by CO2, and then peritoneal lavage was collected for further analysis. a) Cellular D-lactate levels over time (n=3). b) Extracellular D-lactate levels over time (n=3). c) Ratio of cellular L vs D lactate over time (n=3). d) Cellular D-lactate levels in comparison to L-lactate (n=3). Data are presented as the mean of biological replicates +/- SEM. Statistical analysis by multiple unpaired t-tests with Holm-Šídák correction. N refers to the number of mice.

5.2 Conclusions

In conclusion, while we are unsure to what extent D-lactylation or alternate post-translational modification participates in the lactate clock response, we can confirm that MYLS22-mediated mitochondrial fragmentation promotes inflammation resolution *in vivo*, in part by a shift in the lactate clock. Furthermore, impairing lactate accumulation via sodium oxamate promotes inflammation *in vivo*. Thus, histone lactylation is a key component of *in vivo* inflammation resolution induced by mitochondrial fragmentation-mediated lactate accumulation.

Chapter 6: Discussion

6.1 The implications of mitochondrial dynamics in cellular inflammatory responses

Until recently, mitochondrial fission and fusion were believed to be adaptations to meet the metabolic demands of the cell. However, more recent evidence demonstrates that mitochondrial fission and fusion produce specific signals to other organelles to dictate cell differentiation and cell phenotype. For example, neural and muscle stem cell self-renewal is maintained by an elongated mitochondrial network, which produces low ROS stimulation and activates Notch signalling, whereas mitochondrial fragmentation leads to higher ROS levels, activation of NRF2 and transcriptional activation of neuronal commitment program (65, 68, 70). In T cells, commitment to an effector or memory cell phenotype is driven by OPA1 by controlling cristae morphology, thereby impacting metabolic potential. Effector T cells are characterized as having a fission-associated expansion of cristae, leading to inefficient oxidative phosphorylation and a compensatory use of glycolysis as a primary form of metabolism (74). These studies indicate that mitochondrial dynamism is not only a consequence of the cellular environment but rather plays a vital functional role in determining cellular phenotype and function. In this study, we find that a fragmented mitochondrial network is found in macrophages during the pro-resolving phase of inflammation. Mechanistically, this occurs via a faster accumulation of lactate, resulting in the lactylation of histones and a quicker shift towards an anti-inflammatory phenotype. These data are the first to show that mitochondrial dynamics regulate

epigenetic modification of pro-resolving genes in macrophages in response to inflammatory cues.

Previously, LPS was shown to induce a fragmented mitochondrial phenotype, which correlates with the increased glycolysis associated with M1 polarization (107, 108). In contrast, in the present study, we found M1 macrophages have a distinctly elongated mitochondrial network. We evaluated mitochondrial length by staining for an outer membrane protein, Tom20, which is *(i)* not subject to changes in mitochondrial leakage (as is the case with Mitotracker), *(ii)* distinct from other measures of inner mitochondrial membrane proteins that may change with metabolic shifts (i.e. complex I) and *(iii)* more robustly reflects the mitochondrial membrane structure and length (68, 109, 110). Additionally, mitochondrial dyes used in live cell imaging can be toxic to cells and thus cause additional mitochondrial stress, which may be exacerbated upon co-stimulation with inflammatory factors like LPS. We performed additional analyses of mitochondrial length and dynamism using transmission electron microscopy (TEM) where we quantified cristae width and the ratio of mitochondria undergoing dynamic events vs static mitochondria, both of which increased in M1-like macrophages. Elongated mitochondrial networks were also seen in M1 polarized human THP1 macrophages, in murine BMDMs upon pro-inflammatory oxidized low-density lipoprotein (OxLDL) stimulation and in *ex vivo* peritoneal macrophages from mice fed a high-cholesterol diet for 2 weeks. Furthermore, in comparing detailed protocols between our study and those showing fragmented mitochondria upon LPS stimulation, we determined another source of discrepancy based on media supplementation with sodium pyruvate. Sodium pyruvate feeds

into both the TCA cycle and lactate biosynthesis, altering the metabolic pressure presumed to induce mitochondrial network morphology changes (159, 160). Differences in mitochondrial length induced by LPS stimulation can be reduced in correlation with increasing concentrations of sodium pyruvate. In addition, using all the same characterization methods, we found that M2 macrophages and post-inflammatory resolving macrophages have a fragmented mitochondrial morphology. In conclusion, while specific methodologies used across different studies likely account for the different findings of mitochondrial morphology, we conclude that pro-inflammatory macrophages have a predominantly elongated mitochondrial network, whereas resting and M2 macrophages have a predominantly fragmented mitochondrial network.

Previous studies have demonstrated a role for key mitochondrial fission and fusion proteins, namely DRP1, MFN2 and OPA1, in macrophage inflammatory responses, sometimes with disparate results (161–171). Genetic deletion of *Drp1*- a critical mediator of mitochondrial fission- leads to reduced inflammatory responses measured by cytokine expression (107). Additionally, Drp1-mediated ER tethering is required for the phagocytosis of apoptotic bodies (172). Efferocytosis of apoptotic bodies is a critical M2 macrophage function. Similarly, genetic deletion of either *Mfn2* or *Opa1*- each of whom promote mitochondrial fusion- also results in reduced inflammatory gene activation. Collectively, these data suggest that macrophages require a functional and dynamic mitochondrial network to maintain inflammatory responses. It is possible that deletion of a single member of the fission or fusion machinery may have

non-mitochondrial effects (e.g. the non-mitochondrial functions of *Drp1* are also lost) and/or complete loss of these key proteins may result in adaptations that alter cell function. Using an alternative approach, using siRNA knockdown of all 3 major fission or fusion proteins, we similarly observed that loss of functional mitochondrial fission or fusion resulted in impaired cytokine expression in unstimulated cells. However, we observed that loss of mitochondrial fusion machinery in response to LPS resulted in increased *Il1b* gene expression and secretion despite a decrease in the canonical NFκB subunit, p65. Indeed, genetic deletion of *Opa1*, which also demonstrated reduced p65, also resulted in increased IL-1β secretion (115). The authors did not discuss these discrepant findings, but our studies reveal that ATF4 and phospho-c-Jun alternative pro-inflammatory transcription factors are increased when mitochondrial fusion is lost. Therefore, despite lower baseline levels of cytokine expression, the lack of mitochondrial ability to undergo fusion activates the ATF4/cJun axis in response to LPS stimulation, which is likely an explanation for the elevated *Il1b* in these macrophages. It is possible that loss of *Opa1* throughout macrophage differentiation (i.e. genetic loss in bone-marrow-derived macrophage in culture) could impact inflammatory transcriptional pathway differently than the more acute loss of all 3 major fusion mediators, OPA1, MFN1 and MFN2, in mature macrophages. Nevertheless, these data collectively indicate that mitochondrial dynamics, particularly mitochondrial fusion, controls macrophage inflammatory responses.

6.2 Post-inflammatory resolution responses

Following the pro-inflammatory response, in order to return to baseline, macrophages need to adopt an anti-inflammatory and pro-resolving phenotype. This requires the dampening

of pro-inflammatory cytokine production, the activation of pro-reparative gene programs and a switch to an oxidative metabolic phenotype. Arginase 1 is a key mediator of pro-reparative macrophage responses, where it is turned on during the resolution phase to promote the production of proline and polyamines for wound repair and proliferation (173–175). *Arg1* expression is high in M2 macrophages (i.e. upon IL-4 stimulation) and is traditionally viewed as a canonical M2 marker. However, over time following LPS stimulation, *Arg1* expression gradually increases as it engages these pro-resolving programs (173–176). We therefore investigated whether mitochondrial fragmentation and fusion regulate macrophage anti-inflammatory/pro-resolving responses by altering *Arg1* expression following both pro- and anti-inflammatory stimuli. In unstimulated macrophages, preventing mitochondrial fusion increased *Arg1* gene expression which was exacerbated upon LPS stimulation. *Arg1* was similarly increased with IL-4 stimulation. Macrophage phagocytic capacity, a key function of pro-resolving macrophages, was also elevated when mitochondrial fusion was impaired. Our data demonstrate that, by promoting a pro-resolving macrophage phenotype with IL-4 or using a phenocopy siRNA approach, a fragmented mitochondrial network promotes *Arg1* expression and pro-resolving functions in macrophages.

Inflammatory stimulation in macrophages results in high rates of glycolysis as a primary form of metabolism. This results in the accumulation of lactate through lactate dehydrogenase conversion of pyruvate. Recently, lactate and its derivative lactly-CoA have been attributed to a novel form of histone modification known as lactylation,

which activates homeostatic reparatory pathways producing pro-resolving stimuli such as ARG1 (92, 95, 123, 128, 129). Given that promoting mitochondrial fragmentation increased *Arg1* expression following inflammatory stimulation, we hypothesized that this could be a result of increased lactate accumulation and histone lactylation. Indeed, knocking down the mitochondrial fusion machinery resulted in increased lactate and KLA levels after of LPS stimulation. The observed increase in lactate could be a result of decreased pyruvate conversion to acetyl -CoA through the pyruvate dehydrogenase (PDH) pathway, resulting in more pyruvate conversion to lactate via the lactate dehydrogenase (LDH) pathway. Indeed, inhibition of mitochondrial fusion resulted in decreased PDH protein expression, and subsequent blocking of LDH activity prevented the increase in ARG1 expression. Recently, PDH and its inhibitor PDHK have been associated with mitochondrial morphology in the setting of NLRP3 inflammasome activation, which aligns with our findings (127, 130, 177). In summary, by promoting mitochondrial fission in a pro-inflammatory setting results in a shift towards the M2 state through inhibition of PDH, therefore, increasing lactate levels, allowing for histone lactylation and the induction of pro-resolving factors such as ARG1. Whether the lactylation is primarily mediated via a lactyl-CoA dependent mechanism or through a non-enzymatic S-to-N acyl transfer from the glyoxalase cycle intermediate, lactylglutathione (LGSH) remains to be determined (157, 178–182).

In addition to lactate accumulation, the M1 shift towards glycolysis results in the accumulation of multiple by-products that could impact macrophage reparatory programs. The induction of glycolysis mediated by LPS stimulation in macrophages induces two major breaks

in the TCA cycle, resulting in an accumulation of citrate and succinate (23). The succinate is then released into the cytosol, where it can act as a signal that stabilizes HIF1α, inducing pro-inflammatory IL-1β transcription. Succinate can also generate a redox signal by driving mitochondrial ROS production at complex I by reverse electron transport (RET), which also promotes HIF1α. Later in inflammation, the expression of the immune-regulated gene 1 (IRG1) protein in mitochondria can lead to the generation of itaconate from the accumulated citrate. Itaconate inhibits succinate dehydrogenase (SDH) to limit ROS production in response to succinate. Itaconate is also released into the cytosol, where it modifies KEAP1, leading to NRF2 activation and promoting the expression of anti-inflammatory and antioxidant genes (80). Itaconate also induces ATF3, an anti-inflammatory transcription factor. The induction of itaconate by IRG1 could be another part of the macrophage post-inflammatory resolution machinery (26). The impact of mitochondrial fragmentation on IRG1-mediated itaconate accumulation and how lactate may influence this process remains to be explored.

6.3 Alternative lactate mechanisms

The work of this thesis identifies an accumulation of lactate both upon late-stage pro-inflammatory stimulation and upon impaired mitochondrial fusion. This was linked to the induction of histone lactylation turning on post-inflammatory resolution response programs in macrophages. However, recently, lactate itself has been identified as a binding partner of sentrin-specific protease 1 (SENP1), thereby stabilizing the SUMOylation of anaphase-promoting complex (APC), and controlling cell cycle and

proliferation in multiple cancer cell lines (183). In macrophages, SENP1 is upregulated under pro-inflammatory LPS stimulation, promoting the de-SUMOylation of KLF4. De-SUMOylated KLF4 releases p300/CBP-associated factor (PCAF), which enhances the activity of the NF-κB mediated pro-inflammatory signalling (184, 185). Taken together, this suggests that lactate may act as a self-regulating binding factor of SENP1 to prevent de-SUMOylation of KLF4, helping to restore homeostasis post-inflammation. Whether promoting mitochondrial fragmentation induces enough lactate to effectively bind SENP1 remains to be determined. However, this provides another method by which macrophages may restore homeostasis via lactate accumulation.

Because of carbon atom asymmetry, lactate is commonly produced as three isomers: L-lactate, D-lactate, and racemic DL-lactate. L-lactate is the main form in the human body and can be produced from conversion of pyruvate to lactate by L-lactate dehydrogenase (L-LDH). On the other hand, D-lactate is a primary metabolite in gut bacteria (152). Generally, D-LDH is not present in mammals, however, D-lactate can alternatively be converted from pyruvate by D-α-hydroxy acid dehydrogenase, which is only active in a minimal pH range and undergoes catalysis very slowly. The evidence to date has identified that under normal conditions, human D-lactate is not abundant enough to initiate proper catabolism (186). However, recent studies have discovered that D-LDH is expressed in human and mammalian mitochondria (153). Mitochondrial D-LDH converts D-lactate to pyruvate as part of methylglyoxal detoxification using Cytochrome C as an electron acceptor (154, 155). Moreover, D-lactate is metabolized more readily than initially thought, as confirmed by D-lactate half-life studies in plasma and

urine after infusion or oral administration (158, 187). Additionally, D-lactate may be involved in the transport of metabolic substrates in vivo. It is now believed that D-lactate/malate reverse transporters are located in the mitochondrial intima, where D-pyruvate is transported after mitochondrial D-LDH-mediated oxidation, and malic acid is transported in the reverse direction to the cytoplasm (186). Lysine D-lactylation is said to occur but by a non-enzymatic acyl transfer (156). The extent to which histone D-lactylation participates in the lactate clock to initiate post-inflammatory resolution remains to be studied (83, 127, 157, 158). We measured cellular D-Lactate by colorimetric assay and identified relatively high D-Lactate during zymosan-induced peritonitis accumulating in a very similar pattern to L-Lactate. Treatment with sodium oxamate also significantly decreased cellular D-lactate. However, extra-cellular D-lactate was very low, and thus, the zymosan-induced peritonitis D-lactate accumulation cannot be dismissed as gut bacteria leakage from mistaken colon perforation. To what extent D vs L lactate participates in the lactate clock response requires further exploration.

The recent identification of non-enzymatic lactylglutathione (LGSH) mediated acyl transfer directly links histone lactylation with the glyoxalase pathway and D-lactate production (157, 188–190). If the primary form of histone lactly-lysine transfer comes from LGSH as opposed to enzymatic acyltransferases common in other post-translational histone modifications such as acetylation, this provides a self-regulatory method for the production of L vs D lactate. Within the glyoxalase pathway, LGSH can transfer the lactyl group to a histone or feed into glyoxalase 2 (GLO2), producing D-

lactate (178). Therefore, if the primary form of lactyl-transfer is non-enzymatic, we would expect decreased D-lactate when histone lactylation is being mediated. In our in-vivo resolution model, we observed no decrease in D-lactate at 72h and 96h when histone lactylation was being initiated and identified. This data suggests that non-enzymatic acyl transfer is most likely not the primary method of histone lactylation. However, we did identify that the lowest ratio of L vs D lactate was at 72h when lactylation was being initiated; therefore, LGSH-mediated lactyl transfer could still be contributing to the lactate clock post-resolution response. One way to fully elucidate to what proportion LGSH mediated acyl transfer impacts the lactate clock would be to identify the proportion of L vs D lactly isomers on histones via mass spectrometry and experiments are ongoing to assess this.

6.4 Therapeutic implications of targeting mitochondrial dynamics

Our model reveals that macrophages naturally adopt a fragmented mitochondrial phenotype over time following LPS stimulation, which corresponds to the activation of epigenetic changes and increase in Arginase 1 expression and the adoption of a pro-resolving response. Moreover, this process can be accelerated by forcing a fragmented mitochondrial phenotype. This shift in resolution response timeline can also be seen *in vivo* during zymosan-induced peritonitis. This data suggests that inducing fragmentation could be a viable target to promote M2 macrophage phenotype; however, promoting M2 is only beneficial in specific contexts. During cancer progression, a more anti-inflammatory phenotype could lead to increased cancer growth/metastasis through impaired immune detection and a dampening of the cytotoxic inflammatory response. Indeed, tumour-associated macrophages often display

M2-like characteristics and metabolism (191–199). In contrast, in the context of chronic inflammation like that which is found in atherosclerosis and obesity, blocking mitochondrial fusion or promoting mitochondrial fragmentation could promote tissue repair and more rapid resolution. Indeed, M1-like macrophages are abundant within the atherosclerotic plaque and obese adipose tissue, and previous reports have shown that DRP1-mediated mitochondrial fission is essential for efficient efferocytosis and atherosclerosis regression (100, 172, 200–202). We also see an elongated M1-like mitochondrial phenotype under lipid loading conditions both *in vitro* and *ex vivo*, suggesting that preventing mitochondrial fusion in these settings may be beneficial. This theory is supported by recent findings that hearts deficient in fusion machinery MFN1 and MFN2 are protected against acute myocardial infarction (56) and OPA1 deletion has been shown to increase macrophage persistence in muscle regeneration models (115). More work remains to be done to determine the disease and cell-specific context where impaired fusion could be of maximum benefit.

6.5 Study limitations & conclusions

The data presented within this thesis makes a link between changes in mitochondrial morphology and lactate accumulation, which has been associated with promoting post-inflammatory resolution via histone lactylation. We have observed the impact of mitochondrial fragmentation on lactate, histone lactylation and arginase 1. However, as discussed above, lactate can impact post-inflammatory resolution in more ways than the defined lactate clock mechanism. There are several gaps in our observations which may clarify this mechanism. If

histone lactylation via enzymatic acyl transfer is the major mechanism behind the M2-like reparatory *Arg1* expression, we would expect an increase in Lactyl-CoA as well. Alternatively, if the post-inflammatory programming is mediated LGSH lactyl transfer we would expect an increase in LGSH. There could be lactylation of other pro-resolving proteins via either lactyl transfer mechanism that could be adding to the resolution responses we have identified. Additionally, lactate itself could be binding to other proteins, such as SENP1, to further promote inflammation resolution. We can conclude that mitochondrial fragmentation promotes lactate accumulation and inflammatory resolution however, due to the limit of our observations, we can only associate it with histone lactylation. The method of lactylation and other potential pro-reparatory programs remains to be seen.

In conclusion, mitochondrial dynamics play a critical role in directing macrophage function and phenotype. Mitochondrial fusion uniquely controls the late-stage resolving phase of inflammation by controlling metabolite levels and pro-reparative gene expression programs.

References

1. Susser LI, Nguyen M-A, Geoffrion M, Emerton C, Ouimet M, Khacho M, Rayner KJ. 2023. Mitochondrial Fragmentation Promotes Inflammation Resolution Responses in Macrophages via Histone Lactylation. Mol Cell Biol 43:531–546.

2. Chaplin DD. 2010. Overview of the immune response. J Allergy Clin Immunol 125:S3-23.

3. Villani A-C, Sarkizova S, Hacohen N. 2018. Systems Immunology: Learning the Rules of the Immune System. Annu Rev Immunol 36:813–842.

4. Akira S, Uematsu S, Takeuchi O. 2006. Pathogen recognition and innate immunity. Cell 124:783–801.

5. Marshall JS, Warrington R, Watson W, Kim HL. 2018. An introduction to immunology and immunopathology. Allergy Asthma Clin Immunol 14:49.

6. Turvey SE, Broide DH. 2010. Innate immunity. J Allergy Clin Immunol 125:S24-32.

7. Clark M, Kroger CJ, Tisch RM. 2017. Type 1 Diabetes: A Chronic Anti-Self-Inflammatory Response. Front Immunol 8:1898.

8. Miljković D, Spasojević I. 2013. Multiple sclerosis: molecular mechanisms and therapeutic opportunities. Antioxid Redox Signal 19:2286–334.

9. de Mattos BRR, Garcia MPG, Nogueira JB, Paiatto LN, Albuquerque CG, Souza CL, Fernandes LGR, Tamashiro WM da SC, Simioni PU. 2015. Inflammatory Bowel Disease: An Overview of Immune Mechanisms and Biological Treatments. Mediators Inflamm 2015:493012.

10. Deeks SG, Walker BD. 2007. Human immunodeficiency virus controllers: mechanisms of durable virus control in the absence of antiretroviral therapy. Immunity 27:406–16.

11. Allegra A, Tonacci A, Musolino C, Pioggia G, Gangemi S. 2021. Secondary Immunodeficiency in Hematological Malignancies: Focus on Multiple Myeloma and Chronic Lymphocytic Leukemia. Front Immunol 12.

12. van Furth R, Cohn ZA, Hirsch JG, Humphrey JH, Spector WG, Langevoort HL. 1972. The mononuclear phagocyte system: a new classification of macrophages, monocytes, and their precursor cells. Bull World Health Organ 46:845–52.

13. Takahashi K, Yamamura F, Naito M. 1989. Differentiation, maturation, and proliferation of macrophages in the mouse yolk sac: A light-microscopic, enzyme-cytochemical, immunohistochemical, and ultrastructural study. J Leukoc Biol 45:87–96.

14. Ginhoux F, Guilliams M. 2016. Tissue-Resident Macrophage Ontogeny and Homeostasis. Immunity 44:439–449.

15. Guilliams M, Ginhoux F, Jakubzick C, Naik SH, Onai N, Schraml BU, Segura E, Tussiwand R, Yona S. 2014. Dendritic cells, monocytes and macrophages: a unified nomenclature based on ontogeny. Nat Rev Immunol 14:571.

16. Mass E, Nimmerjahn F, Kierdorf K, Schlitzer A. 2023. Tissue-specific macrophages: how they develop and choreograph tissue biology. Nat Rev Immunol 23:563–579.

17. Winkels H, Ehinger E, Vassallo M, Buscher K, Dinh HQ, Kobiyama K, Hamers AAJ, Cochain C, Vafadarnejad E, Saliba A-E, Zernecke A, Pramod AB, Ghosh AK, Anto Michel N, Hoppe N, Hilgendorf I, Zirlik A, Hedrick CC, Ley K, Wolf D. 2018. Atlas of the Immune Cell Repertoire in Mouse Atherosclerosis Defined by Single-Cell RNA-Sequencing and Mass Cytometry. Circ Res 122:1675–1688.

18. Gu W, Ni Z, Tan YQ, Deng J, Zhang SJ, Lv ZC, Wang XJ, Chen T, Zhang Z, Hu Y, Jing ZC, Xu Q. 2019. Adventitial Cell Atlas of wt (Wild Type) and ApoE (Apolipoprotein E)-Deficient Mice Defined by Single-Cell RNA Sequencing. Arterioscler Thromb Vasc Biol 39:1055–1071.

19. Tabas I, Bornfeldt KE. 2016. Macrophage Phenotype and Function in Different Stages of Atherosclerosis. Circ Res 118:653–667.

20. Takeuchi O, Akira S. 2010. Pattern recognition receptors and inflammation. Cell 140:805–20.

21. BIORAD. 2016. Macrophage Polarization Mini Review.

22. Galván-Peña S, O'Neill LAJ. 2014. Metabolic reprogramming in macrophage polarization. Front Immunol 5:1–6.

23. O'Neill LAJ, Kishton RJ, Rathmell J. 2016. A guide to immunometabolism for immunologists. Nat Rev Immunol 16:553–65.

24. Mills E, O'Neill LAJ. 2014. Succinate: a metabolic signal in inflammation. Trends Cell Biol 24:313–320.

25. Williams NC, O'Neill LAJ. 2018. A Role for the Krebs Cycle Intermediate Citrate in Metabolic Reprogramming in Innate Immunity and Inflammation. Front Immunol 9:141.

26. Murphy MP, O'Neill LAJ. 2018. Krebs Cycle Reimagined: The Emerging Roles of Succinate and Itaconate as Signal Transducers. Cell 174:780–784.

27. Mills EL, Kelly B, Logan A, Costa ASH, Varma M, Bryant CE, Tourlomousis P, Däbritz JHM, Gottlieb E, Latorre I, Corr SC, McManus G, Ryan D, Jacobs HT, Szibor M, Xavier RJ, Braun T, Frezza C, Murphy MP, O'Neill LA. 2016. Succinate Dehydrogenase Supports Metabolic Repurposing of Mitochondria to Drive Inflammatory Macrophages. Cell 167:457-470.e13.

28. Tan H-Y, Wang N, Li S, Hong M, Wang X, Feng Y. 2016. The Reactive Oxygen Species in Macrophage Polarization: Reflecting Its Dual Role in Progression and Treatment of Human Diseases. Oxid Med Cell Longev 2016.

29. Ying W, Cheruku PS, Bazer FW, Safe SH, Zhou B. 2013. Investigation of macrophage polarization using bone marrow derived macrophages. J Vis Exp https://doi.org/10.3791/50323.

30. Gordon S, Martinez FO. 2010. Alternative Activation of Macrophages: Mechanism and Functions. Immunity 32:593–604.

31. Rodríguez-Prados J-C, Través PG, Cuenca J, Rico D, Aragonés J, Martín-Sanz P, Cascante M, Boscá L. 2010. Substrate Fate in Activated Macrophages: A Comparison between Innate, Classic, and Alternative Activation. The Journal of Immunology 185:605–614.

32. Pesce JT, Ramalingam TR, Mentink-Kane MM, Wilson MS, Kasmi KCE, Smith AM, Thompson RW, Cheever AW, Murray PJ, Wynn TA. 2009. Arginase-1–Expressing Macrophages Suppress Th2 Cytokine–Driven Inflammation and Fibrosis. PLoS Pathog 5:1000371.

33. Libby P. 2003. Vascular biology of atherosclerosis: overview and state of the art. Am J Cardiol 91:3–6.

34. Moore KJ, Sheedy FJ, Fisher EA. 2013. Macrophages in atherosclerosis: a dynamic balance. Nat Rev Immunol 13:709–721.

35. Moore KJ, Tabas I. 2011. Macrophages in the pathogenesis of atherosclerosis. Cell 145:341–355.

36. Tabas I. 2010. Macrophage death and defective inflammation resolution in atherosclerosis. Nat Rev Immunol 10:36–46.

37. Mills EL, Kelly B, O'Neill LAJ. 2017. Mitochondria are the powerhouses of immunity. Nat Immunol 18:488–498.

38. Ballinger SW. 2005. Mitochondrial dysfunction in cardiovascular disease. Free Radic Biol Med 38:1278–1295.

39. Madamanchi NR, Runge MS. 2007. Mitochondrial dysfunction in atherosclerosis. Circ Res 100:460–473.

40. Shutt T, Geoffrion M, Milne R, McBride HM. 2012. The intracellular redox state is a core determinant of mitochondrial fusion. EMBO Rep 13:909–915.

41. Yue W, Zhu Y, Wang H, Cao C, Chen Q, Liu M, Du L, Zhou J, Tian W, Li D, Song P, Wang B. 2011. Parkin Ubiquitinates Drp1 for Proteasome-dependent Degradation. Journal of Biological Chemistry 286:11649–11658.

42. Polyakov VY, Soukhomlinova MY, Fais D. 2003. Fusion, fragmentation, and fission of mitochondria. Biochemistry (Mosc) 68:838–49.

43. Kleele T, Rey T, Winter J, Zaganelli S, Mahecic D, Perreten Lambert H, Ruberto FP, Nemir M, Wai T, Pedrazzini T, Manley S. 2021. Distinct fission signatures predict mitochondrial degradation or biogenesis. Nature 593:435–439.

44. Chakrabarti R, Ji W-K, Stan R V., de Juan Sanz J, Ryan TA, Higgs HN. 2018. INF2-mediated actin polymerization at the ER stimulates mitochondrial calcium uptake, inner membrane constriction, and division. Journal of Cell Biology 217:251–268.

45. Kraus F, Ryan MT. 2017. The constriction and scission machineries involved in mitochondrial fission. J Cell Sci 130:2953–2960.

46. Kamerkar SC, Kraus F, Sharpe AJ, Pucadyil TJ, Ryan MT. 2018. Dynamin-related protein 1 has membrane constricting and severing abilities sufficient for mitochondrial and peroxisomal fission. Nat Commun 9:5239.

47. Doblado L, Lueck C, Rey C, Samhan-arias AK, Prieto I, Stacchiotti A, Monsalve M. 2021. Mitophagy in Human Diseases. Int J Mol Sci 22:3903.

48. Ma K, Chen G, Li W, Kepp O, Zhu Y, Chen Q. 2020. Mitophagy, Mitochondrial Homeostasis, and Cell Fate. Front Cell Dev Biol 8:531786.

49. Picca A, Faitg J, Auwerx J, Ferrucci L, D'Amico D. 2023. Mitophagy in human health, ageing and disease. Nature Metabolism 2023 5:12 5:2047–2061.

50. Chen G, Kroemer G, Kepp O. 2020. Mitophagy: An Emerging Role in Aging and Age-Associated Diseases. Front Cell Dev Biol 8:527573.

51. Colpman P, Dasgupta A, Archer SL. 2023. The Role of Mitochondrial Dynamics and Mitotic Fission in Regulating the Cell Cycle in Cancer and Pulmonary Arterial Hypertension: Implications for Dynamin-Related Protein 1 and Mitofusin2 in Hyperproliferative Diseases. Cells 12:1897.

52. Jahani-Asl A, Germain M, Slack RS. 2010. Mitochondria: Joining forces to thwart cell death. Biochimica et Biophysica Acta (BBA) - Molecular Basis of Disease 1802:162–166.

53. Cogliati S, Frezza C, Soriano ME, Varanita T, Quintana-Cabrera R, Corrado M, Cipolat S, Costa V, Casarin A, Gomes LC, Perales-Clemente E, Salviati L, Fernandez-Silva P, Enriquez JA, Scorrano L. 2013. Mitochondrial Cristae Shape Determines Respiratory Chain Supercomplexes Assembly and Respiratory Efficiency. Cell 155:160–171.

54. MacVicar T, Langer T. 2016. OPA1 processing in cell death and disease - the long and short of it. J Cell Sci 129:2297–306.

55. Filadi R, Pendin D, Pizzo P. 2018. Mitofusin 2: from functions to disease. Cell Death Dis 9:330.

56. Hall AR, Burke N, Dongworth RK, Kalkhoran SB, Dyson A, Vicencio JM, Dorn GW, Yellon DM, Hausenloy DJ. 2016. Hearts deficient in both Mfn1 and Mfn2 are protected against acute myocardial infarction. Cell Death Dis 7:e2238–e2238.

57. Schrepfer E, Scorrano L. 2016. Molecular Cell Review Mitofusins, from Mitochondria to Metabolism. Mol Cell 61:683–694.

58. Pich S, Bach D, Briones P, Liesa M, Camps M, Testar X, Palacín M, Zorzano A. 2005. The Charcot–Marie–Tooth type 2A gene product, Mfn2, up-regulates fuel oxidation through expression of OXPHOS system. Hum Mol Genet 14:1405–1415.

59. Joshi AU, Saw NL, Shamloo M, Mochly-Rosen D. 2018. Drp1/Fis1 interaction mediates mitochondrial dysfunction, bioenergetic failure and cognitive decline in Alzheimer's disease. Oncotarget 9:6128–6143.

60. Santel A, Fuller MT, Okamoto K, Ryan MT. 2001. Control of mitochondrial morphology by a human mitofusin. J Cell Sci 114:867–74.

61. Aishwarya R, Alam S, Abdullah CS, Morshed M, Nitu SS, Panchatcharam M, Miriyala S, Kevil CG, Bhuiyan MS. 2020. Pleiotropic effects of mdivi-1 in altering mitochondrial dynamics, respiration, and autophagy in cardiomyocytes. Redox Biol 36:101660.

62. Hu J-R, Florido R, Lipson EJ, Naidoo J, Ardehali R, Tocchetti CG, Lyon AR, Padera RF, Johnson DB, Moslehi J. 2019. Cardiovascular toxicities associated with immune checkpoint inhibitors. Cardiovasc Res 115:854.

63. Evans MA, Sano S, Walsh K. 2020. Cardiovascular Disease, Aging, and Clonal Hematopoiesis. Annual Review of Pathology: Mechanisms of Disease 15:419–438.

64. Maxfield FR, Tabas I, de Juan-Sanz J, Barbosa-Lorenzi VC, Wang Y, Ryan TA, Yurdagul A, Cai B, Nomura M, Subramanian M. 2017. Mitochondrial Fission Promotes the Continued Clearance of Apoptotic Cells by Macrophages. Cell 171:331-345.e22.

65. Khacho M, Harris R, Slack RS. 2019. Mitochondria as central regulators of neural stem cell fate and cognitive function. Nat Rev Neurosci 20:34–48.

66. Khacho M, S. Slack R. 2015. Mitochondrial dynamics in neurodegeneration: from cell death to energetic states. AIMS Mol Sci 2:161–174.

67. Khacho M, Slack RS. 2018. Mitochondrial and Reactive Oxygen Species Signaling Coordinate Stem Cell Fate Decisions and Life Long Maintenance. Antioxid Redox Signal 28:1090–1101.

68. Khacho M, Clark A, Svoboda DS, Azzi J, MacLaurin JG, Meghaizel C, Sesaki H, Lagace DC, Germain M, Harper M-E, Park DS, Slack RS. 2016. Mitochondrial Dynamics Impacts Stem Cell Identity and Fate Decisions by Regulating a Nuclear Transcriptional Program. Cell Stem Cell 19:232–247.

69. Ahmed SMU, Luo L, Namani A, Wang XJ, Tang X. 2017. Nrf2 signaling pathway: Pivotal roles in inflammation. Biochimica et Biophysica Acta (BBA) - Molecular Basis of Disease 1863:585–597.

70. Baker N, Wade S, Triolo M, Girgis J, Chwastek D, Larrigan S, Feige P, Fujita R, Crist C, Rudnicki MA, Burelle Y, Khacho M. 2022. The mitochondrial protein OPA1 regulates the quiescent state of adult muscle stem cells. Cell Stem Cell 29:1315-1332.e9.

71. Pearce EL, Pearce EJ. 2013. Metabolic pathways in immune cell activation and quiescence. Immunity 38:633–43.

72. Van Velthoven CTJ, Rando TA. 2019. Stem Cell Quiescence: Dynamism, Restraint, and Cellular Idling. Cell Stem Cell https://doi.org/10.1016/j.stem.2019.01.001.

73. Cheung TH, Rando TA. 2013. Molecular regulation of stem cell quiescence. Nat Rev Mol Cell Biol https://doi.org/10.1038/nrm3591.

74. Buck MD, O'Sullivan D, Klein Geltink RI, Curtis JD, Chang C-H, Sanin DE, Qiu J, Kretz O, Braas D, van der Windt GJW, Chen Q, Huang SC-C, O'Neill CM, Edelson BT, Pearce EJ, Sesaki H, Huber TB, Rambold AS, Pearce EL. 2016. Mitochondrial Dynamics Controls T Cell Fate through Metabolic Programming. Cell 166:63–76.

75. Angiari S, Runtsch MC, Sutton CE, Pearce EL, Mills KHG, O'neill LAJ. 2020. Pharmacological Activation of Pyruvate Kinase M2 Inhibits CD4 + T Cell Pathogenicity and Suppresses Autoimmunity. Cell Metab 31:391–405.

76. Mills EL, O'Neill LA. 2016. Reprogramming mitochondrial metabolism in macrophages as an anti-inflammatory signal. Eur J Immunol 46:13–21.

77. Tannahill GM, Curtis AM, Adamik J, Palsson-Mcdermott EM, McGettrick AF, Goel G, Frezza C, Bernard NJ, Kelly B, Foley NH, Zheng L, Gardet A, Tong Z, Jany SS, Corr SC, Haneklaus M, Caffrey BE, Pierce K, Walmsley S, Beasley FC, Cummins E, Nizet V, Whyte M, Taylor CT, Lin H, Masters SL, Gottlieb E, Kelly VP, Clish C, Auron PE, Xavier RJ, O'Neill LAJ. 2013. Succinate is a danger signal that induces IL-1β via HIF-1α. Nature 496:238.

78. Kelly B, Tannahill GM, Murphy MP, O'Neill LAJ. 2015. Metformin inhibits the production of reactive oxygen species from NADH: Ubiquinone oxidoreductase to limit induction of interleukin-1β (IL-1β) and boosts interleukin-10 (IL-10) in lipopolysaccharide (LPS)-activated macrophages. Journal of Biological Chemistry 290:20348–20359.

79. Nadolski MJ, Tsimikas S, Harkewicz R, Magallon J, Koschinsky ML, Nguyen M, Tabas I, Liao X, Golenbock D, Feric NT, Moore KJ, Witztum JL, Seimon TA. 2010. Atherogenic Lipids and Lipoproteins Trigger CD36-TLR2-Dependent Apoptosis in Macrophages Undergoing Endoplasmic Reticulum Stress. Cell Metab 12:467–482.

80. Mills EL, Ryan DG, Prag HA, Dikovskaya D, Menon D, Zaslona Z, Jedrychowski MP, Costa ASH, Higgins M, Hams E, Szpyt J, Runtsch MC, King MS, McGouran JF, Fischer R, Kessler BM, McGettrick AF, Hughes MM, Carroll RG, Booty LM, Knatko E V., Meakin PJ, Ashford MLJ, Modis LK, Brunori G, Sévin DC, Fallon PG, Caldwell ST, Kunji ERS, Chouchani ET, Frezza C, Dinkova-Kostova AT, Hartley RC, Murphy MP, O'Neill LA. 2018. Itaconate is an anti-inflammatory metabolite that activates Nrf2 via alkylation of KEAP1. Nature 556:113–117.

81. Meiser J, Krämer L, Sapcariu SC, Battello N, Ghelfi J, D'Herouel AF, Skupin A, Hiller K. 2016. Pro-inflammatory Macrophages Sustain Pyruvate Oxidation through Pyruvate Dehydrogenase for the Synthesis of Itaconate and to Enable Cytokine Expression. J Biol Chem 291:3932–46.

82. Brooks GA. 2020. Lactate as a fulcrum of metabolism. Redox Biol 35:101454.

83. Li X, Yang Y, Zhang B, Lin X, Fu X, An Y, Zou Y, Wang J-X, Wang Z, Yu T. 2022. Lactate metabolism in human health and disease. Signal Transduct Target Ther 7:305.

84. Fantin VR, St-Pierre J, Leder P. 2006. Attenuation of LDH-A expression uncovers a link between glycolysis, mitochondrial physiology, and tumor maintenance. Cancer Cell 9:425–34.

85. Min B-K, Park S, Kang H-J, Kim DW, Ham HJ, Ha C-M, Choi B-J, Lee JY, Oh CJ, Yoo EK, Kim HE, Kim B-G, Jeon J-H, Hyeon DY, Hwang D, Kim Y-H, Lee C-H, Lee T, Kim J, Choi Y-K, Park K-G, Chawla A, Lee J, Harris RA, Lee I-K. 2019. Pyruvate Dehydrogenase Kinase Is a Metabolic Checkpoint for Polarization of Macrophages to the M1 Phenotype. Front Immunol 10:944.

86. Soreze Y, Boutron A, Habarou F, Barnerias C, Nonnenmacher L, Delpech H, Mamoune A, Chrétien D, Hubert L, Bole-Feysot C, Nitschke P, Correia I, Sardet C, Boddaert N, Hamel Y, Delahodde A, Ottolenghi C, De Lonlay P. 2013. Mutations in human lipoyltransferase gene LIPT1 cause a Leigh disease with secondary deficiency for pyruvate and alpha-ketoglutarate dehydrogenase. Orphanet J Rare Dis 8:192.

87. Perry JJP, Shin DS, Getzoff ED, Tainer JA. 2010. The structural biochemistry of the superoxide dismutases. Biochimica et Biophysica Acta (BBA) - Proteins and Proteomics 1804:245–262.

88. Ying W, Conclusions VI. 2008. Comprehensive Invited Review NAD /NADH and NADP /NADPH in Cellular Functions and Cell Death: Regulation and Biological Consequences. Antioxid Redox Signal 10.

89. Quinn WJ, Jiao J, TeSlaa T, Stadanlick J, Wang Z, Wang L, Akimova T, Angelin A, Schäfer PM, Cully MD, Perry C, Kopinski PK, Guo L, Blair IA, Ghanem LR, Leibowitz MS, Hancock WW, Moon EK, Levine MH, Eruslanov EB, Wallace DC, Baur JA, Beier UH. 2020. Lactate Limits T Cell Proliferation via the NAD(H) Redox State. Cell Rep 33:108500.

90. Izzo LT, Wellen KE. 2019. Lactate link metabolism to genes. Nature 574:492–493.

91. Wang C, Chen H, Zhang M, Zhang J, Wei X, Ying W. 2016. Malate-aspartate shuttle inhibitor aminooxyacetic acid leads to decreased intracellular ATP levels and altered cell cycle of C6 glioma cells by inhibiting glycolysis. Cancer Lett 378:1–7.

92. Zhang D, Tang Z, Huang H, Zhou G, Cui C, Weng Y, Liu W, Kim S, Lee S, Perez-Neut M, Ding J, Czyz D, Hu R, Ye Z, He M, Zheng YG, Shuman HA, Dai L, Ren B, Roeder RG, Becker L, Zhao Y. 2019. Metabolic regulation of gene expression by histone lactylation. Nature 574:575–580.

93. Irizarry-Caro RA, McDaniel MM, Overcast GR, Jain VG, Troutman TD, Pasare C. 2020. TLR signaling adapter BCAP regulates inflammatory to reparatory macrophage transition by promoting histone lactylation. Proc Natl Acad Sci U S A 117:30628–30638.

94. Noe JT, Rendon BE, Geller AE, Conroy LR, Morrissey SM, Young LEA, Bruntz RC, Kim EJ, Wise-Mitchell A, De Souza Rizzo MB, Relich ER, Baby B V., Johnson LA, Affronti HC, McMasters KM,

Clem BF, Gentry MS, Yan J, Wellen KE, Sun RC, Mitchell RA. 2021. Lactate supports a metabolic-epigenetic link in macrophage polarization. Sci Adv 7:8602.

95. Manoharan I, Prasad PD, Thangaraju M, Manicassamy S. 2021. Lactate-Dependent Regulation of Immune Responses by Dendritic Cells and Macrophages. Front Immunol 12:691134.

96. Cui H, Xie N, Banerjee S, Ge J, Jiang D, Dey T, Matthews QL, Liu R-M, Liu G. 2021. Lung Myofibroblasts Promote Macrophage Profibrotic Activity through Lactate-induced Histone Lactylation. Am J Respir Cell Mol Biol 64:115–125.

97. Zhao Y, Zhao B, Wang X, Guan G, Xin Y, Sun Y, Wang J, Guo Y, Zang Y. 2019. Macrophage transcriptome modification induced by hypoxia and lactate. Exp Ther Med 18:4811.

98. Caldwell RB, Toque HA, Priya Narayanan S, William Caldwell R. 1459. Arginase: an old enzyme with new tricks. Trends Pharmacol Sci 36:395–405.

99. Dowling JK, Afzal R, Gearing LJ, Cervantes-Silva MP, Annett S, Davis GM, De Santi C, Assmann N, Dettmer K, Gough DJ, Bantug GR, Hamid FI, Nally FK, Duffy CP, Gorman AL, Liddicoat AM, Lavelle EC, Hess C, Oefner PJ, Finlay DK, Davey GP, Robson T, Curtis AM, Hertzog PJ, Williams BRG, McCoy CE. 2021. Mitochondrial arginase-2 is essential for IL-10 metabolic reprogramming of inflammatory macrophages. Nature Communications 2021 12:1 12:1–14.

100. Yurdagul A, Subramanian M, Wang X, Crown SB, Ilkayeva OR, Darville L, Kolluru GK, Rymond CC, Gerlach BD, Zheng Z, Kuriakose G, Kevil CG, Koomen JM, Cleveland JL, Muoio DM, Tabas I. 2020. Macrophage Metabolism of Apoptotic Cell-Derived Arginine Promotes Continual Efferocytosis and Resolution of Injury. Cell Metab 31:518-533.e10.

101. Cowburn AS, Crosby A, Macias D, Branco C, Colaço RDDR, Southwood M, Toshner M, Alexander LEC, Morrell NW, Chilvers ER, Johnson RS. 2016. HIF2α-Arginase axis is essential for the development of pulmonary hypertension. Proc Natl Acad Sci U S A 113:8801–8806.

102. Ross EA, Devitt A, Johnson JR. 2021. Macrophages: The Good, the Bad, and the Gluttony. Front Immunol 12:708186.

103. Sheu KM, Hoffmann A. 2022. Functional Hallmarks of Healthy Macrophage Responses: Their Regulatory Basis and Disease Relevance. Annu Rev Immunol 40:295–321.

104. Mosser DM, Hamidzadeh K, Goncalves R. 2021. Macrophages and the maintenance of homeostasis. Cell Mol Immunol 18:579–587.

105. Mosser DM, Edwards JP. 2008. Exploring the full spectrum of macrophage activation. Nat Rev Immunol 8:958–969.

106. Rodríguez-Morales P, Franklin RA. 2023. Macrophage phenotypes and functions: resolving inflammation and restoring homeostasis. Trends Immunol 44:986–998.

107. Kapetanovic R, Afroz SF, Ramnath D, Lawrence GM, Okada T, Curson JE, Bruin J, Fairlie DP, Schroder K, St John JC, Blumenthal A, Sweet MJ. 2020. Lipopolysaccharide promotes Drp1-dependent mitochondrial fission and associated inflammatory responses in macrophages. Immunol Cell Biol 98:528–539.

108. Gao F, Reynolds MB, Passalacqua KD, Sexton JZ, Abuaita BH, O'Riordan MXD. 2021. The Mitochondrial Fission Regulator DRP1 Controls Post-Transcriptional Regulation of TNF-α. Front Cell Infect Microbiol 10:593805.

109. Patten DA, Wong J, Khacho M, Soubannier V, Mailloux RJ, Pilon-Larose K, MacLaurin JG, Park DS, McBride HM, Trinkle-Mulcahy L, Harper M, Germain M, Slack RS. 2014. OPA1-dependent cristae modulation is essential for cellular adaptation to metabolic demand. EMBO J 33:2676–2691.

110. Khacho M, Tarabay M, Patten D, Khacho P, MacLaurin JG, Guadagno J, Bergeron R, Cregan SP, Harper M-E, Park DS, Slack RS. 2014. Acidosis overrides oxygen deprivation to maintain mitochondrial function and cell survival. Nat Commun 5:3550.

111. Kelley N, Jeltema D, Duan Y, He Y. 2019. The NLRP3 Inflammasome: An Overview of Mechanisms of Activation and Regulation. Int J Mol Sci 20:3328.

112. He Y, Hara H, Núñez G. 2016. Mechanism and Regulation of NLRP3 Inflammasome Activation. Trends Biochem Sci 41:1012–1021.

113. Ichinohe T, Yamazaki T, Koshiba T, Yanagi Y. 2013. Mitochondrial protein mitofusin 2 is required for NLRP3 inflammasome activation after RNA virus infection. Proceedings of the National Academy of Sciences 110:17963–17968.

114. Park S, Won J-H, Hwang I, Hong S, Lee HK, Yu J-W. 2015. Defective mitochondrial fission augments NLRP3 inflammasome activation. Sci Rep 5:15489.

115. Sánchez-Rodríguez R, Tezze C, Agnellini AHR, Angioni R, Venegas FC, Cioccarelli C, Munari F, Bertoldi N, Canton M, Desbats MA, Salviati L, Gissi R, Castegna A, Soriano ME, Sandri M, Scorrano L, Viola A, Molon B. 2023. OPA1 drives macrophage metabolism and functional commitment via p65 signaling. Cell Death Differ 30:742–752.

116. Dorrington MG, Fraser IDC. 2019. NF-κB Signaling in Macrophages: Dynamics, Crosstalk, and Signal Integration. Front Immunol 10:705.

117. Zhou R, Yazdi AS, Menu P, Tschopp J. 2011. A role for mitochondria in NLRP3 inflammasome activation. Nature 469:221–225.

118. Lu Y-C, Yeh W-C, Ohashi PS. 2008. LPS/TLR4 signal transduction pathway. Cytokine 42:145–151.

119. Corcoran SE, O'Neill LAJ. 2016. HIF1α and metabolic reprogramming in inflammation. Journal of Clinical Investigation 126:3699–3707.

120. Zhang C, Bai N, Chang A, Zhang Z, Yin J, Shen W, Tian Y, Xiang R, Liu C. 2013. ATF4 is directly recruited by TLR4 signaling and positively regulates TLR4-trigged cytokine production in human monocytes. Cell Mol Immunol 10:84–94.

121. Koppula P, Zhuang L, Gan B. 2021. Cystine transporter SLC7A11/xCT in cancer: ferroptosis, nutrient dependency, and cancer therapy. Protein Cell 12:599–620.

122. Pourcet B, Pineda-Torra I. 2013. Transcriptional regulation of macrophage arginase 1 expression and its role in atherosclerosis. Trends Cardiovasc Med 23:143–152.

123. Dichtl S, Lindenthal L, Zeitler L, Behnke K, Schlösser D, Strobl B, Scheller J, El Kasmi KC, Murray PJ. 2021. Lactate and IL6 define separable paths of inflammatory metabolic adaptation. Sci Adv 7:3505–3528.

124. Bhattacharjee A, Shukla M, Yakubenko VP, Mulya A, Kundu S, Cathcart MK. 2013. IL-4 and IL-13 employ discrete signaling pathways for target gene expression in alternatively activated monocytes/macrophages. Free Radic Biol Med 54:1–16.

125. Yunna C, Mengru H, Lei W, Weidong C. 2020. Macrophage M1/M2 polarization. Eur J Pharmacol 877:1–9.

126. Liu Y, Xu R, Gu H, Zhang E, Qu J, Cao W, Huang X, Yan H, He J, Cai Z. 2021. Metabolic reprogramming in macrophage responses. Biomark Res 9:1.

127. Noe JT, Rendon BE, Geller AE, Conroy LR, Morrissey SM, Young LEA, Bruntz RC, Kim EJ, Wise-Mitchell A, Barbosa de Souza Rizzo M, Relich ER, Baby B V, Johnson LA, Affronti HC, McMasters KM, Clem BF, Gentry MS, Yan J, Wellen KE, Sun RC, Mitchell RA. 2021. Lactate supports a metabolic-epigenetic link in macrophage polarization. Sci Adv 7:eabi8602.

128. Chen A-N, Luo Y, Yang Y-H, Fu J-T, Geng X-M, Shi J-P, Yang J. 2021. Lactylation, a Novel Metabolic Reprogramming Code: Current Status and Prospects. Front Immunol 12:688910.

129. Xin Q, Wang H, Li Q, Liu S, Qu K, Liu C, Zhang J. 2022. Lactylation: a Passing Fad or the Future of Posttranslational Modification. Inflammation 45:1419–1429.

130. Meyers AK, Wang Z, Han W, Zhao Q, Zabalawi M, Duan L, Liu J, Zhang Q, Manne RK, Lorenzo F, Quinn MA, Song Q, Fan D, Lin H-K, Furdui CM, Locasale JW, McCall CE, Zhu X. 2023. Pyruvate dehydrogenase kinase supports macrophage NLRP3 inflammasome activation during acute inflammation. Cell Rep 42:111941.

131. Hollenberg AM, Smith CO, Shum LC, Awad H, Eliseev RA. 2020. Lactate Dehydrogenase Inhibition With Oxamate Exerts Bone Anabolic Effect. Journal of Bone and Mineral Research 35:2432–2443.

132. Altinoz MA, Ozpinar A. 2022. Oxamate targeting aggressive cancers with special emphasis to brain tumors. Biomedicine & Pharmacotherapy 147:112686.

133. Ye W, Zheng Y, Zhang S, Yan L, Cheng H, Wu M. 2016. Oxamate Improves Glycemic Control and Insulin Sensitivity via Inhibition of Tissue Lactate Production in db/db Mice. PLoS One 11.

134. Fredman G, Li Y, Dalli J, Chiang N, Serhan CN. 2012. Self-limited versus delayed resolution of acute inflammation: temporal regulation of pro-resolving mediators and microRNA. Sci Rep 2:639.

135. Kamaly N, Fredman G, Subramanian M, Gadde S, Pesic A, Cheung L, Fayad ZA, Langer R, Tabas I, Farokhzad OC. 2013. Development and in vivo efficacy of targeted polymeric inflammation-resolving nanoparticles. Proc Natl Acad Sci U S A 110:6506–6511.

136. Li X, Liu Z, Jin H, Fan X, Yang X, Tang W, Yan J, Liang H. 2014. Agmatine Protects against Zymosan-Induced Acute Lung Injury in Mice by Inhibiting NF-κB-Mediated Inflammatory Response. Biomed Res Int 2014.

137. Fujieda Y, Manno A, Hayashi Y, Rhodes N, Guo L, Arita M, Bamba T, Fukusaki E. 2013. Inflammation and Resolution Are Associated with Upregulation of Fatty Acid β-Oxidation in Zymosan-Induced Peritonitis. PLoS One 8:e66270.

138. Rombouts Y, Jónasdóttir HS, Hipgrave Ederveen AL, Reiding KR, Jansen BC, Freysdottir J, Hardardottir I, Ioan-Facsinay A, Giera M, Wuhrer M. 2016. Acute phase inflammation is characterized by rapid changes in plasma/peritoneal fluid N-glycosylation in mice. Glycoconj J 33:457–470.

139. Watzlawick R, Kenngott EE, Liu FDM, Schwab JM, Hamann A. 2015. Anti-Inflammatory Effects of IL-27 in Zymosan-Induced Peritonitis: Inhibition of Neutrophil Recruitment Partially Explained by Impaired Mobilization from Bone Marrow and Reduced Chemokine Levels. PLoS One 10:e0137651.

140. Chen W, Wang J, Jia L, Liu J, Tian Y. 2016. Attenuation of the programmed cell death-1 pathway increases the M1 polarization of macrophages induced by zymosan. Cell Death & Disease 2016 7:2 7:e2115–e2115.

141. Noguchi M, Kohno S, Pellattiero A, Machida Y, Shibata K, Shintani N, Kohno T, Gotoh N, Takahashi C, Hirao A, Scorrano L, Kasahara A. 2023. Inhibition of the mitochondria-shaping protein Opa1 restores sensitivity to Gefitinib in a lung adenocarcinomaresistant cell line. Cell Death Dis 14.

142. Varanita T, Soriano ME, Romanello V, Zaglia T, Quintana-Cabrera R, Semenzato M, Menabò R, Costa V, Civiletto G, Pesce P, Viscomi C, Zeviani M, Di Lisa F, Mongillo M, Sandri M, Scorrano L. 2015. The Opa1-Dependent Mitochondrial Cristae Remodeling Pathway Controls Atrophic, Apoptotic, and Ischemic Tissue Damage. Cell Metab 21:834–844.

143. Dai W, Wang Z, Wang QA, Chan D, Jiang L. 2022. Metabolic reprogramming in the OPA1-deficient cells. Cellular and Molecular Life Sciences 79:1–11.

144. Herkenne S, Ek O, Zamberlan M, Pellattiero A, Chergova M, Chivite I, Novotná E, Rigoni G, Fonseca TB, Samardzic D, Agnellini A, Bean C, Di Benedetto G, Tiso N, Argenton F, Viola A, Soriano

ME, Giacomello M, Ziviani E, Sales G, Claret M, Graupera M, Scorrano L. 2020. Developmental and Tumor Angiogenesis Requires the Mitochondria-Shaping Protein Opa1. Cell Metab 31:987-1003.e8.

145. Zamberlan M, Boeckx A, Muller F, Vinelli F, Ek O, Vianello C, Coart E, Shibata K, Christian A, Grespi F, Giacomello M, Struman I, Scorrano L, Herkenne S. 2022. Inhibition of the mitochondrial protein Opa1 curtails breast cancer growth. Journal of Experimental and Clinical Cancer Research 41:1–18.

146. Jiang HL, Yang HH, Liu YB, Zhang CY, Zhong WJ, Guan XX, Jin L, Hong JR, Yang JT, Tan XH, Li Q, Zhou Y, Guan CX. 2022. L-OPA1 deficiency aggravates necroptosis of alveolar epithelial cells through impairing mitochondrial function during acute lung injury in mice. J Cell Physiol 237:3030–3043.

147. Jiang HL, Yang HH, Liu YB, Zhang CY, Zhong WJ, Guan XX, Jin L, Hong JR, Yang JT, Tan XH, Li Q, Zhou Y, Guan CX. 2022. L-OPA1 deficiency aggravates necroptosis of alveolar epithelial cells through impairing mitochondrial function during acute lung injury in mice. J Cell Physiol 237:3030–3043.

148. Schuler MH, Hughes AL. 2020. OPA1 and Angiogenesis: Beyond the Fusion Function. Cell Metab 31:886–887.

149. Muramatsu H, Sumitomo M, Morinaga S, Kajikawa K, Kobayashi I, Nishikawa G, Kato Y, Watanabe M, Zennami K, Kanao K, Nakamura K, Suzuki S, Yoshikawa K. 2019. Targeting lactate dehydrogenase-A promotes docetaxel-induced cytotoxicity predominantly in castration-resistant prostate cancer cells. Oncol Rep 42:224–230.

150. Zhai X, Yang Y, Wan J, Zhu R, Wu Y. 2013. Inhibition of LDH-A by oxamate induces G2/M arrest, apoptosis and increases radiosensitivity in nasopharyngeal carcinoma cells. Oncol Rep 30:2983–2991.

151. Xiang J, Zhou L, He Y, Wu S. 2021. LDH-A inhibitors as remedies to enhance the anticancer effects of PARP inhibitors in ovarian cancer cells. Aging 13:25920–25930.

152. Stolberg L, Rolfe R, Gitlin N, Merritt J, Mann L, Linder J, Finegold S. 1982. D-Lactic Acidosis Due to Abnormal Gut Flora. New England Journal of Medicine 306:1344–1348.

153. Flick MJ, Konieczny SF. 2002. Identification of putative mammalian D-lactate dehydrogenase enzymes. Biochem Biophys Res Commun 295:910–6.

154. Welchen E, Schmitz J, Fuchs P, García L, Wagner S, Wienstroer J, Schertl P, Braun H-P, Schwarzländer M, Gonzalez DH, Maurino VG. 2016. d-Lactate Dehydrogenase Links Methylglyoxal Degradation and Electron Transport through Cytochrome c. Plant Physiol 172:901–912.

155. Jain M, Aggarwal S, Nagar P, Tiwari R, Mustafiz A. 2020. A D-lactate dehydrogenase from rice is involved in conferring tolerance to multiple abiotic stresses by maintaining cellular homeostasis. Sci Rep 10:12835.

156. Latham T, Mackay L, Sproul D, Karim M, Culley J, Harrison DJ, Hayward L, Langridge-Smith P, Gilbert N, Ramsahoye BH. 2012. Lactate, a product of glycolytic metabolism, inhibits histone deacetylase activity and promotes changes in gene expression. Nucleic Acids Res 40:4794–803.

157. Gaffney DO, Jennings EQ, Anderson CC, Marentette JO, Shi T, Schou Oxvig A-M, Streeter MD, Johannsen M, Spiegel DA, Chapman E, Roede JR, Galligan JJ. 2020. Non-enzymatic Lysine Lactoylation of Glycolytic Enzymes. Cell Chem Biol 27:206-213.e6.

158. de Vrese M, Koppenhoefer B, Barth CA. 1990. D-lactic acid metabolism after an oral load of DL-lactate. Clin Nutr 9:23–8.

159. Abusalamah H, Reel JM, Lupfer CR. 2020. Pyruvate affects inflammatory responses of macrophages during influenza A virus infection. Virus Res 286:198088.

160. Viola A, Munari F, Sánchez-Rodríguez R, Scolaro T, Castegna A. 2019. The Metabolic Signature of Macrophage Responses. Front Immunol 10:1462.

161. Mclelland G-L, Goiran T, Yi W, Ve Dorval G, Chen CX, Lauinger ND, Krahn AI, Valimehr S, Rakovic A, Rouiller I, Durcan TM, Trempe J-FO, Fon EA. 2018. Mfn2 ubiquitination by PINK1/parkin gates the p97-dependent release of ER from mitochondria to drive mitophagy. Elife 7:1–35.

162. Yu W, Wang X, Zhao J, Liu R, Liu J, Wang Z, Peng J, Wu H, Zhang X, Long Z, Kong D, Li W, Hai C. 2020. Stat2-Drp1 mediated mitochondrial mass increase is necessary for pro-inflammatory differentiation of macrophages. Redox Biol 37:101761.

163. Otera H, Wang C, Cleland MM, Setoguchi K, Yokota S, Youle RJ, Mihara K. 2010. Mff is an essential factor for mitochondrial recruitment of Drp1 during mitochondrial fission in mammalian cells. Journal of Cell Biology 191:1141–1158.

164. Bordt EA, Clerc P, Roelofs BA, Saladino AJ, Tretter L, Adam-Vizi V, Cherok E, Khalil A, Yadava N, Ge SX, Francis TC, Kennedy NW, Picton LK, Kumar T, Uppuluri S, Miller AM, Itoh K, Karbowski M, Sesaki H, Hill RB, Polster BM. 2017. The Putative Drp1 Inhibitor mdivi-1 Is a Reversible Mitochondrial Complex I Inhibitor that Modulates Reactive Oxygen Species. Dev Cell 40:583-594.e6.

165. Kim H, Park SJ, Jou I. 2022. STAT6 in mitochondrial outer membrane impairs mitochondrial fusion by inhibiting MFN2 dimerization. iScience 25:104923.

166. Lloberas J, Muñoz JP, Hernández-Álvarez MI, Cardona PJ, Zorzano A, Celada A. 2020. Macrophage mitochondrial MFN2 (mitofusin 2) links immune stress and immune response through reactive oxygen species (ROS) production. Autophagy 16:2307.

167. Rogne M, Chu DT, Küntziger TM, Mylonakou MN, Collas P, Tasken K. 2018. OPA1-anchored PKA phosphorylates perilipin 1 on S522 and S497 in adipocytes differentiated from human adipose stem cells. Mol Biol Cell 29:1487–1501.

168. Herkenne S, Ek O, Zamberlan M, Pellattiero A, Chergova M, Chivite I, Novotná E, Rigoni G, Fonseca TB, Samardzic D, Agnellini A, Bean C, Di Benedetto G, Tiso N, Argenton F, Viola A, Soriano ME, Giacomello M, Ziviani E, Sales G, Claret M, Graupera M, Scorrano L. 2020. Developmental and Tumor Angiogenesis Requires the Mitochondria-Shaping Protein Opa1. Cell Metab 31:987-1003.e8.

169. Civiletto G, Varanita T, Cerutti R, Gorletta T, Barbaro S, Marchet S, Lamperti C, Viscomi C, Scorrano L, Zeviani M. 2015. Opa1 overexpression ameliorates the phenotype of two mitochondrial disease mouse models. Cell Metab 21:845–54.

170. Bean C, Audano M, Varanita T, Favaretto F, Medaglia M, Gerdol M, Pernas L, Stasi F, Giacomello M, Herkenne S, Muniandy M, Heinonen S, Cazaly E, Ollikainen M, Milan G, Pallavicini A, Pietiläinen KH, Vettor R, Mitro N, Scorrano L. 2021. The mitochondrial protein Opa1 promotes adipocyte browning that is dependent on urea cycle metabolites. Nature Metabolism 2021 3:12 3:1633–1647.

171. Tezze C, Romanello V, Desbats MA, Salviati L, Scorrano L, Correspondence MS. 2017. Age-Associated Loss of OPA1 in Muscle Impacts Muscle Mass, Metabolic Homeostasis, Systemic Inflammation, and Epithelial Senescence. Cell Metab 25:1374-1389.e6.

172. Wang Y, Subramanian M, Yurdagul A, Barbosa-Lorenzi VC, Cai B, de Juan-Sanz J, Ryan TA, Nomura M, Maxfield FR, Tabas I. 2017. Mitochondrial Fission Promotes the Continued Clearance of Apoptotic Cells by Macrophages. Cell 171:331-345.e22.

173. Rath M, Müller I, Kropf P, Closs EI, Munder M. 2014. Metabolism via Arginase or Nitric Oxide Synthase: Two Competing Arginine Pathways in Macrophages. Front Immunol 5:532.

174. Yang Z, Ming X-F. 2014. Functions of Arginase Isoforms in Macrophage Inflammatory Responses: Impact on Cardiovascular Diseases and Metabolic Disorders. Front Immunol 5:533.

175. Wang X, Chen Y, Qin W, Zhang W, Wei S, Wang J, Liu FQ, Gong L, An FS, Zhang Y, Chen Z-Y, Zhang M-X. 2011. Arginase I Attenuates Inflammatory Cytokine Secretion Induced by Lipopolysaccharide in Vascular Smooth Muscle Cells. Arterioscler Thromb Vasc Biol 31:1853–1860.

176. El Kasmi KC, Qualls JE, Pesce JT, Smith AM, Thompson RW, Henao-Tamayo M, Basaraba RJ, König T, Schleicher U, Koo M-S, Kaplan G, Fitzgerald KA, Tuomanen EI, Orme IM, Kanneganti T-D, Bogdan C, Wynn TA, Murray PJ. 2008. Toll-like receptor–induced arginase 1 in macrophages thwarts effective immunity against intracellular pathogens. Nat Immunol 9:1399–1406.

177. Thoudam T, Chanda D, Sinam IS, Kim BG, Kim MJ, Oh CJ, Lee JY, Kim MJ, Park SY, Lee SY, Jung MK, Mun JY, Harris RA, Ishihara N, Jeon JH, Lee IK. 2022. Noncanonical PDK4 action alters mitochondrial dynamics to affect the cellular respiratory status. Proc Natl Acad Sci U S A 119:e2120157119.

178. Trujillo MN, Jennings EQ, Hoffman EA, Zhang H, Phoebe AM, Mastin GE, Kitamura N, Reisz JA, Megill E, Kantner D, Marcinkiewicz MM, Twardy SM, Lebario F, Chapman E, McCullough RL,

D'Alessandro A, Snyder NW, Cusanovich DA, Galligan JJ. 2024. Lactoylglutathione promotes inflammatory signaling in macrophages through histone lactoylation. Mol Metab 81:101888.

179. Luense LJ, Wang X, Schon SB, Weller AH, Lin Shiao E, Bryant JM, Bartolomei MS, Coutifaris C, Garcia BA, Berger SL. 2016. Comprehensive analysis of histone post-translational modifications in mouse and human male germ cells. Epigenetics Chromatin 9:1–15.

180. Lin Y, Qiu T, Wei G, Que Y, Wang W, Kong Y, Xie T, Chen X. 2022. Role of Histone Post-Translational Modifications in Inflammatory Diseases. Front Immunol 13:852272.

181. Liu R, Wu J, Guo H, Yao W, Li S, Lu Y, Jia Y, Liang X, Tang J, Zhang H. 2023. Post-translational modifications of histones: Mechanisms, biological functions, and therapeutic targets. MedComm (Beijing) 4:e292.

182. Ramazi S, Allahverdi A, Zahiri J. 2020. Evaluation of post-translational modifications in histone proteins: A review on histone modification defects in developmental and neurological disorders. J Biosci 45:135.

183. Liu W, Wang Y, Bozi LHM, Fischer PD, Jedrychowski MP, Xiao H, Wu T, Darabedian N, He X, Mills EL, Burger N, Shin S, Reddy A, Sprenger H-G, Tran N, Winther S, Hinshaw SM, Shen J, Seo H-S, Song K, Xu AZ, Sebastian L, Zhao JJ, Dhe-Paganon S, Che J, Gygi SP, Arthanari H, Chouchani ET. 2023. Lactate regulates cell cycle by remodelling the anaphase promoting complex. Nature 616:790–797.

184. Wang K, Xiong J, Lu Y, Wang L, Tian T. 2023. SENP1-KLF4 signalling regulates LPS-induced macrophage M1 polarization. FEBS J 290:209–224.

185. Wang K, Zhou W, Cai Q, Cheng J, Cai R, Xing R. 2017. SUMOylation of KLF4 promotes IL-4 induced macrophage M2 polarization. Cell Cycle 16:374–381.

186. de Bari L, Atlante A, Guaragnella N, Principato G, Passarella S. 2002. D-Lactate transport and metabolism in rat liver mitochondria. Biochem J 365:391–403.

187. Oh MS, Uribarri J, Alveranga D, Lazar I, Bazilinski N, Carroll HJ. 1985. Metabolic utilization and renal handling of D-lactate in men. Metabolism 34:621–5.

188. Chakraborty S, Gogoi M, Chakravortty D. 2015. Lactoylglutathione lyase, a critical enzyme in methylglyoxal detoxification, contributes to survival of Salmonella in the nutrient rich environment. Virulence 6:50.

189. Allaman I, Bélanger M, Magistretti PJ. 2015. Methylglyoxal, the dark side of glycolysis. Front Neurosci 9:123680.

190. Stewart BJ, Navid A, Kulp KS, Knaack JLS, Bench G. 2013. D-Lactate Production as a Function of Glucose Metabolism in Saccharomyces cerevisiae. Yeast 30:81.

191. Pan Y, Yu Y, Wang X, Zhang T. 2020. Tumor-Associated Macrophages in Tumor Immunity. Front Immunol 11:1–9.

192. Vitale I, Manic G, Coussens LM, Kroemer G, Galluzzi L. 2019. Macrophages and Metabolism in the Tumor Microenvironment. Cell Metab 30:36–50.

193. Li J, DeNicola GM, Ruffell B. 2022. Metabolism in tumor-associated macrophages, p. 65–100. *In* International review of cell and molecular biology. NIH Public Access.

194. Zhang Q, Wang J, Yadav DK, Bai X, Liang T. 2021. Glucose Metabolism: The Metabolic Signature of Tumor Associated Macrophage. Front Immunol 12:2525.

195. Zhou H-C, Xin-Yan Yan, Yu W-W, Liang X-Q, Du X-Y, Liu Z-C, Long J-P, Zhao G-H, Liu H-B. 2022. Lactic acid in macrophage polarization: The significant role in inflammation and cancer. Int Rev Immunol 41:4–18.

196. Israelsen WJ, Vander Heiden MG. 2015. Pyruvate kinase: Function, regulation and role in cancer. Semin Cell Dev Biol 43:43–51.

197. Ayob AZ, Ramasamy TS. 2018. Cancer stem cells as key drivers of tumour progression. J Biomed Sci 25:20.

198. De R, Sarkar S, Mazumder S, Debsharma S, Siddiqui AA, Saha SJ, Banerjee C, Nag S, Saha D, Pramanik S, Bandyopadhyay U. 2018. Macrophage migration inhibitory factor regulates mitochondrial dynamics and cell growth of human cancer cell lines through CD74–NF-κB signaling. J Biol Chem 293:19740.

199. Spera I, Sánchez-Rodríguez R, Favia M, Menga A, Venegas FC, Angioni R, Munari F, Lanza M, Campanella A, Pierri CL, Canton M, Castegna A. 2021. The J2-immortalized murine macrophage cell line displays phenotypical and metabolic features of primary BMDMs in their M1 and M2 polarization state. Cancers (Basel) 13:5478.

200. Wong YC, Ysselstein D, Krainc D. 2018. Mitochondria–lysosome contacts regulate mitochondrial fission via RAB7 GTP hydrolysis. Nature 2018 554:7692 554:382–386.

201. Kleele T, Rey T, Winter J, Zaganelli S, Mahecic D, Lambert HP, Ruberto F, Nemir M, Wai T, Pedrazzini T, Manley S. 2020. Distinct molecular signatures of fission predict mitochondrial degradation or proliferation. bioRxiv. Nature Publishing Group https://doi.org/10.1101/2020.11.11.372557.

202. Civenni G, Bosotti R, Timpanaro A, Vàzquez R, Merulla J, Pandit S, Rossi S, Albino D, Allegrini S, Mitra A, Mapelli SN, Vierling L, Giurdanella M, Marchetti M, Paganoni A, Rinaldi A, Losa M, Mira-Catò E, D'Antuono R, Morone D, Rezai K, D'Ambrosio G, Ouafik LH, Mackenzie S, Riveiro ME, Cvitkovic E, Carbone GM, Catapano C V. 2019. Epigenetic Control of Mitochondrial Fission Enables Self-Renewal of Stem-like Tumor Cells in Human Prostate Cancer. Cell Metab 30:303-318.e6.

Contribution of Collaborators

Collaborator	Contribution
Dr. Katey Rayner	Supervisor
Dr. Mireille Khacho	Co-Supervisor
Dr. Mireille Ouimet	Thesis Advisory Committee Member
Dr. Erin Mulvihill	Thesis Advisory Committee Member
Dr. Julie St. Pierre	Thesis Advisory Committee Member
Dr. My-Anh Nguyen	Mentorship, editing & training
Michele Geoffrion	Mentorship & training
Christina Emerton	Seahorse assay training and supervision

Copyright Permission

Article Title: Mitochondrial Fragmentation Promotes Inflammation Resolution Responses in Macrophages via Histone Lactylation

Author List: Leah I Susser, My-Anh Nguyen, Michele Geoffrion, Christina Emerton, Mireille Ouimet, Mireille Khacho, & Katey J Rayner

Journal Title: Molecular and Cellular Biology

Our Ref: tmcb/03638992

1/3/2024

Dear Requester,

Thank you for your correspondence requesting permission to reproduce content from a Taylor & Francis Group journal content in your thesis to be posted on your university's repository.

We will be pleased to grant free permission on the condition that your acknowledgement must be included showing article title, author, full Journal title, and **© copyright # [year]**, reprinted by permission of Informa UK Limited, trading as Taylor & Taylor & Francis Group, http://www.tandfonline.com

This permission does not cover any third party copyrighted work which may appear in the article by permission. Please ensure you have checked all original source details for the rights holder and if need apply for permission from the original rightsholder.

Please note that this license **does not allow you to post our content on any other third-party websites.**

Please note permission does not provide access to our article, if you are affiliated to an institution and your institution holds a subscription to the content you are requesting you will be able to view the article free of charge, if your institution does not hold a subscription or you are not affiliated to an institution that has a subscription then you will need to purchase this for your own personal use as we do not provide our articles free of charge for research.

Thank you for your interest in our Journal.

With best wishes,

Taylor & Francis Journal Permissions
Web: www.tandfonline.com
4 Park Square, Milton Park, Abingdon, OX14 4RN
(+44 (0)20 8052 0600

Disclaimer: T&F publish Open Access articles in our subscription priced journals, please check if the article you are interested in is an OA article and if so, which license was it published under.

Before printing, think about the environment.

ref:!00D0Y035Iji.!5007T0awQgh:ref

Curriculum Vitae

Leah Isabelle Susser

Scholarships

- University of Ottawa Heart Institute Endowed Scholarship **2020 – 2022**
- Queen Elizabeth II Graduate Scholarship in Science and Technology **2020 – 2021**
- University of Ottawa Graduate Admission Scholarship **2019 – 2023**
- University of Ottawa Merit Scholarship **2016 – 2017**
- University of Ottawa Undergraduate Admission Scholarship **2013 – 2017**

Honours & Awards

- CIHR Travel Award – Institute Community Support **2019**
- Deans Honour List **2017**

Education & Research Experience

University of Ottawa: Ottawa, Ontario **2017 –2024**

- ***Doctorate of Science in Biochemistry. Candidate***
  Supervisor: Dr. Katey Rayner Co-Supervisor: Dr. Mireille Khacho
  Faculty of Medicine; Biochemistry Microbiology and Immunology Program
  (Transfer completed from MSc. of the same name)

  Investigate the role of mitochondrial dynamics in the macrophage post-inflammatory resolution response. We found and later published in the Journal of "*Molecular and Cellular Biology"*, that mitochondrial fragmentation is a critical component in the post inflammatory macrophage response mediated through lactate accumulation causing histone lactylation. These findings required planning, organizing and designing both in-vivo and in-vitro scientific studies where I developed the following lab skills; cell culture, siRNA transfection, RNA isolation, RT-qPCR, protein isolation, western blot, cellular immunofluorescence microscopy, & flow cytometry. Throughout this process I also developed the following soft skills; critical analysis of literature, presenting, writing (both a literature review and primary research), statistical analysis, mentorship, & publication review (I reviewed two publications for two major journals: "*Circulation Research*" and "*Nature Cardiovascular Research*"). Throughout my degree I also had the opportunity to collaborate and participate in numerous multidisciplinary studies resulting in publication across numerous fields of interest in addition to my own.

University of Ottawa: Ottawa, Ontario **2013 – 2017**
Honours Bachelor of Biomedical Science Degree. Cum Laude
Specialist, Cell and Molecular Biology

- **Honours Student** (University of Ottawa Heart Institute) **2016 – 2017**
  Supervisor: Dr. Katey Rayner
  Studying the effect of hyperglycemia on inflammation and cell death in the context of atherosclerosis, as a result of diabetes. As diabetics have much worse atherosclerosis my projects aim was to better characterize this relationship between hyperglycemia and inflammatory cell death in macrophages. Skills learned: cell culture, protein assay, LDH viability assay, western blot, RNA isolation, RT-qPCR.
- **Research Assistant** (University of Ottawa) **Summer 2015**
  Supervisor: Dr. Christopher Boddy
  Developed new formulations for the thioesterase enzyme in lyophilized form. The goal was to increase the stability on the enzyme over time in powder form and maintain the activity when solubilized in organic solution. Skills learned: plasmid transformation, protein expression, protein purification, lyophilisation, SDS-PAGE and agar gels.
- **Research Assistant** (University of Ottawa Heart Institute) **Summer 2014**
  Supervisor: Dr. Robert deKemp
  Collected and investigated data on several multidisciplinary studies involving Positron Emission Tomography (PET) scans. I processed and analyzed patient scans. The goal of the project was to measure calcium deposit in arteries. Analyses were performed to find the best attenuation correction factor in order to automate analysis of patient scans. My work was published in "*Nuclear Cardiology"*. I also worked on analysis of polar map to quantify abnormal myocardial blood flow. This research data was presented in a poster at the SNM in 2015. Skills learned: minor C++ coding, large data set management, & patient blinding procedures.
- **Research Assistant** (University of Ottawa Heart Institute) **Summer 2013**
  Supervisor: Dr. Robert deKemp
  Worked on several projects involving Positron Emission Tomography (PET) scans. I processed these images using the software Flowquant and analyzed the data. The work resulted in a change in imaging protocol for Time-of-flight imaging (a form of PET). The results were included in a recent publication. Skills learned: polar map analysis, large data set management, & statistical analysis.
- **Research Assistant** (Ottawa Hospital Research Institute Cancer Center) **Summer 2012**
  Supervisor: Dr. John Bell
  Studied the mode of action of viruses on tumor cell by doing immunohistochemistry and staining of tumor sections. Performed numerous method optimizations. Skills learned: tissue sectioning, tissue immunohistochemistry staining, hematoxylin staining, & tissue morphology imaging.

Publications

1. **Susser, L. I.,** Nguyen, M.-A., Geoffrion, M., Emerton, C., Ouimet, M., Khacho, M., & Rayner, K. J. (2023). Mitochondrial Fragmentation Promotes Inflammation Resolution Responses in Macrophages via Histone Lactylation. *Molecular and Cellular Biology*, *43*(10), 531–546.

2. **Susser, L. I.,** & Rayner, K. J. (2022). Through the layers: how macrophages drive atherosclerosis across the vessel wall. *The Journal of Clinical Investigation*, *132*(9), 1–9.

3. Nguyen, M.-A., Hoang, H.-D., Rasheed, A., Duchez, A.-C., Wyatt, H., Cottee, M. L., Graber, T. E., **Susser, L.I.,** Robichaud, S., Berber, İ., Geoffrion, M., Ouimet, M., Kazan, H., Maegdefessel, L., Mulvihill, E. E., Alain, T., & Rayner, K. J. (2022). miR-223 Exerts Translational Control of Proatherogenic Genes in Macrophages. *Circulation Research*, *131*(1), 42.

4. Nguyen, M.-A., Wyatt, H., **Susser, L**. **I**., Geoffrion, M., Rasheed, A., Duchez, A.-C., . . . Rayner, K. J. (2019). Delivery of microRNAs by Chitosan Nanoparticles to Functionally Alter Macrophage Cholesterol Efflux In Vitro and In Vivo. *ACS Nano 2019,* 13(6), 6491-6505.

5. Heberlig, G., Brown, J., Simard, R., Wirz, M., Zhang, W., Wang, M., **Susser, L.I.,** Horsman, M.E., and Boddy, C. (2018). Chemoenzymatic macrocycle synthesis using resorcylic acid lactone thioesterase domains. *Organic & Biomolecular Chemistry, 16*(32), 5771-5779.

6. Kaster, T. S., Dwivedi, G., **Susser, L. I.,** Renaud, J. M., Beanlands, R. S., Chow, B. J., & Dekemp, R. A. (2014). Single low-dose CT scan optimized for rest-stress PET attenuation correction and quantification of coronary artery calcium. *Journal of Nuclear Cardiology, 22*(3), 419-428. doi:10.1007/s12350-014-0026-y

National & International Conference Presentations

1. **Susser, L.I.,** M., Nguyen, Geoffrion, M., Khacho, M., & Rayner, K. *Mitochondrial fragmentation promotes inflammation resolution responses in macrophages via histone lactylation;* Keystone Symposia: Mitochondria Signaling and Disease, Banff, AB, Canada, Feb 14, 2024.

2. **Susser, L.I.,** M., Nguyen, Geoffrion, M., Khacho, M., & Rayner, K. *Mitochondrial fragmentation promotes inflammation resolution responses in macrophages via histone lactylation;* Canadian Vascular and Lipid Summit, Prince Edward County, ON, Canada, Sept 29, 2023.

3. **Susser, L.I.,** M., Nguyen, Geoffrion, M., Khacho, M., & Rayner, K. *Mitochondrial fragmentation promotes inflammation resolution responses in macrophages via histone lactylation;* Ontario Cell Biology Symposium, Guelph, ON, Canada, August 11, 2023.

4. **Susser, L.I.,** M., Nguyen, Rasheed, A., Geoffrion, M., Khacho, M., & Rayner, K. *Mitochondrial dynamics directs macrophage polarization during atherosclerosis: implications for disease regression;* Keystone Symposia: Mitochondrial Biochemistry in Health and Disease, Whistler, BC, Canada, May 18, 2020. (Abstract accepted but Conference Canceled due to COVID-19)

5. **Susser, L.I.,** M., Nguyen, Rasheed, A., Geoffrion, M., Khacho, M., & Rayner, K. *Mitochondrial dynamics directs macrophage polarization during atherosclerosis: implications for disease regression;* Canadian Vascular and Lipid Summit, Banff, AB, Canada, Oct 4, 2019.

6. **Susser, L.I.,** Geoffrion, M., Nguyen, M., Khacho, M., & Rayner, K. *Mitochondrial dynamics a Tale of Two Fs;* Canadian Lipoprotein Conference, Toronto, ON, Canada, June 12, 2018. (Selected for an Oral Presentation)

7. Almufleh, A., Rayner, K., Zhang, L., **Susser, L.I.,** Mielniczuk, L., Stadnick, E., Davies, R., Liu, P., & Chih, S. *Biomarker Discovery in Cardiac Allograft Vasculopathy: Novel Aptamer Proteomic and MicroRNA Profiling*; International Society for Heart and Lung Transplantion Conference, Nice, France, April 13,2018.

8. **Susser, L.I.,** Karunakaran, D., & Rayner, K. *Diabetic Induced Hyperglycemia is a Trigger for Inflammation and Cell Death in Atherosclerotic Macrophages;* Canadian Society for Molecular Medicine Conference, Ottawa, ON, May 19, 2017.

Local Conference Presentations

1. **Susser, L.I.,** M., Nguyen, Geoffrion, M., Khacho, M., & Rayner, K. *Mitochondrial fragmentation promotes inflammation resolution responses in macrophages via histone lactylation;* Ottawa Cardiovascular Research Day, Ottawa, ON May 15-16, 2023.

2. **Susser, L.I.,** M., Nguyen, Geoffrion, M., Khacho, M., & Rayner, K. *Mitochondrial dynamics directs macrophage polarization during atherosclerosis: implications for disease regression;* Ottawa Cardiovascular Research Day, Ottawa, ON May 26-27, 2022.

3. **Susser, L.I.,** M., Nguyen, Geoffrion, M., Khacho, M., & Rayner, K. *Mitochondrial dynamics directs macrophage polarization during atherosclerosis: implications for disease regression;* Ottawa Cardiovascular Research Day, Ottawa, ON May 10, 2021.

4. **Susser, L.I.,** M., Nguyen, Rasheed, A., Geoffrion, M., Khacho, M., & Rayner, K. *Mitochondrial dynamics directs macrophage polarization during atherosclerosis: implications for disease regression;* Ottawa Heart Institute Research Day, Ottawa, On April 27, 2020. (Abstract accepted but Conference Canceled due to COVID-19)

5. **Susser, L.I.,** M., Nguyen, Rasheed, A., Geoffrion, M., Khacho, M., & Rayner, K. *Mitochondrial dynamics directs macrophage polarization during atherosclerosis: implications for disease regression;* Ottawa Heart Institute Research Day, Ottawa, On May 12, 2019.

6. Almufleh, A., Rayner, K., **Susser, L.I.,** Mielniczuk, L.M., Stadnick, E., Davies, R.A., P. Liu, P., Chih, S. *MicroRNA Biosignatures in Cardiac Allograft Vasculopathy;* Ottawa Heart Conference, Ottawa, ON, May 2, 2019.

7. **Susser, L.I.,** Geoffrion, M., Nguyen, M., Khacho, M., & Rayner, K. *Mitochondrial dynamics and the effects on macrophage polarization in the context of atherosclerosis;* Ottawa Heart Institute Research Day, Ottawa, ON, April 30, 2018.

8. **Susser, L.I.,** Geoffrion, M., Nguyen, M., Khacho, M., & Rayner, K. *Mitochondrial dynamics and the effects on macrophage polarization in the context of atherosclerosis;* Ottawa Heart Conference, Ottawa, ON, April 26, 2018.

9. **Susser, L.I.,** Karunakaran, D., & Rayner, K. *Diabetic Induced Hyperglycemia is a Trigger for Inflammation and Cell Death in Atherosclerotic Macrophages;* University of Ottawa Heart Institute Research Day, Ottawa, ON, May 1, 2017.

Volunteer Experience

Let's Talk Science in Ottawa (uOttawa) **2018 – 2022**

Volunteer: Organized and ran educationnal activities in schools for children ages 11-12 in 2018, 7-8 in 2019 & 2021 and 9-10 in 2020 & 2022. As well as participated as a judge for multiple science fairs and evaluated high school student research proposals.

UOHI Trainee Committee (oHEART Committee) **2020 – 2021**

Treasurer elect: Manage a budget to fund a variety of social and academic activities with emphasis on improving moral for all trainees during a global pandemic. This includes inviting four world renowned speakers from around the world via a new virtual format.

UOHI Trainee Committee (oHEART Committee) **2019 – 2020**
Treasure elect: Managed a deficit budget to fund a variety of social and academic activities. This included inviting and hosting one national and one international speakers. Those speakers were postponed due to COVID-19.

Hillel Lodge Longterm Care Center **2013 – 2017**
Volunteer activity leader: Organized and ran weekly activities for the senior residents including concerts, BINGO and card games.
Alzheimer's Ward Therapy Specialist (Snoozelan): Ran soothing and memory stimulating activities for residents within the Alzheimers ward.

B'nai B'rith Youth Organization (BBYO) **2011 – 2013**
BBYO Ottawa chapter president elect: Led the Ottawa chapter electoral board in planning charity, leadership and team building activities for Jewish youth.